INFORMATION TO USERS

This manuscript has been reproduced from the microfilm master. UMI films the text directly from the original or copy submitted. Thus, some thesis and dissertation copies are in typewriter face, while others may be from any type of computer printer.

The quality of this reproduction is dependent upon the quality of the copy submitted. Broken or indistinct print, colored or poor quality illustrations and photographs, print bleedthrough, substandard margins, and improper alignment can adversely affect reproduction.

In the unlikely event that the author did not send UMI a complete manuscript and there are missing pages, these will be noted. Also, if unauthorized copyright material had to be removed, a note will indicate the deletion.

Oversize materials (e.g., maps, drawings, charts) are reproduced by sectioning the original, beginning at the upper left-hand corner and continuing from left to right in equal sections with small overlaps. Each original is also photographed in one exposure and is included in reduced form at the back of the book.

Photographs included in the original manuscript have been reproduced xerographically in this copy. Higher quality 6" x 9" black and white photographic prints are available for any photographs or illustrations appearing in this copy for an additional charge. Contact UMI directly to order.

UMI

A Bell & Howell Information Company
300 North Zeeb Road, Ann Arbor MI 48106-1346 USA
313/761-4700 800/521-0600

FLUORESCENCE STUDY OF THE STRUCTURE AND DYNAMICS OF MODEL PHOSPHOLIPID BILAYERS USING CORONENE AND 4-CORONENYL BUTYRIC-PHOSPHATIDYLCHOLINE

by

Bo Shen

A dissertation submitted to the Graduate Faculty in Chemistry in partial fulfillment of the requirements for the degree of Doctor in Philosophy, The City University of New York

1998

This manuscript has been read and accepted for the Graduate Faculty in Chemistry in satisfaction of the dissertation requirement for the degree of Doctor of Philosophy.

9/11/98
Date

Chairman of Examining Committee

9/15/98
Date

Executive Officer

Supervisory Committee

The City University of New York

ABSTRACT

Fluorescence Study of the Structure and Dynamics of Model Phospholipid Bilayers using Coronene and 4-Coronenyl Butyric-Phosphatidylcholine

by

Bo Shen

Advisor: Professor Lesley Davenport

Melittin (26 amino acids in length) is the major bioactive peptide of bee venom and is very similar in amino acid sequence to several important signal sequence peptides. The effects of this peptide on *submicrosecond* lipid dynamics have been investigated using the long-lived fluorescence probes, coronene and a 2'-(4-coronenylbutyric) ester of lyso egg phosphatidylcholine (Cor-PC). For Cor-PC, the fluorophore is attached at the Sn2' position on the glycerol backbone of the phospholipid, and consequently resides at a fixed location within the lipid bilayer. Both coronene (τ_{av} = 200ns) and Cor-PC (τ_{av} = 120ns) exhibit long mean fluorescence lifetimes and strong rotational sensitivity to lipid bilayer disordering ('gel-fluid' lipid melting) events occuring on the submicrosecond timescale. The new probe, Cor-PC, has the additional advantage that it can provide both structural and dynamic information arising from specific sites within the bilayer. Measurements of the steady-state and time-resolved fluorescence emission anisotropy for these probes have been

used to examine the effects of melittin on the submicrosecond gel-fluid lipid equilibrium in DMPC small unilamellar vesicles (SUVs). Additionally, the effects of melittin on the rotational motions of the popular short-lived (<τ> ~ 10ns) fluorescence probe, 1,6-diphenyl-1,3,5-hexatriene (DPH), have been examined. Steady-state emission anisotropy values, <r>, were measured as a function of increasing temperature for DMPC/melittin SUVs (1:50 peptide to phospholipid mole labeling ratio) labeled with either coronene, Cor-PC or DPH. Below the lipid phase transition temperature (T_c = 23 °C for DMPC) in 'gel' phase lipid, an increase in emission anisotropy values (<r>) was detected for both coronene and Cor-PC labeled SUVs, suggesting an ordering of the lipid packing. In contrast, the short-lived DPH probe reports little change in <r>, and appears not to be sensitive to submicrosecond lipid dynamics. Cor-PC is particularly sensitive to the presence of melittin in the gel phase, exhibiting an increase in <r> values of ~45% over non-peptide containing bilayers, suggesting that this fluorophore is reporting more directly on lipid-peptide interactions. The increased <r> values observed for the coronene probes do not arise from quenched fluorescence lifetime values when in the presence of peptide, which are relatively insensitive to the presence of peptide. Time-resolved emission anisotropy decays for Cor-PC and coronene labeled DMPC SUVs at 14 °C were fitted using two rotational correlation times. For both probes, a fast rotational correlation time (ϕ_1), invariant to the presence of melittin, was observed. In contrast the slower rotational correlation times (ϕ_2) increased in the presence of peptide, suggesting that melittin has a significant effect on lipid dynamics within the submicrosecond 'time

window', resulting in a decrease in rotational motions for these long-lived fluorophores arising from decreased gel-fluid lipid fluctuations. For Cor-PC, ϕ_2 ranged from 240ns to 520 ns with addition of melittin (1:50), while the rotational correlation time (ϕ_2) of coronene embedded in lipid bilayer showed somewhat less sensitivity to the peptide. This may be attributed in part, to the non-fixed location of coronene within the lipid bilayers. For DPH, time-resolved emission anisotropy data were best analyzed as a single rotational correlation time and a residual anisotropy term (r_∞). The 'wobbling-in cone' model was used to interpret the origins of this persistent anisotropy term. While less sensitive to the effect of peptide on the gel-phase lipid dynamics compared with the longer-lived fluorescence bilayer probes, a decreased freedom of wobble for DPH was observed in the presence of melittin, where the semiangle of the cone (θ_c) is reduced, suggesting increased average bilayer ordering.

Fluorescence quenching experiments were performed to assess the location of the coronene and Cor-PC probes within DMPC bilayers, with or without melittin. Lipid embedded Cor-PC demonstrated more accessibility to the extrinsically added iodide quencher, suggesting that coronene is located deeper within the apolar region of the lipid bilayers compared with Cor-PC. In the presence of melittin, fluorescence quenching of Cor-PC labeled DMPC SUVs proved more difficult, with the probe appearing to be less accessible, presumably arising because of the more ordered or rigid lipid bilayers in the presence of peptide. This ordering of the bilayers is further supported from excimer studies using pyrene labeled DMPC vesicles. In the presence

of melittin, excimer formation is hindered, and is due to the decreased bilayer microviscosity in the presence of melittin.

ACKNOWLEDGMENTS

I would like to express my gratitude to my mentor, Professor Lesley Davenport, for all her help and excellent scientific guidance, and for being so encouraging and supportive throughout the course of this work and my graduate life.

I wish to thank Dr. Piotr Targowski and Sal Atzeni for all their help, support and friendship. I wish to thank the Department of Chemistry at Brooklyn College for their support, for their help, and for most of my valuable graduate career I spent there.

I would like to thank Professor Richard Pizer for his guidance and encouragement with my graduate program.

Special thanks are due to Professor Ross and Professor Strekas, members of my committee, for stimulating conversations and other assistance during the course of my graduate study at The City University of New York.

This thesis is dedicated to my wife Qifang Li, my son Kevin Shen, my father Minglong Shen and my mother Yongshun Wang.

TABLE OF CONTENTS

LIST OF TABLES

LIST OF FIGURES

LIST OF ABREVIATIONS

ADC	Analogue-to-digital converter
CD	Circular dichroism
Cor	Coronene
Cor-PC	4-coronenyl butyric-phosphatidylcholine
DMPC	L-α-dimyristoylphosphatidylcholine
DPH	all-*trans*-1,6-diphenyl-1,3,5-hexatriene
DPO	1,6-diphenyl-1,3,5,7-octatetraene
DSC	Differential scanning calorimetry
EA	Emission anisotropy
EDTA	Ethylenediaminetetraacetic acid
E/M	Ratio of excimer to monomer fluorescence intensities
ESR	Electron spin resonance
FWHM	Full width at half maximum
HPLC	High performance liquid chromatography
IR	Infrared spectra
LMLVs	Large multilamellar vesicles
LUVs	Large unilamellar vesicles
MCA	Multi-channel analyzer
MFPM	Multi-frequency phase modulation
MLT	Melittin

NMR	Nuclear magnetic resonance
PMT	Photomultiplier Tube
Pyr	Pyrene
RP-HPLC	Reverse-phase high performance liquid chromatography
S/N	Signal to noise ratio
SUVs	Small Unilamellar Vesicles
T_c	Lipid phase transition temperature
TAC	Time-to-amplitude convertor
TCSPC	Time-correlated single photon counting
THF	Tetrahydrofuran
Tris.HCl	Tris(hydroxymethyl)aminomethane.HCl
TLC	Thin-layer chromatography
TREA	Time-resolved fluorescence emission anisotropy

1. Introduction

1.1. Rationale

Experiments are described here which examine the interactions of peptides on *submicrosecond* bilayer lipid dynamics and packing. In particular, we have focussed our studies on the dynamics of melittin-lipid interactions. Melittin (MLT), a single Trp-containing peptide with 26 amino acids, isolated from European honey bee (*Apis mellifera*) venom [1, 2] has the amino acid sequence: Gly-Ile-Gly-Ala-Val-Leu-Lys-Val-Leu-Thr-Thr-Gly-Leu-Pro-Ala-Leu-Ile-Ser-Trp-Ile-Lys-Arg-Lys-Arg-Gln-Gln-NH_2 [3], which closely resembles the primary structure of several previously isolated important signal sequence peptides, *e.g.*, hen egg lysozyme [4]. While many previous studies have focussed on the interactions of melittin with lipid bilayers [3], comparatively few have examined its effect on lipid dynamics, and more specifically, dynamic effects occurring on the *submicrosecond* time scale. Our interests here thus focus on the application of fluorescence probe methods which span this critical *submicrosecond* region, for investigating lipid dynamics and lipid-protein interactions.

We reasoned that *submicrosecond* lipid relaxation processes occurring within the lipid bilayer might be accessible to fluorescence investigations, if the fluorescence lifetime of the adopted membrane probes were on the order of several hundreds of nanoseconds. Fluorescence probes with short (nanosecond) lifetimes can only provide information about lipid-peptide interactions occurring on this time scale. When the average fluorescence lifetime ($<\tau>$) is longer than possible slower (and persistent) lipid relaxation processes (*e.g.*, gel-to-fluid lipid exchange) then equilibrium is established. Under such conditions, where intermediate lipid relaxation processes are absent [5], then differences between the NMR and

fluorescence experimental averaging times become irrelevant, and fluorescence techniques may be successfully employed for studies of *submicrosecond* lipid dynamics. In particular, time-resolved and steady-state fluorescence emission anisotropy studies of long-lived fluorescence membrane probes can provide a convenient tool for investigation of gel-fluid lipid acyl-chain motions, and their modulation by introduction of a simple peptide to the bilayer structure.

1.2. Membrane Function and Dynamics

Biological membranes are the "skins" of living cells, maintaining cell shape and preventing loss of important cellular components to the environment. They are comprised of a variety of lipids and associated proteins. The proteins may be inserted into or through the membrane matrix, and can facilitate important membrane mediated processes, *e.g.*, transportation.

The physical chemistry of membrane structure is a fundamental aspect of normal cell activity and is connected with a number of important cellular functions. By providing a highly selective permeability barrier (between exterior and interior compartments) which contains specific protein molecular pumps and gates, membranes can regulate the molecular and ionic composition of the intracellular medium and play an important role in the control and flow of information between cells and their environment. Additionally, membranes are critical for biological communication by generating signals, which can be chemical or electrical, through specific membrane receptors which are sensitive to external stimuli. As such, membranes are an indispensable component of the living organism.

The ability of membrane lipids to assume the basic bilayer organization is associated with their amphipathic character, which arises because of their polar (or hydrophilic; water loving) head group region and nonpolar (or hydrophobic; water hating) region. In the presence of water, the polar regions of the lipid molecules tend to orient towards the aqueous phase, while the hydrophobic sections will exclude and separate from water. Thus, in the aqueous phase, lipid bilayers are the preferred ordered structures resulting in the lowest free energy.

As a direct consequence of the lateral diffusion of lipids ($D \sim 1\ \mu m^2 s^{-1}$) and proteins ($D \sim 1.0 \times 10^{-4}$-$0.4\ \mu m^2 s^{-1}$) within the plane. membranes are fluid in nature. Additionally, membrane components are able to rotate about an axis perpendicular to the membrane surface (rotational diffusion). It has been demonstrated [6, 7] that the activity of membrane enzymes, the transport of certain metabolites and ions such as Na^+, K^+ and H^+, which are vital for establishing membrane potentials, are examples of processes that are greatly influenced by the mobility and packing of membrane lipids.

In general the fluidity of a membrane depends on the nature of the fatty-acyl chain region of the membrane lipid. Most lipid species undergo a phase transition from a so-called viscous "gel" (frozen) state to a more "fluid" (melted) or liquid-crystalline state ($L_\beta' - L_\alpha$) as a function of temperature, pressure or in the presence of proteins, *etc*. Consequently, at the transition temperature (T_c), a dramatic change of 'microscopic' viscosity within the nonpolar acyl-chain region of the lipid bilayer occurs. The particular lipid phase transition depends on the length of the acyl chain and its degree of unsaturation. At physiological temperature, because of the heterogeneous lipid composition of cell membranes they usually exist in the

fluid state. As a consequence, for a given temperature or pressure, it is expected that a chemically heterogeneous mixture of 'gel' and 'fluid phospholipids will coexist, giving rise to observed lipid phase separations or domains [8, 9]. The size distribution of these domains and their dynamics and modulation have been the subject of numerous studies [9].

Interestingly, microheterogeneity or gel-fluid clusters (several hundreds of molecules) have been reported for model bilayer systems composed of a single phospholipid type, and have been implicated in several important biological processes, *e.g.*, passive ion transport (for a review, see [10]). In the following studies, we examine the effects of melittin on bilayer microheterogeneity and associated 'gel-fluid' lipid dynamics.

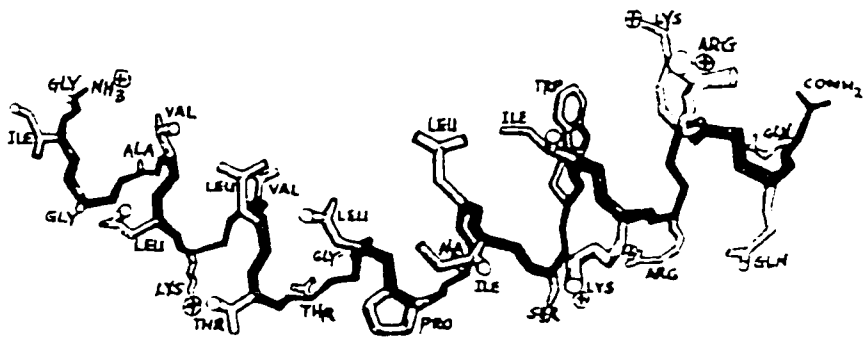

Figure 1. Proposed conformation of the monomeric subunits of melittin forming a crystalline tetramer.

1.3. Previous Lipid Dynamics Studies

A wide variety of biophysical methods have been used to study the structure and dynamic processes occurring within the membrane bilayer over an extensive time span from picoseconds to seconds. Translational (diffusion) and rotational diffusion studies (rotational rate) have provided evidence for the 'fluidity' of phospholipid bilayers [11]. This 'fluidity' arises from the flexibility of fatty acyl chains of the lipid, and is related to the *conformational* lipid order parameter, S [where $S=N^{-1}\sum_n(S_n)$ and $S_n = [(3\langle\cos^2\theta_n\rangle - 1)/2]$, where N is the total number of methylene segments [12] and θ_n is the angle made by the individual methylene bond (n) of the acyl chain backbone of the lipid and the bilayer normal. When acyl chains exist in the rigid (L_β' gel) phase, $S\sim1$ whereas $S\sim0$ for the fluid (or liquid-crystalline, L_α) phase. Differential scanning calorimetry [13, 14], ESR [15, 16], NMR [17, 18], Raman [19, 20], IR [21] and fluorescence spectroscopic [14, 22] studies have all successfully provided detailed information regarding lipid phase transitional behavior from measurements of the ordering and dynamics of lipids within liposomes as well as in bilayers containing pure lipid [22], mixed lipid [23] or proteins [24].

During the past several decades, fluorescence techniques have been successfully applied to numerous problems in biochemistry. Both intrinsic and extrinsic fluorophores [11, 25, 26] have been used to obtain both structural and conformational information about protein, nucleic acids and membranes. In particular, fluorescence methods for studying membrane structure and dynamics represent an area of particularly intense activity (see [11, 25] for a review).

Many highly fluorescent dyes have been widely used as extrinsic probes (for

example: 1,6-diphenyl-1,3,5-hexatriene, (DPH); 1,6-diphenyl-1,3,5,7-octatetraene, (DPO); perylene and coronene) for membrane heterogeneity studies [5, 11, 25, 26]. These probes preferentially partition into the hydrophobic region of membranes, and distribute between both 'fluid' and 'gel' regions of the bilayer according to their gel-fluid partition coefficient ($K_p^{g/f}$). Sensitivity of these probes to their surrounding lipid environment is detected *via* altered fluorescence parameters, such as the fluorescence lifetime (τ) or the rotational correlation time (ϕ) where probes are located in different regions of the bilayer. Hence, measured fluorescence lifetimes (τ) or rotational correlation times (ϕ) can provide a detailed picture of the structural and dynamic aspects of lipid bilayers.

The fluorescence decay for a probe within an isotropic solvent is expected to be monoexponential. However, when embedded within pure or mixed lipid heterogeneous lipid systems, the decay is often multi-exponential. For some probes (*e.g. trans*-parinaric acid) the measured lifetime values may be associated with a particular lipid environment, *e.g.*, 'gel' or 'fluid' lipid [27]. For other probes the origins for the multi-exponential fluorescence decay profiles are less clear (see [28], for a review).

Restriction of the range of reorientational motion of a fluorophore (probe molecule) when embedded in the acyl chain region of lipid bilayers, may also be revealed by using time-resolved anisotropy measurements. Thus time-dependent anisotropy measurements, r(t), can provide a picture of lipid reorientational motion on the 0.1 ns to 100 ns time scale or even longer. Anisotropic probe motion is again revealed as a sum of multi-exponential components in the decay of the emission anisotropy, r(t). Evidence for anisotropic rotational behavior of probes in bilayer membranes has been reported by several laboratories [11, 26].

1.4. Previous Studies of Lipid-Peptide Interactions and Dynamics

Interactions between proteins and membranes are of fundamental biological importance [6, 24, 29, 30 and 31]. In particular, the mechanism of protein secretion and translocation across membranes is not fully understood. It is now known that signal peptides [32, 33] or 'leader' sequences are required for the initiation of membrane protein insertion and translocation [34, 35]. These signal peptides sequences are generally 15-30 amino acids long and have a positively charged amino-terminal region followed by a stretch of highly hydrophobic amino acids. Studies have indicated that signal sequences may help to provide the information necessary for proper insertion of a protein into or through a membrane [36].

There are several hypotheses concerning the initiation of translocation of proteins across membrane. One postulates the existence of a membrane associated protein which recognizes the signal peptide and forms an aqueous channel through which the protein is extruded [37, 38]. The other view suggests direct partitioning of proteins into the lipid bilayer wherein translocation is initiated by interaction of signal sequences with the lipid bilayer [39, 40]. In either case, the signal peptide must interact with the membrane. The effect of these small polypeptides on lipid membranes and their interaction with lipids are thus of extreme importance in understanding the overall mechanism of protein transfer across membranes.

Melittin is one of a class of water-soluble peptides that binds strongly to membranes, altering bilayer permeability and resulting in hemolysis [3]. Melittin also induces a voltage-dependent ion-conductance across planar lipid bilayers (forming anion-selective pores in lipid membranes) and causes selective micellarization of bilayers [3]. Since this small peptide closely resembles signal sequences with respect to size, amphiphilicity and secondary

structure, it is of particular interest as a model for the studying of mechanism of protein-lipid interactions and the general feature of membrane protein structure and conformation.

Melittin is predominantly a hydrophobic peptide, with a net charge of +6. However, conformational studies of melittin suggest a skewed distribution of polar and non-polar amino-acids when the peptide exists in an α-helical conformation [3]. The polar amino-acids lie on one face of the helix with the non-polar amino-acids segregated almost completely on the opposite side of the helix. This amphipathic nature is characteristic of many membrane-binding peptides. In solution, the usual structure for melittin is a random coil or a tetrameric aggregate, whereas in methanol melittin is monomeric and α-helical [3]. Upon insertion into the lipid bilayer, melittin assumes the α-helical form [41].

With addition of melittin to a stirred population of erythrocytes, the peptide binds within seconds [42]. It has been suggested that melittin binds to the phospholipids as a tetramer [43] and that lipid packing is affected. Usually the tetramer consists of melittin monomers existing predominantly in a helical conformation, as confirmed by circular dichroism and Raman spectroscopic studies [44]. This association state of melittin in membranes is an important issue regarding the voltage-gated channel forming properties of the peptide which presumably requires self-association of monomers to produce a 'pore' [45]. In the gel phase of DMPC, the α-helical segments of melittin are oriented roughly perpendicular to the plane of the membrane bilayer [46, 47]. The affinity of melittin for membranes composed of negatively charged lipids is about 100-fold greater than for zwitterionic lipids [48], indicating the potential for a strong electrostatic component in the binding of melittin to the membrane. Figure 1 shows the proposed conformation of melittin

when associated with the bilayer.

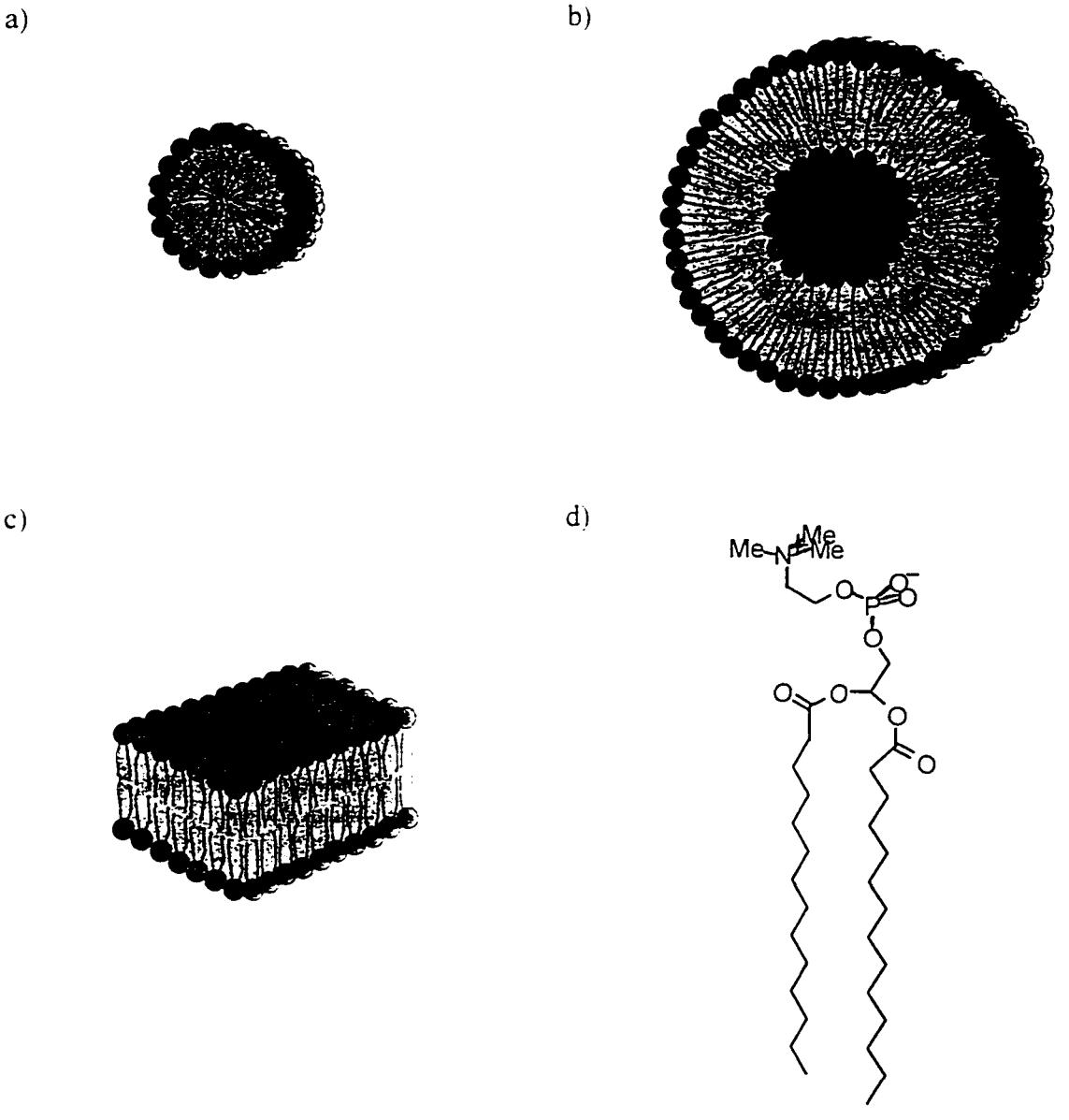

Figure 2. Different lipid assemblies and ordered structures: a) micelle; b) unilamellar vesicles; c) bilayers; d) dimyristoylphosphatidylcholine (DMPC).

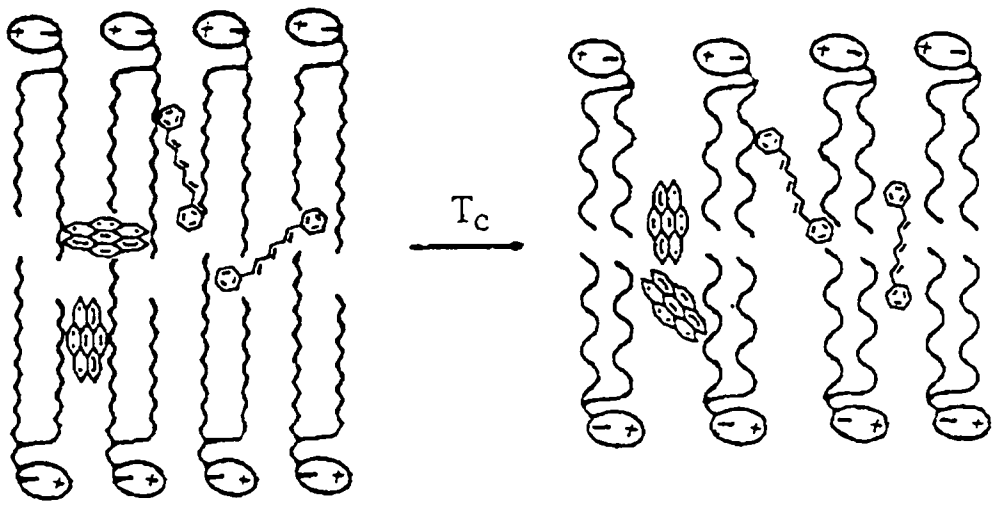

Figure 3. Cartoon showing the space available for the rotational motions of DPH and coronene below (gel phase) and above (fluid phase) the phase transition temperature (T_c) of lipid bilayers.

1.5. Systems Used in This Study

Studies of the effects of a simple peptide on *submicrosecond* lipid dynamics were performed using time-resolved emission anisotropy studies of long-lived fluorescence probes embedded within model bilayer systems containing melittin. Among the different model systems available for studying membranes, the phospholipid bilayer has been used extensively to investigate both the structural and functional aspects of biological membranes. Figure 2 summarizes different possible lipid membrane structures. A particular structure is determined by the ratio of head group to acyl chain length and number of lipid molecules [49]. In this study, small unilamellar vesicles (SUVs) composed of L-α-dimyristoylphosphatidylcholine (DMPC) were chosen for the model lipid membrane structures of choice (diameter 250-300Å) where the composition may be carefully controlled.

There are several available fluorescence membrane probes which exhibit long fluorescence lifetimes (τ >100ns) including *cis* and *trans*-parinaric acids [11], various pyrene derivatives [50, 51] and coronene [5]. The long fluorescence lifetime component of parinaric acid affords this probe a high degree of sensitivity to lipid phase transitional behavior, and the different isomers exhibits preferential partitioning for 'gel' (*trans*) or 'fluid' (*cis*) lipid phases [11]. Pyrene and its various derivatives when embedded in lipid bilayer systems exhibit fluorescence lifetimes (τ) of around 100 ns, and are useful for lateral diffusion [50, 51] and anisotropy studies in bilayer membranes [52]. Previous studies using coronene [5, 53, 54, 55] have shown that this fluorescence probe, with a mean lifetime (τ_{AV}) greater than 200 nanoseconds, is sensitive to chain disordering events on *submicrosecond* time scale which occur well after the fluorescence decay of most other popular fluorescence membrane probes

such as 1,6-diphenyl-1,3,5-hexatriene (DPH) [56].

In these studies, coronene and a coronene phospholipid analogue have been employed as fluorescence emission anisotropy probes. The latter probe was synthesized, purified and characterized [28] with the goal of positioning the long-lived fluorescence probe at a fixed location in the lipid bilayer. Figure 3 shows the proposed location for DPH and coronene embedded within DMPC lipid bilayers. Both these hydrophobic probes are expected to reside within the apolar region of the bilayer. However, different probes can locate in different parts of bilayer, resulting in varying local rotational volumes available for probe motions. Rotational motions of embedded probes are sensitive to the physical state of the bilayer. Below the phospholipid phase transition temperature (T_c), the lipid acyl chains are more tightly packed which results in restricted rotational motions for the embedded fluorophores. Above T_c however, the fluorescence bilayer probes have less hindered rotations. The range of reorientational motion of a fluorophore (probe molecule) may be revealed using time-resolved fluorescence emission anisotropy (TREA) measurements of the embedded probe residing within the acyl chain region of the lipid bilayer. Such polarized measurements provide information regarding both the dynamics (rotational correlation times; ϕ) and structural ordering of the bilayer (the residual anisotropy term; r_∞) which may be represented in terms of the *conformational* lipid order parameter (S, where $S^2 = r_\infty/r_0$). Bilayer lipid order parameters have been determined using a variety of spectroscopic (NMR, ESR, Raman, fluorescence, ultrasound) and calorimetric techniques [57, 58, 59, 60]. The magnitude of the order parameters reflects both the time scale and dimensionality (*i.e.*, micro- *versus* macro-) over which the experimental averaging occurs. Typically the values determined by the

various methods do not agree and differences between values determined from the nanosecond *versus* the microsecond time range may be taken as presumptive evidence for 'slow' lipid motions, which may be rationalized in terms of acyl-chain motions occurring within the bilayer matrix during the 10^{-7}-10^{-8} s time window. Previous studies using long-lived fluorescence probes have demonstrated such sensitivity to *submicrosecond* lipid dynamics [5].

1.6. Theoretical Background of Fluorescence Methods

Fluorescence spectroscopic methods provide a unique approach for the investigation of the basic physical properties of membrane systems. The high sensitivity of this spectroscopic tool, combined with the time scale of the technique and advances in analyses of complex fluorescence decay profiles, permits measurement of rapid relaxation and excited-state processes of embedded lipid fluorophores. The measured fluorescence signals (excitation and/or emission spectra; fluorescence lifetime and rotational properties) are exquisitely sensitive to the environment surrounding the fluorophore following excitation [52]. As such information regarding the nature of the lipid environment may be obtained. Similarly, time-resolved fluorescence measurements may be used to monitor reorientation processes on the nanosecond time scale [11, 61].

Caution must be exercised when using extrinsic probes for bilayer studies, and minimization or exclusion of potential local "perturbation" effects caused by the addition of extrinsic probes to the bilayer must be considered in order to fully interpret the rotational behavior of added embedded fluorophores as probes of the surrounding lipid environment.

Possible probe induced perturbations for the present studies will be discussed below.

1.6.1. Fluorescence Emission Spectrum

The emission spectrum is a measure of the wavelength dependence of the fluorescence intensity at a fixed excitation wavelength. Since fluorescence almost always takes place exclusively from the lowest vibrational level of the first excited state (S_1 to S_0 transition), the shape of the emission spectrum of a molecule is independent of the excitation wavelength, and will be exhibit a Stokes' shift to lower energies (longer wavelength) compared to the absorption spectrum.

For many fluorophores the emission spectrum reveals sensitivity to the environmental polarity surrounding the fluorophore. The molecule may exhibit 'solvent relaxation', where the observed emission spectrum is red-shifted to longer wavelengths due to either specific (hydrogen bonding) or non-specific solvent (induced dipole) effects. Similarly, the fluorescence intensity, which is related to the emission quantum yield (Φ_f), is also sensitive to the local probe environment. Often Φ_f is lower in polar solvents where solvent effects occur. Additionally, the overall band shape of the fluorescence spectrum can provide insights into possible molecular geometry differences of the chromophore when in the ground versus excited states. Normally, in the absence of any excited-state rearrangements, the excitation/absorption and emission spectra are mirror images of each other.

1.6.2. Fluorescence Excitation Spectrum

The excitation spectrum is a measure of the dependence of the fluorescence intensity

changes with variation of the excitation wavelength. The fluorescence intensity will be proportional to $\epsilon\Phi_f$ if the intensity of the exciting light is kept constant. For most fluorescent molecules the quantum yield is almost independent of the wavelength of excitation, so that the excitation spectrum is proportional to the extinction coefficient (ϵ) for a single absorbing species, and will be a replica of the absorption spectrum of the compound.

1.6.3. The Fluorescence Lifetime

If we have a number of excited molecules, and the only route for return to the ground-state is that involving the emission of light, then the intensity of the fluorescence decays exponentially, and the radiative lifetime (τ_f) is defined as the time taken for the intensity of fluorescence to fall to 1/e of its initial value, assuming no radiationless processes are occurring [61]. A Jablonski diagram representing the conventional kinetic scheme for the excitation and emission behavior of molecules in the condensed phase is shown in Figure 4. Here S_0 represents the ground singlet state, S_1 is the first excited singlet state and S_n is the nth excited state, where as $n \neg \infty$, ionization occurs. T_1 represents the lowest energy first triplet state. The rate constants are defined as follows: k_f is the intrinsic or radiative fluorescence decay rate, and represents a first order rate constant; k_{isc} is the rate of intersystem crossing from the singlet to the triplet states and k_{ic} is the rate describing the radiationless decay processes back down to the ground state. Initial excitation (10^{-15} sec) by absorption of radiation to a higher excited singlet state (S_n) results in fast (10^{-12}sec) radiationless internal conversion to the lowest vibrational levels of the first singlet state (S_1). The molecule may decay back to the ground-state without emission of light (resulting in thermal solvent effects), undergo

intersystem crossing to the first triplet state, or result in fluorescence emission.

The actual time dependence of the fluorescence emission is described by the combined rate constant:

$$k = [k_f + k_{isc} + k_{ic}] \equiv k_f + k_{nr} \quad (1)$$

where: k_{nr} represents the total nonradiative decay processes and k_f is the radiative rate for $S_1 \rightarrow S_0$, which is related to the strength of the transition between these states. Strongly allowed transitions have short radiative lifetimes [11]. The actual fluorescence lifetime is thus defined as:

$$k = \frac{1}{\tau} \quad (2)$$

where τ is experimentally determined. Hence for a single fluorophore which decays exponentially [62], the decay of the fluorescence intensity is described by:

$$I(t) = I_0 \cdot e^{-\frac{t}{\tau}} \quad (3)$$

where I_0 is the fluorescence intensity at $t = 0$. In general, however, fluorescence decays for fluorophores embedded within biological systems are not adequately described by a simple single exponential decay function. Several factors can affect the fluorescence decay, *e.g.*, interactions of the fluorophore with its surrounding environment resulting in heterogeneous ground-state locations for the fluorophore, or alternatively, from excited-state processes such as the interaction with potential quenching agents [63], energy transfer to a second fluorophore [42] or excited state reactions, including proton transfer or dimer (excimer)

formation [63]. As a consequence the resultant decay profile may be more complex. In these cases, the observed fluorescence decay is fitted using a sum of exponentials, *i.e.*

$$I(t) = \sum \alpha_i \cdot e^{-t/\tau_i} \quad (4)$$

where τ_i represent the lifetime of component 'i' and α_i is a preexponential factor representing the contribution of component τ_i to the time-resolved decay. Values for α_i and τ_i can provide important physical insights into complex biological systems. The fractional contribution (f_i) of each species to the total fluorescence intensity is given by:

$$f_i = \frac{\alpha_i \cdot \tau_i}{\sum_i \alpha_i \cdot \tau_i} \quad (5)$$

1.6.4. The Fluorescence Quantum Yield

The quantum yield (Φ) for the fluorescence process is defined as:

$$\Phi_f = \frac{k_f}{(k_f + k_{nr})} = \frac{k_f}{k} = k_f \cdot \tau = \frac{\tau}{\tau_f} \quad (6)$$

where τ_f is defined as the natural or intrinsic fluorescence lifetime.

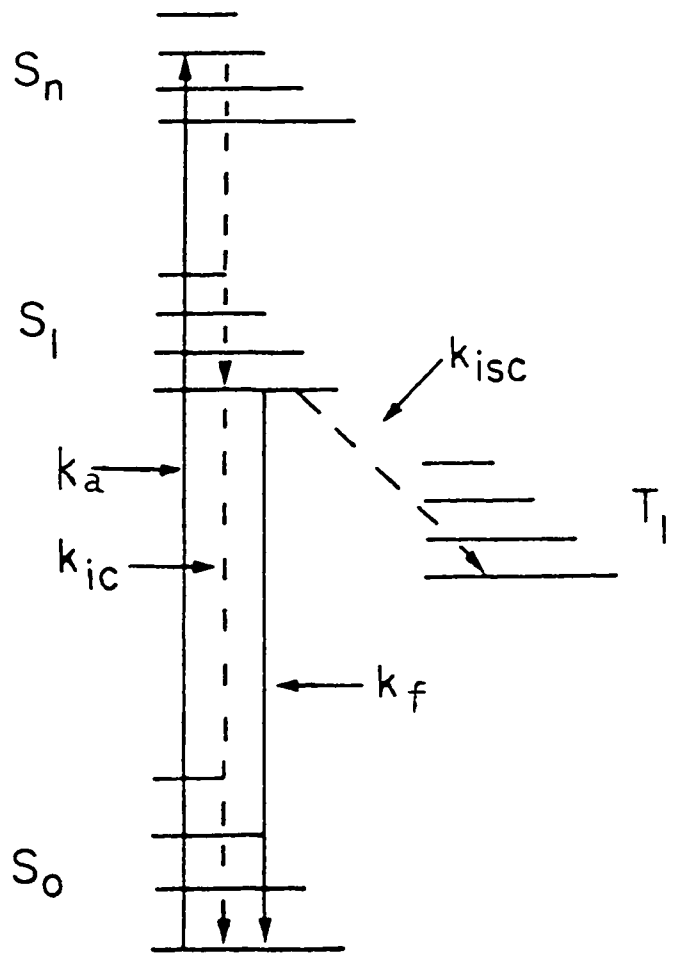

$M + h\nu \rightarrow {}^1M^*$	k_a (absorption)
${}^1M^* \rightarrow M + h\nu$	k_f (fluorescence)
${}^1M^* \rightarrow {}^3M^*$	k_{isc} (intersystem~crossing)
${}^1M^* \rightarrow M$	k_{ic} (internal~conversion)

Where M represents a polyatomic molecule and ${}^1M^*$ is the polyatomic molecule in the excited singlet state. ${}^3M^*$ is the polyatomic molecule in the excited triplet state.

Figure 4. Jablonski diagram outlining the energy levels and the excitation and decay processes for a polyatomic molecule.

1.6.5. Fluorescence Emission Anisotropy

Excitation of a randomly oriented or macroscopically isotropic sample of fluorophores with polarized light results in photoselection of a particular molecular subset within a given angular distribution, such that their absorption transition dipoles are oriented along the polarization vector of the incident radiation. In the absence of fast excited-state reorientational motions of the fluorophore, the resulting fluorescence emission is also polarized. The extent of depolarization of the emission of a fluorophore thus reflects the degree to which a population of photoselected excited fluorophores has lost its initial selective orientation and becomes randomized. Such depolarizing events usually arise from rotational diffusion and/or energy transfer.

The steady-state fluorescence emission anisotropy (<r>), which quantitates the degree of polarization, is defined [51] for linearly polarized excitation light as follows:

$$\langle r \rangle = \frac{[I_{VV} - I_{VH}]}{[I_{VV} + 2 \cdot I_{VH}]} \qquad (7)$$

where the first subscript refers to the orientation of the excitation polarizer, and the second to that of the emission polarizer.

In the limiting case, where the excitation and emission dipoles of a fluorophore are collinear, and no molecular reorientation of radiationless decay (S_n–S_1) occurs on excitation, the theoretically expected (or fundamental) emission anisotropy value, r_f, is 0.4. However, the measured maximum emission anisotropy, r_0, is often less than this fundamental value, due to radiationless decay, and nonparallel absorption and emission transition dipoles. A more

general expression defining the measured, or limiting anisotropy is thus defined:

$$r_0 = (\frac{2}{5}) \cdot P_2 \cos(\delta) = (\frac{2}{5}) \cdot \frac{(3\cos^2\delta - 1)}{2} \quad (8)$$

where δ defines the angle between the $S_0 \rightarrow S_n$ and $S_1 \rightarrow S_0$ transition dipoles, and P_2 is the second Legendre polynomial. Values for r_0 ($-0.2 < r_0 < 0.4$, for the range $90° > \delta > 0°$) can be determined experimentally by measuring the emission anisotropy for the molecule in a rigid matrix, where no molecular reorientations occur. The value of r_0 will depend on the excitation wavelength because of the variation in the angle between the excitation and emission dipoles for a particular photoselected initial state S_n. For example, if the excitation and emission dipoles are orthogonal, then $\delta = 90°$, and from Equation 8, $r_0 = -0.2$.

The time dependence of the decay of the anisotropy from its initial limiting value (r_0) depends on the effective motion of the transition dipoles of the chromophore during its excited state. The decay of the emission anisotropy for a general rigid ellipsoid [44, 62] can be described by the sum of five exponential terms:

$$r(t) = \sum_j^5 \beta_j \cdot e^{-\frac{t}{\phi_j}} \quad (9)$$

However, in practice, for many cases no more than three rotational correlation times (ϕ_j) will be experimentally resolved. Additionally, if two pairs of rotational correlation times are approximately equal, then no more than three exponential terms will be observed. This is the case for ellipsoids of revolution. The emission anisotropy is now more simply described as a

sum of three exponentials terms [64]:

$$r(t) = \beta_1 \cdot e^{\frac{-t}{\Phi_1}} + \beta_2 \cdot e^{\frac{-t}{\Phi_2}} + \beta_1 \cdot e^{\frac{-t}{\Phi_3}} \quad (10)$$

The preexponential β_j terms represent trigonometric function describing the angles between the absorption (μ_a) and emission (μ_e) transition dipoles (θ and θ, respectively) and the symmetry axis (Z) of the ellipsoid.

$$\beta_1 = 0.3\sin^2\theta_a \cdot \sin^2\theta_e \cdot cos2\psi_{ae}$$
$$\beta_2 = 0.1(3\cos^2\theta_a - 1)(3\cos^2\theta_e - 1) \quad (11)$$
$$\beta_3 = 1.2 \cdot \sin\theta_a \cdot \cos\theta_a \cdot \sin\theta_e \cdot \cos\theta_e \cdot \cos\psi_{ae}$$

The definition of angles is shown in Figure 5 where Z is symmetry axis. μ_a is absorption dipole, μ_e is emission dipole, θ_a is the angle between μ_a and the symmetry axis, θ_e is the angle between μ_e and the symmetry axis, and ψ_{ae} is the angle between azimuth projections of μ_a and μ_e. δ is the angle between μ_a and μ_e.

The zero-point or limiting emission anisotropy term (Equation 8) arises from:

$$r_0 = r(0) = \beta_1 + \beta_2 + \beta_3 = 0.2(3\cos^2\delta - 1) \quad (12)$$

The pre-exponential (β_j) terms will depend on the wavelength of excitation, since θ_a (the angle between $S_0 \rightarrow S_n$ absorption transition dipoles and the symmetry axis) varies with the excitation wavelength on exciting the fluorophore to different S_n.

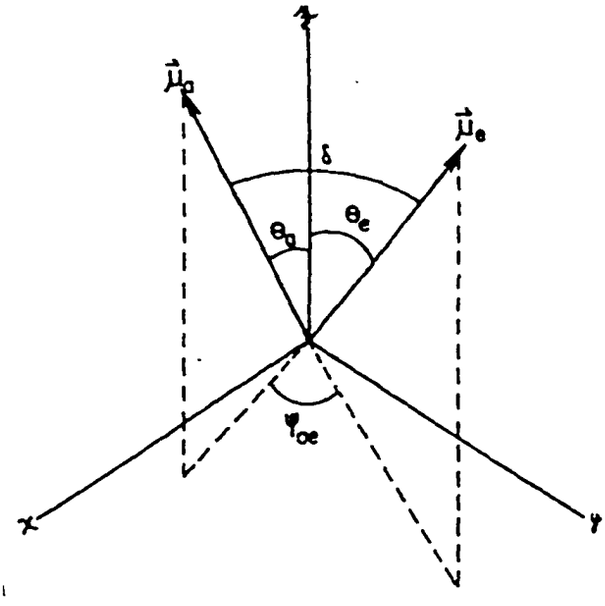

Figure 5. Definition of transition dipole directions, for a molecule with D_{2h} symmetry, which define the preexponential terms (β).

The rotational correlation times (ϕ) are related to the diffusion rates $D_\perp$ and $D_\parallel$, defined as the rate of rotation about an axis perpendicular and parallel to the symmetry axis, respectively:

$$\begin{aligned} \phi_1 &= (2D_\perp + 4D)^{-1} \\ \phi_2 &= (6D_\perp)^{-1} \\ \phi_3 &= (5D_\perp + D)^{-1} \end{aligned} \tag{13}$$

where:

$$\begin{aligned} D_\perp &= \frac{3\rho[(2\rho^2 - 1)S - \rho]D}{2(\rho^2-1)} \\ D_\parallel &= \frac{3\rho(\rho - S)D}{2(\rho^2-1)} \end{aligned} \tag{14}$$

and ρ is the axial ratio, and D is the rotational diffusion coefficient for a sphere of volume V, equal to that of the ellipsoid:

$$D=\frac{kT}{6\eta V} \tag{15}$$

Here k is the Boltzmann constant. For a prolate ellipsoid, $\rho > 1$,

$$S=(\rho^2-1)^{1/2}\ln[\rho+(\rho^2-1)^{1/2}] \tag{16}$$

and for an oblate ellipsoid, $\rho < 1$:

$$S=(\rho^2-1)^{1/2}\tan^{-1}\left[\frac{(1-\rho^2)^{1/2}}{\rho}\right] \tag{17}$$

The principal diffusion coefficients ($D_{\perp}$, $D_{\parallel}$) are thus functions of the size and shape of the rotating fluorophore, and will be dependent on the temperature T and viscosity η of the surrounding solvent, or in this case, the lipid. Their values will also depend on the nature of any interaction between the lipid molecule and the surface of the probe molecule. These interactions may fall in to two classes:

A. The Sticking Boundary Condition: Several cases are involved here:

1. For a prolate rotator: $D_{\parallel} > D_{\perp}$ and $\phi_1 > \phi_3 > \phi_2$

2. For an oblate rotator: $D_{\perp} \geq D_{\parallel}$ and $\phi_1 \cong \phi_2 \cong \phi_3$

B. Slipping Boundary Condition (i.e., free diffusion about the symmetry axis): For both prolate and oblate rotators:

1. $D_{\parallel}(\neg\infty) >> D_{\perp}$ and $\phi_1 >> \phi_2 \cong \phi_3 \neg 0$

2. The values of $D_{\perp}$(slip)/$D_{\perp}$(stick) decreases from infinity for a sphere to almost unity for very elongated prolate or very flattened oblate ellipsoids.

So depending on the orientations of the absorption and emission dipoles of the fluorophore and its interaction with lipid molecules or solvent, different relationships of pre-exponential terms and rotational correlation times will be observed in the emission anisotropy decay.

From Equation 10, if one of the transition dipoles (μ_a or μ_e) is directed along a principal diffusion axis *(i.e.*, θ_e or $\theta_a = 0$ then $_3\beta = 0$), then the decay of the emission

anisotropy reduces to double exponential:

$$r(t)=\beta_1 \cdot e^{-(\frac{t}{\phi_1})}+\beta_2 \cdot e^{-(\frac{t}{\phi_2})} \quad (18)$$

Furthermore, if this axis coincides with the symmetry axis of the ellipsoid ($\beta_2 = \beta_3 = 0$), then the expression for r(t) is further reduced to a single exponential:

$$r(t)=\beta_1 \cdot e^{-(\frac{t}{\phi_1})} \quad (19)$$

The decay is obviously monoexponential in the case of an isotropic rotor (i.e., $D_{\perp} = D_{\parallel}$), where $\phi_1 = \phi_2 = \phi_3$,

$$r(t)=(\beta_1+\beta_2+\beta_3) \cdot e^{-(\frac{t}{\phi})} \quad (20)$$

The decay of the emission anisotropy is dependent on either: 1) the shape of the probe molecule, or 2) the surroundings around the probe. We can have an isotropic rotor in an anisotropic environment or an anisotropic rotor in an anisotropic environment.

For fluorophores in lipid bilayers, anisotropic rotational behavior can thus potentially provide important insights into the magnitude of the principal diffusion coefficients as well as the interaction of the probe molecule with the lipid molecule, which yields further understanding of the structure of the lipid membrane, on the order of the lifetime of the fluorescence probe employed.

Often the anisotropic rotational motions of a fluorophore can be more easily unraveled

by investigating its anisotropic decay profiles obtained from time-resolved pulsed nanosecond fluorimetry using several excitation wavelengths, or by varying the temperature at a fixed excitation wavelength. By appropriate linkage of the preexponential terms (dependent on excitation wavelength, but independent of temperature) and the rotational correlation times (dependent on temperature, but independent of the excitation wavelength) the two anisotropy decay profiles may be 'globally' analyzed for an appropriate set of β and ϕ terms [62, 64 and 65].

Often for heterogeneous or anisotropic systems such as lipid bilayers, a residual or limiting anisotropy term is required for analysis r(t):

$$r(t) = \sum \beta_j \cdot e^{-\frac{t}{\Phi_j}} + r_\infty \qquad (21)$$

Here r_∞ is defined as the residual or limiting anisotropy; ϕ_j is the rotational correlation time or reorientational relaxation time and β_i is the associated pre-exponential term. When t=0:

$$r(0) = \sum_j \beta_j + r_\infty = r_0 \qquad (22)$$

Origins for the constant term (r_∞) include: 1) a subpopulation of excited-state fluorophores which remain immobilized during the excited-state of the molecule (heterogeneous model), or, 2) restricted rotational motion of all probes (homogeneous model). Most likely both models contribute. For the homogeneous model, if the probe is cylindrically symmetric then the restricted motion is given by:

$$r_\infty = r_0(\langle P_2[\cos(\chi)]\rangle)^2 \quad (23)$$

where P_2 is the second Legendre polynomial, and χ is the angle between the orientation of the emission transition dipole and the normal to the plane of the bilayer, for an average ensemble of probes (represented by $\langle\rangle$). For unrestricted rotational motion $r_\infty = 0$, where $\chi = 90°$, and $r_0 = \sum\beta_j$.

Equation 23 is more normally represented as the probe order parameter, S, and provides information about the ordering of the surrounding lipid environment:

$$\frac{r_\infty}{r_0} = S^2 \quad (24)$$

The range for S is, $0<S<1$, and represents a fully ordered (S=1) and disordered (S=0) ensemble of probe molecules.

1.7. Measurement of Fluorescence Lifetime and Emission Anisotropy Decays

1.7.1. Fluorescence Lifetimes

Two methods that are widely used to determine the fluorescence lifetime of a particular fluorophore [61, 66] are time-correlated single photon counting (TCSPC) and multi-frequency phase-modulation (MFPM). In TCSPC, the sample is excited using a short pulse (~2 nsecs) of light and the time-dependence of the exponential decay of the fluorescence intensity back to the ground state provides estimates of the fluorescence lifetime [64].

When a sample is excited using repetitive pulses (typically 25-50 kHz for a thyratron-

gated flash lamp system and 4 Mhz for laser-based systems) fast timing electronics are employed to measure the time taken between the excitation pulse and the arrival of the first emitted photon at the detection device (*e.g.* a phototube or multichannel plate). A 'start-pulse' arising from a lamp flash initiates a linear voltage ramp on a time-to-amplitude convertor (TAC). The 'stop-pulse' is derived from a high gain detection photomultiplier. The amplitude of the voltage ramp from the TAC is proportional to the time between the excitation and emission events, which is converted to time and stored in an appropriate time bin using a multichannel analyzer (MCA). If the photon counting event is measured many times (10^5~10^6), then a histogram of photon arrival times is built-up in the MCA, and represents the time-resolved fluorescence decay.

Available pulsed light sources for TCSPC are not true δ-pulses. As a consequence the observed exponential fluorescence decay represents a convolution of the true decay with the excitation profile. This 'contamination', which results in instrumental broadening of the measured decay profile, can be eliminated by deconvolution [61]. Lifetime resolution of a few hundred picoseconds is possible *via* deconvolution even when the excitation pulse has a full width at half maximum (FWHM) of ~2 nsec.

The second method used to measure fluorescence lifetimes routinely is the phase modulation method. In this method, the sample is excited with sinusoidally modulated excitation light of a particular frequency. The emission is a forced response to the excitation and is modulated at the same circular frequency ($\omega = 2\pi \times$ frequency in Hz) as the excitation. However, the modulated fluorescence is delayed in phase by an angle ϕ relative to the excitation due to the finite lifetime of the excited state, and the intensity is demodulated (m)

relative to the excitation. The phase angle (ϕ) and demodulation factor (m) are both measured and used to calculate the phase (τ_p) and modulation (τ_m) lifetime using:

$$\tau_p = \omega^{-1}\tan\phi \quad (25)$$

and

$$\tau_m = \omega^{-1}[(1/m^2)-1]^{1/2} \quad (26)$$

where m = (Ba/bA), such that the relative amplitude of the variable portion of the emission (B/A) is smaller than that of the excitation (b/a). For a single exponential decay:

$$\tau_p = \tau_m = \tau \quad (27)$$

where τ is the actual fluorescence lifetime. However, if the decay law is more complicated then $\tau_p \neq \tau_m$, and the fluorescence decay represents a multiexponential function.

In the following discussion, we emphasize the pulsed or TCSPC method, since this technique is used most often in our laboratory.

1.7.2. Time Resolved Emission Anisotropy Decays

The emission anisotropy decay may also be obtained experimentally using the pulsed excitation method. For a fluorescent sample which is excited using vertically excited excitation light (I_V), the time dependence of the emission components polarized parallel $I_{VV}(t)$ and perpendicular $I_{VH}(t)$ to the vertical excitation director can be used to determine the decay

of the emission anisotropy r(t) according to the following equation [67]:

$$r(t) = \frac{G \cdot I_{VV}(t) - I_{VH}(t)}{G \cdot I_{VV}(t) + 2 \cdot I_{VH}(t)} \equiv \frac{D(t)}{S(t)}$$

$$D(t) = S(t) \cdot r(t) = (\Sigma_i \alpha_i \cdot e^{-\frac{t}{\tau_i}}) \cdot (\Sigma_j \beta_j \cdot e^{-\frac{t}{\phi_j}}) \qquad \textbf{(28)}$$

where D(t) is the difference (of polarized emission intensities) decay and S(t) is the total intensity (or sum of polarized emission intensities) decay. The G-factor (or grating factor [64]) is an instrumental parameter that corrects for any imbalance in the efficiency of the detection path for transmission of vertical or horizontal polarized emission intensities. Usually:

$$G = \frac{I_{HH}}{I_{HV}} \qquad \textbf{(29)}$$

An alternative approach for analyzing polarized decay profiles involves vector analysis where $I_{VV}(t)$ and $I_{VH}(t)$ polarized decay profiles are simultaneously analyzed using global analysis for consistent lifetime and rotational parameters:

$$I_{VV}(t) = \Sigma_i \, s_i(t) \, [1 + 2r_i(t)] \, / \, 3 \qquad \textbf{(30)}$$

and

$$I_{VH}(t) = \Sigma_i \, s_i(t) \, [1 - r_i(t)] \, / \, 3 \qquad \textbf{(31)}$$

In these studies, sum and difference analyses (Equation 28, and Section 2.6) were performed.

1.8. Fluorescence Membrane Probes Used in These Studies

Long-lived fluorescence probes used in this study include: coronene (Cor) and the phospholipid adduct, 4-coronenyl-butyric phosphatidylcholine (Cor-PC). In addition, 1,6-diphenyl-1,3,5-hexatriene (DPH) was examined as an example of a short-lived rotationally sensitive probe. Studies were performed using pyrene (Pyr), as a long-lived probe which provides sensitivity to lateral diffusion dynamics within the bilayer matrix.

1.8.1. Coronene

Coronene, a long-lived fluorescent polycyclic hydrocarbon, has been the subject of intense photophysical studies [68, 69, 70]. Figure 6 shows the highly symmetrical and planar (D_{6h}) structure of coronene.

Coronene was chosen as a fluorescence probe of lipid dynamics and structure for several important reasons: 1) as an unsubstituted non-polar polyaromatic hydrocarbon, coronene is expected to preferentially partition into the hydrophobic region of the bilayer; 2) due to the long fluorescence lifetime ($<\tau>\sim$200ns) when embedded in phospholipid bilayers, this molecule will provide sensitivity to submicrosecond lipid dynamics; 3) due to the D_{6h} planar symmetry, the in-plane principal transition probabilities [70] are averaged over the plane of the molecule (r_0=0.1). As a consequence, in-plane rotational motions are not detected in the fluorescence experiment and depolarizing motions of coronene are exclusively due to

out-of-plane rotations (Figure 6).

Previous studies have shown that because of the long lifetime, the steady-state emission anisotropy for coronene reflects 'slow' out-of-plane probe rotational motions ($<r>_{op}$) only [5], and is sensitive to submicrosecond gel-fluid lipid fluctuations.

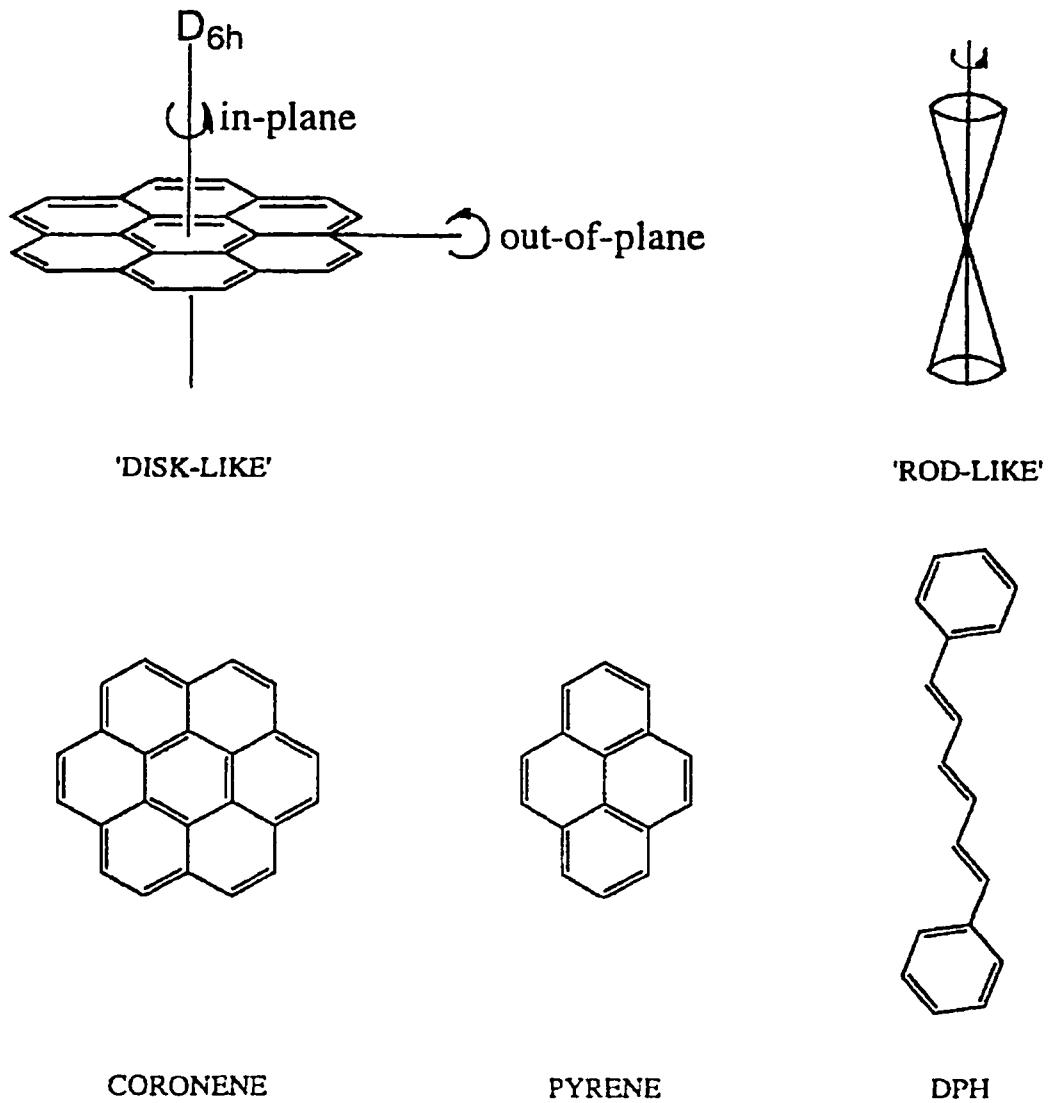

Figure 6. Molecular structures of the fluorescence probes used in these studies: coronene; pyrene and DPH.

1.8.2. Cor-PC

A common problem related to any probe study is the uncertainty of the location of the probe within the membrane bilayer. Sometimes a fluorescence probe can exchange through the solution and redistribute itself at some other location within the membrane bilayer [71]. In order to preclude the uncertaininty of probe location, we have synthesized a fluorescent adduct of a phosphatidylcholine molecule with coronene located at the 2' position on the glycerol backbone, *i.e.* 4-coronenyl butyric-phosphatidyl choline (Cor-PC). The structure of Cor-PC is shown in Figure 7. As such, the Cor-PC probe has the following advantages: 1) the probe molecule is expected to preferentially partition within the apolar region of the bilayer and undergo minimal exchange between the solvent and the bilayer; 2) the position of the chromophore relative to the bilayer structure is known and fixed; 3) although the origins of its rotational motions are unclear and most likely arise from both complex in- and out-of-plane contributions due to the altered symmetry of the molecule, the molecule does provide sensitvity to submicrosecond lipid dynamics, since Cor-PC exhibits a long fluorescence lifetime (τ_{av}=120ns). Since the lifetime is somewhat quenched compared to coronene (see below for a discussion), the quantum yield (Φ) is also correspondingly lower.

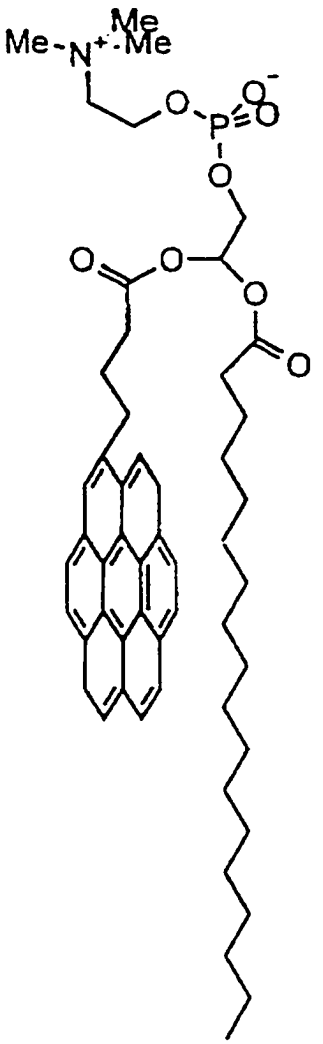

Figure 7. The molecular structure of 4-coronenyl butyric acid (Cor-PC)

2. Experimental

2. 1. Reagents

Tris buffer was prepared from 0.01M Tris.HCl, 0.1M NaCl and 1mM EDTA. The pH was adjusted to 8.3 by adding diluted sodium hydroxide (NaOH). Deionized water (resistivity of 15MΩ/cm or greater) was obtained using a Milli-Q water filtration system (Millipore, Bedford, MA). DMPC and melittin were purchased from Sigma Chemical Co (MO). DMPC was used as supplied, after checking its purity using thin-layer chromatography (silica gel G) using chloroform:methanol:water (65:25:4; by vol.) as the running solvent. A single spot, indicative of a phosphodiester bond containing species, was observed when using an ammonium molybdate spray reagent. Fluorescence probes (coronene, DPH and pyrene) were obtained from Molecular Probes (Oregon). All other chemicals were purchased from Sigma or Aldrich Chemical Companies and used as supplied.

The purity of the commercially obtained melittin (HPLC grade) was assessed by HPLC (Perkin-Elmer 1020 LC Plus) using a C-18 analytical column (4×250 mm). The solvents employed were as follows: solvent A (0.1% trifluoroacetic acid (TFA) in water) and solvent B (0.1% TFA in 75% acetonitrile/water). The mobile phase used was a 20 minute linear gradient (from 45-100%, by volume) of solvent B at 1.0 mL/minute, with an absorption detection wavelength set at 215 nm. Under these conditions, a single resolved peak (retention time = 10.08minutes) was observed. No phospholipase A_2 contamination was detected in the commercially obtained melittin sample. As a further precaution EDTA (1 mM) was added to the Tris buffer used in these experiments in order to chelate any divalent calcium ions (Ca^{2+}) which are required for phospholipase A_2 activity.

2.2. Synthesis of Cor-PC

Coronene-phospholipid analogue, the 2'-(4-coronenylbutyric) ester of lyso-egg phosphatidylcholine (Cor-PC), was synthesized according to the scheme shown in Figure 8. Synthesis of Compounds II and III, were essentially as described elsewhere (see reference[72]), however the procedure here was modified to provide a micro synthetic scheme. Other modifications are described. The three-step synthesis involves a Friedel-Crafts acylation of the succinic anhydride with coronene, followed by a Huang-Minlon reduction [73] of the resultant keto-acid, and finally conjugation of the fluorescent fatty acid with a phospholipid through an ester linkage, essentially as described by Morgan *et al.* [71]. ^{1}H-NMR spectra were obtained using a Bruker CXP300 spectrometer, operating at 4T. FT-IR spectra were recorded using a Perkin-Elmer (Paragon 500) with KBr pellets. The synthesized Cor-PC was further analyzed using reverse-phase HPLC (Hewlett Packard: HP1100) with an analytical C-18 column (4×250 mm). The mobile phase used was 100% acetonitrile and the flow rate was 1 mL/min. The absorbance of the eluant was monitored at 308 nm.

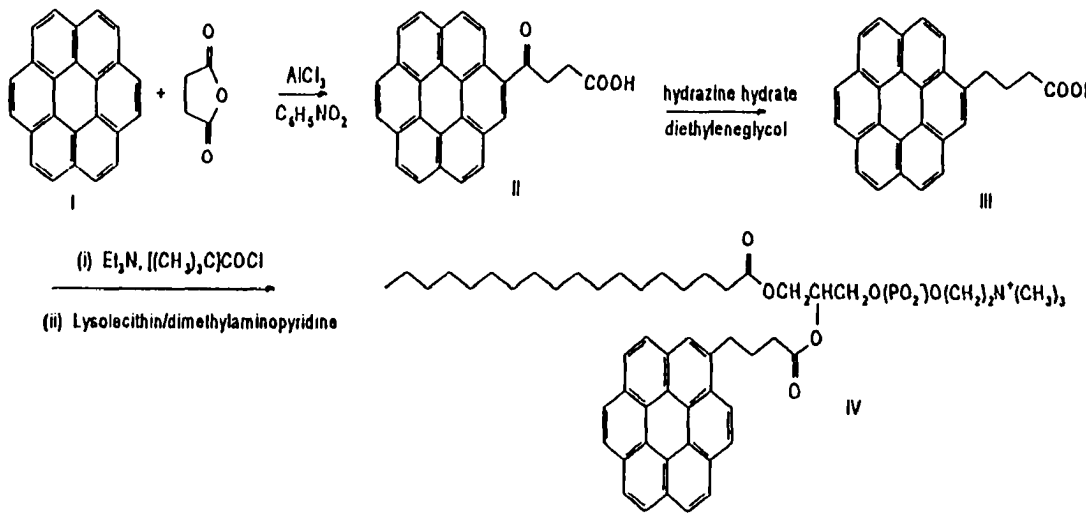

Figure 8. Synthetic Scheme for Coronene Phosphatidylcholine (Cor-PC).

2.2.1. 3-coronenoyl propionic acid (Compound II)

Coronene (100 mg) and succinic anhydride (73.4 mg) were placed in a 10 mL round-bottomed flask. Aluminium chloride (400 mg) was dissolved in 3 mL of nitrobenzene and injected slowly over a period of one hour at 0°C with stirring. The mixture was then flushed with nitrogen, sealed and left to stir for four hours at room temperature. Cold 2M HCl was added by injection and the solution was boiled for 10 minutes. A greenish-yellow precipitate was observed. The reaction mixture was allowed to cool and the green-yellow crystals were harvested by vacuum filtration using a Whatman No. 1 filter paper, washed with benzene, methanol and 2M HCl, and dried overnight under reduced pressure (<0.1 mm Hg) at 25°C. The product (108 mg; 82% yield) was recrystallized from xylene and judged pure after TLC analysis (R_f = 0.53), using ethanol/THF (50/50; by volume) as the developing solvent with silica gel G (40 micron) as the support medium. The keto acid product (Compound II, Figure 8) demonstrated a melting point of 243°C. The NMR (measured in pyridine-d_5) and IR spectra (measured using potassium bromide) were fully consistent with the expected molecular structure, and in xylene exhibited an absorption band at 444nm, with ϵ_{340} in THF = 24,914±80 $M^{-1}.cm^{-1}$.

2.2.2. 4-coronenyl butyric acid (Compound III)

The Huang-Minlon method was used essentially as described previously [73] but modified to increase the overall yield of the acid on a micro-scale. This method was preferred over the Clemmensen reduction which produced significantly lower yields. 3-coronenoyl propionic acid (100 mg), 80% hydrated hydrazine (74.8 µL), NaOH (60 mg), and diethylene

glycol (249 μL) were combined in a 5 mL round-bottomed flask. The mixture was refluxed for 90 minutes at 180°C at which time excess hydrazine and water were distilled off until the temperature rose to 200°C. The mixture was refluxed for an additional 3.5 hours at 195°C, cooled to room temperature and diluted with water and 2M HCl. The resulting solid was collected by vacuum filtration and washed with cold water and 2M HCl. The reduced product was recrystallized from xylene and dried under vacuum for 48 hours. 50 mg of crystalline product was further purified by flash chromatography on a silica gel G column (100 cm x 2.5 cm; 40 micron particle size) with a nitrogen pressure of 5-10 p.s.i. using ethyl acetate/xylene (2:1; v/v) as the running solvent. The pure 4-coronenyl butyric acid (compound III, Figure 8) exhibited a single spot (R_f = 0.65) under these elution conditions. Fractions containing pure product were pooled and dried by rotary evaporation. A yield of 86% was obtained (66.4 mg) with a melting point of 273°C. IR and NMR analysis showed spectra consistent with the expected product. Compound III in THF has an absorption band ϵ_{294} = 23,644±97.80 $M^{-1}cm^{-1}$.

2.2.3. 4-coronenyl butyric-phosphatidylcholine (Cor-PC; Compound IV)

Redistilled triethylamine (9 μL) was added to a stirred suspension of compound III (20 mg) in dry methylene chloride (2 mL), followed by 30 μL of trimethylacetylchloride. The mixture was incubated at 25°C to form the mixed anhydride. The reaction mixture was evaporated to dryness and held under 1 mm Hg vacuum for 60 minutes at 25 °C. The residue was treated with 2 mL of methylene chloride, excess L-α-lysophosphatidylcholine and dimethylaminopyridine (9 mg). The solution was stirred for 12 hours at 25°C. The Cor-PC

(Compound IV; Figure 8) was isolated from the reaction mixture by first diluting with chloroform and then extracting with three 10 mL portions of cold 0.01M HCl. The organic layer was dried by evaporation, redissolved in chloroform/methanol/acetic acid/water (75/25/7.5/2.5; v/v) and flash chromatographed using a silica gel G column (100 cm x 2.5 cm; 40 micron particle size) with a nitrogen pressure of 5-10 p.s.i. Fractions (2 mL) were collected and TLC analysis using silica gel G plates with the column solvent system, showed that unreacted compound III eluted first, followed by pure Cor-PC (R_f = 0.36). Fractions containing pure product were pooled and dried by rotary evaporation. Pure Cor-PC was stable for several months when dissolved in 95% ethanol and stored at -11 °C under nitrogen. The concentration of the fluorescent lipid analog (0.181 mM) was determined by phosphorus assay [74]. Typical yields were 7% based on compound III. The material was homogeneous by TLC examination exhibiting a single fluorescent spot which gave a positive spray reaction with phosphorus staining ammonium molybdate reagent [75].

Incubation of pure Cor-PC (200 μL of 0.181 mM solution taken to dryness under nitrogen and redissolved in diethylether/methanol (95/5; by volume)) with phospholipase A_2 (1 mg in 1mL of 0.22M NaCl-0.02M $CaCl_2$-0.001M EDTA-0.05M MOPS, pH 7.2) as described elsewhere [76], yielded compound III and lysophosphatidylcholine, both identified by TLC. Pure Cor-PC in THF has an absorption band at 305 nm (ϵ_{304} = 11,581 $cm^{-1}M^{-1}$).

2. 3. Preparation and Labeling of Vesicle Systems

2.3.1. DMPC Vesicles

Labeling of vesicles was performed *via* two methods. In the first, the chosen

fluorescent probe (in this case Cor-PC or pyrene) was cosonicated with the lipid during the preparation of the SUVs. DMPC (5-10 mg) from a stock phospholipid solution (10mg/mL in chloroform), together with small aliquots of the appropriate fluorophore were co-evaporated using dry nitrogen, onto the inner surface of a thick-walled, wide diameter boiling tube. One hour vacuum desiccation (0.5~1.0 mmHg) was applied to ensure that all the residual chloroform had been removed. The resultant dried residue was resuspended in 3 mL of 0.01M Tris.HCl containing 0.1M NaCl, 1mM EDTA (pH = 8.3) and vortexed. The phospholipid/fluorophore suspension was then sonicated using a probe sonifier (Heat System Ultrasonics Inc., Farmingdale, NY, Model W225) at 30°C (above the phospholipid phase transition temperature; T_c =23.5°C for DMPC) in 3 minute bursts (total sonication time was typically 15 minutes) and under nitrogen. These precautions were necessary in order to minimize lipid peroxidation artifacts from local over heating. SUVs were produced when the milky white multilamellar suspension turned clear and faintly opalescent. The solution was ultracentrifuged [77] (Beckman Airfuge) at 108,000xg (82,000 rpm) for sixty minutes in order to remove titanium particles from the sonicator probe, aggregated fluorophore and any large lipid aggregates. Removal of the center core after ultracentrifugation produced DMPC SUVs, which were carefully transferred using a Pasteur pipet to a test tube and stored in a water-bath (30°C). The concentration of the SUV preparation was determined from the lipid phosphorus concentration, using an ammonium molybdate complex calorimetric assay [74]. A stock phosphorus solution made from Na_2HPO_4 (anhydrous) was used to standardize the assay. Blank (non-labeled) SUVs were prepared in the same way but without the fluorophores. The probe to phospholipid molar labeling ratio was typically 1:200 or 1:100 for

Cor-PC, and 1:50 or 1:25 for pyrene.

In contrast, labeling with coronene and DPH was achieved by direct injection of small aliquots of a stock probe solution (1 mM in THF) into a vortexing suspension of preformed vesicles (DMPC/DPH = 500:1, DMPC/Coronene = 200:1, molar labeling ratio) above T_c. The labeled SUVs were gently shaken overnight to ensure complete incorporation of the probe into the bilayer vesicles (30°C). Incorporation of the fluorescent probes into the vesicles was followed by monitoring the increasing emission anisotropy values, below the phase transition temperature of the lipid (room temperature), reaching a final plateau value when full incorporation was achieved.

To eliminate the presence of any unincorporated and/or adsorbed probe molecules, usually the labeled SUVs were passed over a Pharmacia PD-10 Sephadex G-25M size-exclusion column using Tris buffer as the running solvent. A second phosphorus assay was performed to determine the final concentration of vesicle phospholipid.

Large unilamellar vesicles (LUVs) [78], were prepared by extrusion. Again, the DMPC stock solution (10 mg/mL in chloroform) was dried (in the presence or absence of fluorescent probe at the appropriate labeling ratio) by evaporation using nitrogen followed by vacuum desiccation for one hour as described above, mixed by vortex in the presence of Tris buffer (3 mL), and finally subjected to three freeze-thaw cycles using liquid nitrogen [78]. The resultant large multilamellar vesicle (LMLVs) dispersion was extruded through two stacked 25 mm diameter polycarbonate filters of 0.1 μm pore size, to produce homogeneous LUVs of 100Å diameter. Briefly, LMVs were carefully pipetted into the central chamber of a lipid extruder (Lipex Biomembrane Inc., Vancouver, B.C., Canada) above the

polycarbonate filters and a positive nitrogen pressure, typically 100-500 lb/in.^{2}, was applied via a gas cylinder fitted with a high pressure regulator (0-400 lb/in.^{2}). LUVs were collected and extruded twice more. All extrusion procedures were conducted at 30°C, above the phase transition temperature (T_c) for DMPC.

After preparation, a sample (3 mL) of the phospholipid vesicle suspension was transferred to a 1cm × 1cm × 4 cm quartz fluorescence cuvette. A matched phosphorus concentration blank vesicle sample was also prepared and used as the experimental control to correct measured fluorescence signals for any potential light scattering effects arising from the vesicle suspension alone.

Fluorescently labeled DMPC SUVs and LUVs were stored in a water-bath at 30°C and always used for fluorescence studies within two days of preparation.

2.3.2. Melittin Containing Vesicles

Melittin (usually 1.00 mM in Tris buffer) was added by direct injection to the diluted vesicles solution with either fixed or increasing molar ratio from 1:1000 to 1:20 (peptide to lipid molar ratio). All the samples were incubated (at 30°C) for at least 30 minutes before fluorescence spectroscopic measurements were performed, in order to ensure full incorporation of the melittin into the lipid vesicles. Penetration of the peptide was followed spectroscopically since the fluorescence emission spectrum of melittin exhibits a blue wavelength shift (~5nm) when embedded in lipid bilayers, relative to that in aqueous solution [43, 79, 80].

2.4. Fluorescence Spectroscopic Measurements

Fluorescence spectra were measured using a Perkin-Elmer MPF2A or a Perkin-Elmer LS-50B spectrofluorimeter, each equipped with a thermostatically controlled sample holder (home built feedback controller interfaced to a Fisher water bath) for accurate control of the experimental temperature. Excitation wavelengths employed were: 306 nm for coronene, 308 nm for Cor-PC, 355 nm for DPH and 340 nm for pyrene, respectively. Emission wavelengths were: 448 nm for coronene and Cor-PC, 430 nm for DPH and 396 and 470nm for the monomer (M) and excimer (E) of pyrene, respectively. For both excitation and emission spectra the bandwidths used were typically 4.0 nm, each, respectively or optimized to maximize the signal to noise (S/N) ratio.

For fluorescence investigations, all samples were diluted to 0.05-0.1 absorbance units at the appropriate excitation wavelength, in order to avoid possible inner filter effects [81], and reduce light scattering arising from the vesicle suspensions. As mentioned previously, any light scattering from the vesicle suspension was always corrected for by subtracting the signal from the blank SUVs solution from that of the fluorophore labeled SUVs, measured using identical excitation and emission conditions.

2.4.1. Steady-State Emission Anisotropy Measurements (<r>)

Steady-state emission anisotropies (<r>) were measured as a function of different parameters (*e.g.* temperature, concentration of melittin, concentration of quenching agent and probe to lipid molar labeling ratios, etc.). The appropriate excitation or emission polarization direction (vertical or horizontal) was selected using polarizers mounted between the cuvette

and the focusing or collecting lenses to the monochromaters, respectively (Figure 9). The steady-state emission anisotropy (<r>) was calculated from the four possible polarizer combinations according to:

$$\langle r \rangle = \frac{G \cdot I_{VV} - I_{VH}}{G \cdot I_{VV} + 2 \cdot I_{VH}} \qquad (32)$$

where the first and second subscripts refer to the orientation of the excitation and emission polarizer, respectively. The G-factor [82], defined as: $G = I_{HH} / I_{HV}$, represents a correction for the inequality of sensitivity of the detection system to the transmission of horizontally and vertically polarized emissions.

Background polarized signals, arising from light scattering of the vesicle suspension and/or membrane autofluorescence, were measured using a blank SUV sample and were each subtracted from the corresponding measured polarized fluorescence intensity, before determination of <r>.

FLUORESCENCE EMISSION ANISOTROPY

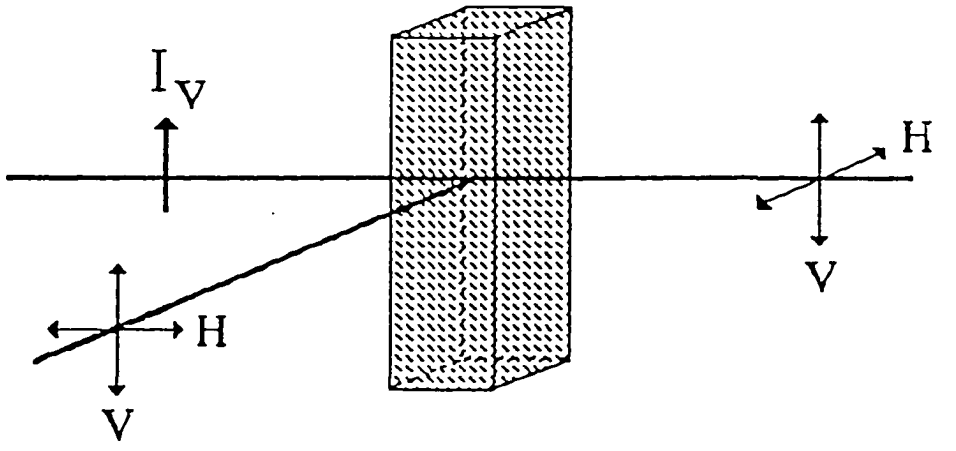

$$\langle r \rangle = \frac{G \cdot I_{VV} - I_{VH}}{G \cdot I_{VV} + 2 \cdot I_{VH}} \qquad (33)$$

$$\text{where:} \quad G = \frac{I_{HH}}{I_{HV}}$$

Figure 9. Optical configuration for steady-state emission anisotropy measurements.

2.4.2. Pyrene Excimer/Monomer Ratio Measurements

Intermolecular excimer formation of pyrene when embedded within lipid bilayers has been extensively employed as a probe of molecular mobility within the hydrocarbon interior of phospholipid bilayers [50]. In these studies, we conducted a series of experiments to determine the effects of melittin on phospholipid packing by measurement of the diffusion controlled excited-state dimer (or excimer) formation arising from the encounter of a pyrene molecule during its excited-state lifetime, with a second ground-state molecule while embedded within the phospholipid bilayer.

Steady-state fluorescence emission spectra were recorded from 360 nm to 600 nm., using an excitation wavelength of 340 nm. From the fluorescence emission spectra, an excimer to monomer intensity ratio (E/M) was determined from the blank corrected emission intensities corresponding to the pyrene excimer (I_E at 470 nm) and monomer (I_M at 390 nm):

$$\frac{Excimer}{Monomer} = \frac{E}{M} = \frac{I_E(\lambda = 470nm)}{I_M(\lambda = 390nm)} \qquad (34)$$

The E/M intensity ratio for pyrene labeled DMPC vesicles was measured as a function of temperature and peptide labeling ratios.

2.4.3. Fluorescence Quenching Experiments

Fluorescence quenching experiments can provide information about the location of a fluorescence probe within a lipid bilayer system through its accessibility to an extrinsically added fluorescence quencher molecule [65]. A fluorophore which is located on the surface

of lipid vesicle is readily accessible to a solute quencher dissolved in the aqueous phase. However, a fluorophore embedded deeper within the lipid bilayer or residing on the inner leaflet of the bilayer may be quenched to a lesser degree or inaccessible to the solute quencher. Fluorescence quenching experiments were performed here in an effort to determine the location of the coronene moiety of Cor-PC when embedded within the phospholipid bilayers. This information aids in the interpretation of complex time-resolved fluorescence signals.

Stock solutions of KI (2.0M in Tris.HCl buffer) were prepared either immediately before the experiment or a few days earlier, and stored in the dark at 0-5°C. Sodium thiosulfate ($Na_2S_2O_3$; 0.1 mM) was added both to the KI stock solutions and Tris.HCl (used for dilution) to prevent the production of I_2 which is subsequently reduced to form I_3^-, which due to its strong absorption extinction interferes with the fluorescence quenching measurements.

Quenching experiments were conducted using lipid vesicle suspensions (5 trials) containing either Cor-PC or coronene, to which increasing amounts (0 to ~0.2M) of the extrinsic heavy atom quencher, potassium iodide, was added. Aliquots of sodium chloride (NaCl) were also added to keep the ionic strength of the vesicle suspensions constant. Samples were allowed to incubate before the fluorescence intensities were measured at 14°C using the Perkin-Elmer LS-50B spectrofluorimeter. Excitation wavelengths were 306 nm for coronene and 308 nm for Cor-PC, with the emission intensity measured at 448 nm for both probes. The slit width for both the excitation and emission monochromaters were each 4.0 nm. Corrections were made for any background vesicle blank scattering, using control

samples.

For the measurement of the interaction of melittin with lipid, the melittin (1 mM in Tris buffer) was added by direct injection to the diluted probe-labeled and blank vesicle samples. Samples were incubated for at least 30 minutes, as described above, before the quenching experiments were performed to ensure full incorporation of melittin into the SUV samples.

The quenching effect of KI on the fluorophore was determined by calculating the fluorescence intensity ratio ($I_0/I([Q])$), where I_0 is the fluorescence intensity of the bilayer embedded probe in the absence of quencher and I([Q]) is the resulting dilution-corrected fluorescence intensity, after addition of quencher at concentration [Q].

2.5. Time-Resolved Fluorescence Measurements

Nanosecond time-resolved fluorescence measurements were performed using a home-built time-correlated single-photon counting fluorometer (Figure 10) equipped with a 340 nm excitation interference filter (typical bandpass of 10nm, Ealing Optical) and an emission monochromator (Model H-10, Instruments-SA, New Jersey). A coaxial nanosecond flash lamp (Photochemical Research Associates, Model 510B or an IBH (Glasgow, UK) nanosecond flash lamp, Model 5000) was used as the excitation source. The lamp discharge was gated using a hydrogen filled thyratron, resulting in discharge pulses across two thoriated-tungsten electrodes at a frequency of 15-50 kHz. The lamp housing was filled with ultra pure nitrogen gas (Matheson) at typically 0.5 atm pressure, resulting in all of the emission spectral lines for nitrogen. The electrode gap was set typically at about a width of

0.8-1.2 mm. Under these conditions, the lamp displayed pulse widths of about 2 nanosecond full width at half maximum (FWHM).

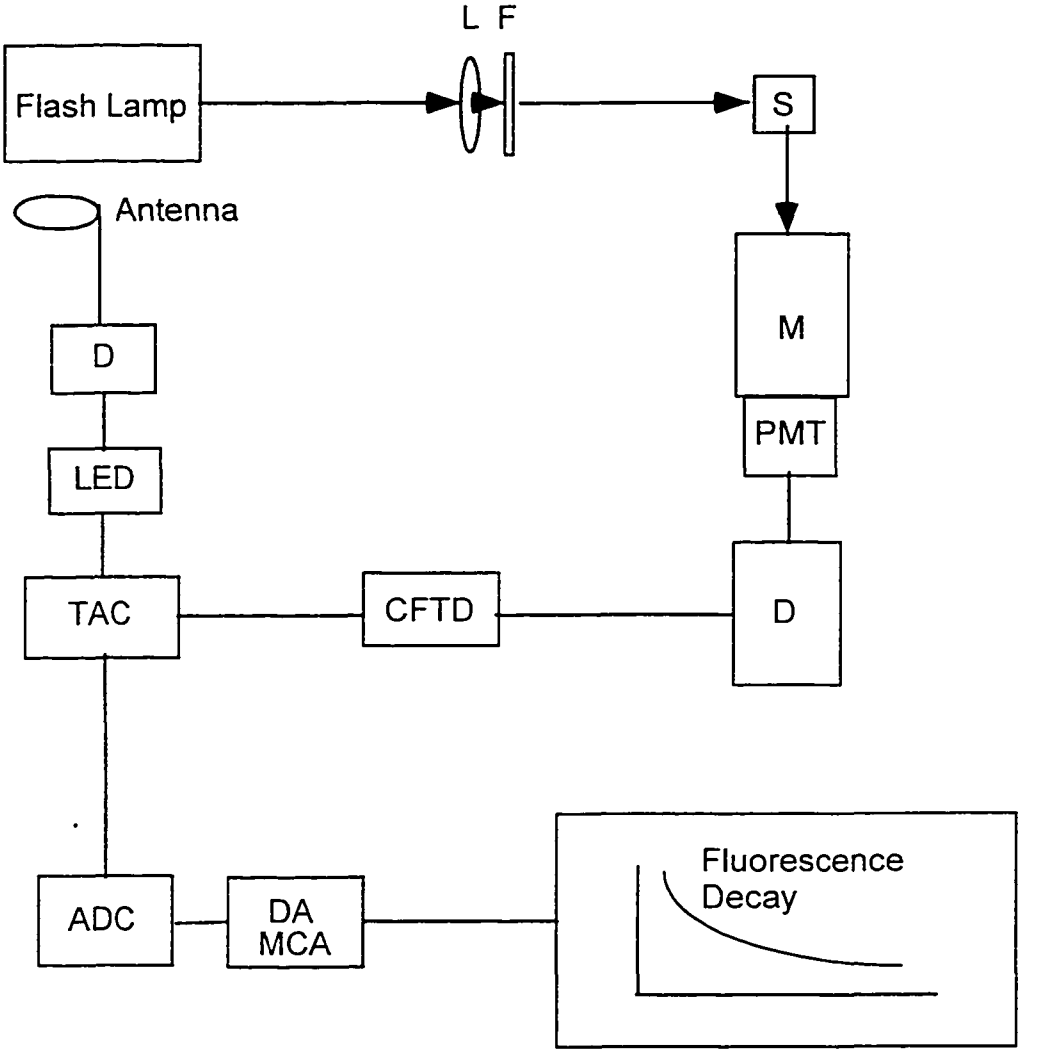

Figure 10. Schematic block diagram of the home-built single photon counting fluorometer used in these studies: L, focusing lens; F, excitation filter; S, sample holder; M, emission monochromator; PMT, fast photomultiplier tube; D, delay cable; CFTD, constant fraction timing discriminator; LED, leading edge time discriminator; TAC, time-to-amplitude converter; ADC, analogue-to digital converter; DA, data acquisition; MCA, multichannel analyzer.

A discriminated 'start-pulse' (Ortec 436 100MHz constant fraction discriminator) which initiates a linear voltage ramp on a time-to-amplitude (Ortec 566 TAC) converter, was derived from a fiber optic detection system (RCA IP28 photomultiplier) observing the pulsed flashlamp. The 'stop-pulse' was obtained using a high gain detection photomultiplier (for our studies we employed a water cooled Phillips XP-2020Q phototube), after discrimination and amplification using a Tennelec 455 quad fast discriminator (CFD). The amplitude of the voltage ramp from the TAC is proportional to the time between the excitation and emission events, which is converted to time and stored in an appropriate time bin using a multichannel analyzer (Ortec 918A-MCA-ADCAM). If the photon counting event is measured many times (10^5~10^6), then a histogram of photon arrival times is built-up in the multichannel analyzer (MCA), and represents the time-resolved fluorescence decay. A timing calibration (τ_{cal}) of 0.432 ns/channel was used for all the time-resolved experiments performed. For a typical fluorescence decay profile, the peak counts collected were 15,000 for the fluorescent sample and 20,000 for the scattering profile (diluted colloidal silica/Ludox, Dupont, DE) subsequently used for the lamp deconvolution.

The compound, 9-cyanoanthracene (9-CNA) in methanol (τ = 4 ns) was used as a standard reference material demonstrating a single exponential decay time, which could be used to: a) test the performance of the single-photon counting instrument, and b) serve as a lifetime standard for determining the color (or "Q") shift resulting from the varying transit times for the different energy photons arising from the fluorescent (emission wavelength) or scattering (excitation wavelength) samples impinging on the detector [83, 84]. For our experiments, these values were usually less than 200 ps.

The time between excitation pulses was adjusted to be greater than about five times the fluorescence decay time in order to avoid wrap around effects arising from a second excitation pulse interfering with the fluorescence emission decay arising from an earlier excitation pulse. This effect is of particular importance when studying long-lived fluorophores as discussed here. In addition, the emitted light intensity must be adjusted using the appropriate discriminators to ensure that only a single photon for each excitation pulse is detected at the phototube, hence excluding 'pile-up' artifacts [64], which leads to distortion and weighting of the decay profiles to shorter fluorescence lifetimes.

The emission anisotropy decay was obtained experimentally by measuring the time dependence of the parallel ($I_{VV}(t)$) or perpendicularly ($I_{VH}(t)$) polarized emission light, with respect to the excitation polarizer which was fixed in the vertical orientation. The G-factor, defined according to Equation 29, was determined before and after the emission anisotropy decay experiment, by extending the time window of the multichannel analyzer, such that all photons in all channels were integrated to provide essentially a steady-state (or time-averaged) measurement for a particular polarized intensity (I_{fV} and I_{fH}). Similarly a steady-state <r> value was determined in the same fashion (Equation 33). The extended time window was employed here in order to obviate possible truncation errors of decay profiles arising from the use of long-lived lifetime probes. The resultant polarized emission decay profiles were then analyzed using sum and difference analysis as discussed below.

2.6. Analysis of Time-Resolved Fluorescence Decay Data

All data analyses was performed using an 80486 66MHz personal computer system

equipped with a math coprocessor.

For pulse fluorometry, the true fluorescence decay, F(t), is defined as the impulse response decay function following the excitation of the sample by an infinitely short or 'delta' pulse of light. This narrow excitation pulse precisely defines the time origin from which the decay is measured. In reality however, the excitation pulse has a finite width which does not allow for a clear definition of the true 'time zero'. The experimentally obtained fluorescence decay is thus distorted by convolution with the lamp flash profile. This artifact is described by the convolution integral:

$$R(t) = \int L(t')F(t-t')dt' \qquad (35)$$

where F(t) represents the true fluorescence decay, L(t) is the time profile of the excitation pulse, and R(t) is the experimental decay response which is obtained from the single photon counting instrument following the excitation pulse. Making a change of variables, $t' = t - \mu$, we have:

$$R(t) = \int L(t-\mu)F(\mu)d\mu \qquad (36)$$

Thus, with a knowledge of the experimental functions R(t) and L(t), the true fluorescence decay profile F(t), uncontaminated by the convolution integral, can be determined, from which the decay components (α, τ and β, ϕ) can be determined. A large variety of numerical procedures are available for carrying out the deconvolution procedure [64].

A Marquardt non-linear least-squares minimization method [61, 64, 85a] was

employed in our studies to analyze single-photon counting decay data. This method provides excellent and reliable results. The basis of the least-squares minimization method is the calculation of the expected value for R(t) given assumed values α_i and τ_i from:

$$F(t) = \Sigma \alpha_i \cdot e^{\frac{-t}{\tau_i}} \tag{37}$$

The convolution integral R(t) is then constructed using the assumed values of α_i and τ_i (or another assumed decay law) and the measured time-profile of the lamp pulse, L(t). The calculated function, $R_C(t)$, is compared with the observed function, R(t). The α_i and τ_i values are adjusted until the best fit is obtained. The goodness of fit is judged from:

(a). Evaluation of Chi-squared (χ^2) values:

$$\chi^2 = \Sigma \omega_i [R(t) - R_c(t)]^2 \tag{38}$$

where:

$$\omega_i = \frac{1}{R(t)} \tag{39}$$

and is a statistical weighing factor which accounts for the expected error in each value of R(t). A minimum value of χ^2 indicates the best fit. Usually χ^2 values larger than 2 indicate a poor fit and χ^2 values less than 1.2 indicate a good fit.

(b). Evaluation of the weighted residual, given by:

$$r(t_i) = \sqrt{(\omega_i)}\,[R_c(t_i) - R(t_i)] \qquad \textbf{(40)}$$

Here, a random distribution around zero indicates a good fit.

(c). Evaluation of the autocorrelation function of the residuals: the autocorrelation function, C(t), of the residuals is defined as:

$$C(t_j) = \frac{(\frac{1}{m})\ \sum r(t_i) r(t_{i-j})}{(\frac{1}{n})\ \sum [r(t_i)]^2} \qquad \textbf{(41)}$$

where $C(t_j)$ is the correlation between the residual in channel I and the residual in channel I+j summed over a selected number of I channels, r(t) is defined in Equation 40, n is the number of time intervals for which experimental data are available, and m is the number of terms in the numerator. The index j can assume the values 1, 2, ..., (n-m). An upper limit for j is set at n/2 so that the number of terms in the numerator, m, may be sufficient for proper averaging.

The autocorrelation function plot is a more sensitive indication of poor fitting than the plot of residuals. Usually a good fit shows the low amplitude oscillation about zero of the autocorrelation function when plotted against j.

Analyses of the time dependent emission anisotropy decays were achieved from construction of difference and sum curves (see Section 1.7.2), and determination of the steady-state emission anisotropy value (as discussed above, Section 2.4.1, Figure 9). Since

the difference decay may be expressed as the product of the sum curve and the steady-state emission anisotropy value (Equation 28), by fixing preexponential (α) and lifetime (τ) values from an independent analysis of the total intensity decay, values for β and ϕ values may be determined from fits to the experimentally derived difference decay data:

$$d(t) = I_{VV}(t) - I_{VH}(t)$$

$$d(t) = (\Sigma_j \beta_j e^{-\frac{t}{\phi_j}}) \cdot (\Sigma_i \alpha_i e^{-\frac{t}{\phi_i}}) \qquad (42)$$

Time-resolved fluorescence data summarized and shown in the following data tables are representative of several (N = 1-4) data set collected for each experimental variable (*e.g.*, temperature, added melittin concentration). For each decay data set analyzed (several thousand counting events - Gaussian distribution), errors for the retrieved parameters using non-linear least square regression analyses are typically about 5-10%, and fall within the experimental confidence interval as set by the change in calculated χ^2 values [85b]. Alternatively, standard deviations for the recovered parameters from several data sets (N > 1) did not typically exceed ~15%.

3. Experimental Results and Discussion

3.1. The Synthesis and Analysis of Cor-PC Adduct

The synthetic procedure described for Cor-PC provided a pure target compound with high yield (85%). The compound was chromatographed over a Silica gel G column using chloroform/methanol/acetic acid/water (75/25/7.5/2.5; by volume) as the eluant. Eluted fractions revealed a single fluorescent spot on TLC which additionally gave a positive phosphodiester stain with an ammonium molybdate spray reagent [75], reacted negatively with Ninhydrin reagent [86] (a stain for α-amino groups), and revealed a single spot on charring with sulfuric acid reagent (2% in methanol, by vol.). Reversed-phase HPLC analysis using a C-18 column for Cor-PC (Figure 11a) revealed a single elution peak with a retention time (RT) of 6.71 minutes, providing further evidence for the purity of the synthesized Cor-PC. This single peak was characterized from the UV-visible absorption spectrum of the coronenyl moiety, determined using a photo-diode array detector on the HPLC (Figure 11b), which reveals strong absorption bands at 308 nm and 342 nm [70]. For comparison, a sample of pure coronene was chromatographed using the same reversed-phase HPLC system, which provided a single elution peak with a retention time of 13.09 minutes (Figure 12a) and a UV-visible absorption spectrum characteristic for coronene (Figure 12b). The much longer retention time for coronene compared to Cor-PC may be attributed to its more non-polar character, resulting in a stronger adsorption on to the C-18 HPLC column. In contrast, the coronene fluorophore of Cor-PC is attached to the more polar phosphatidylcholine molecule and, as a consequence, is more easily eluted from the column.

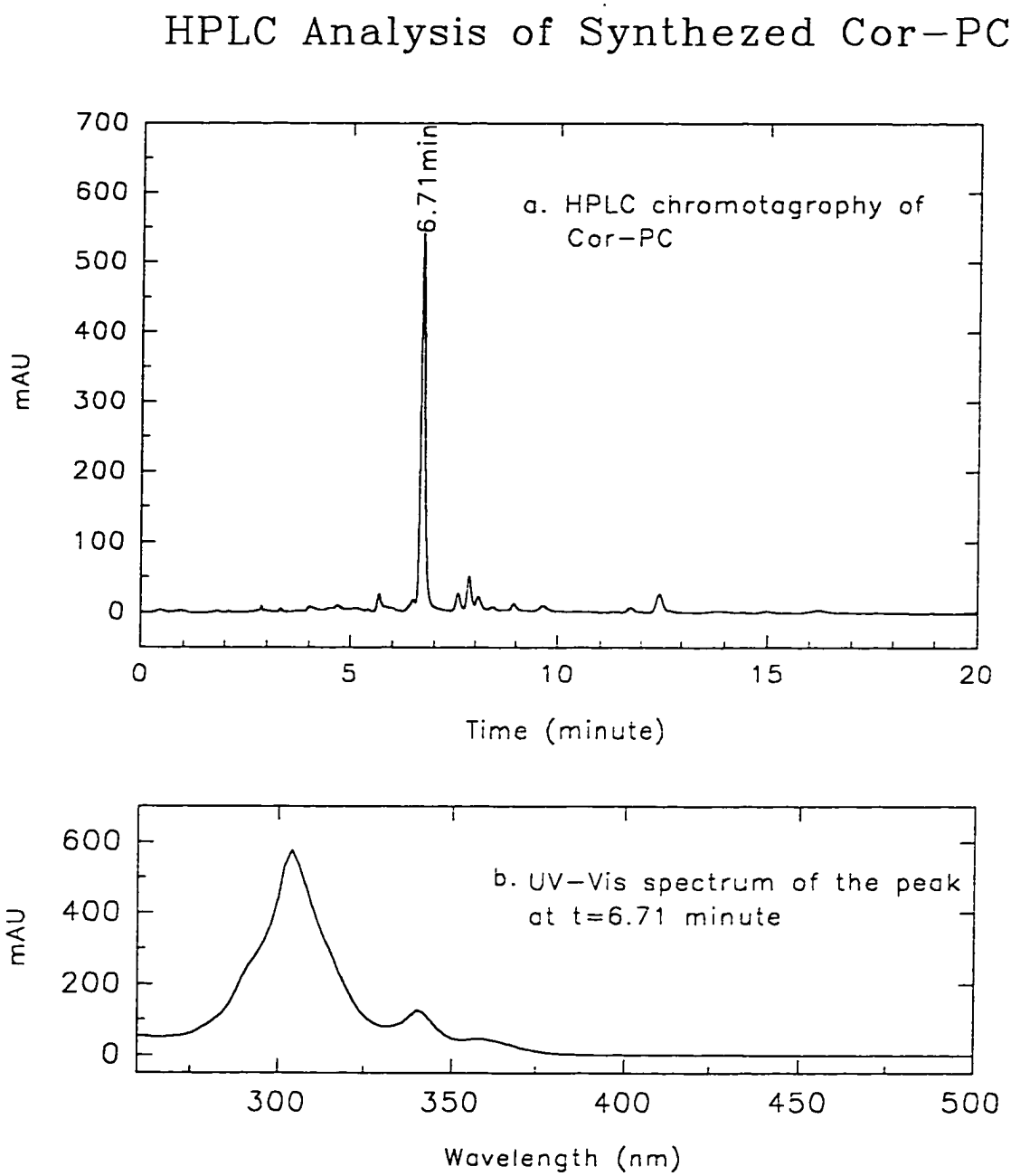

Figure 11. a). Reversed-phase HPLC analysis of synthesized Cor-PC using a C-18 column. The absorbance of the eluant was monitored at 308 nm. The mobile phase was acetonitrile with a flow rate of 1 mL/min. b). UV-visible absorption spectrum of the eluted Cor-PC HPLC peak.

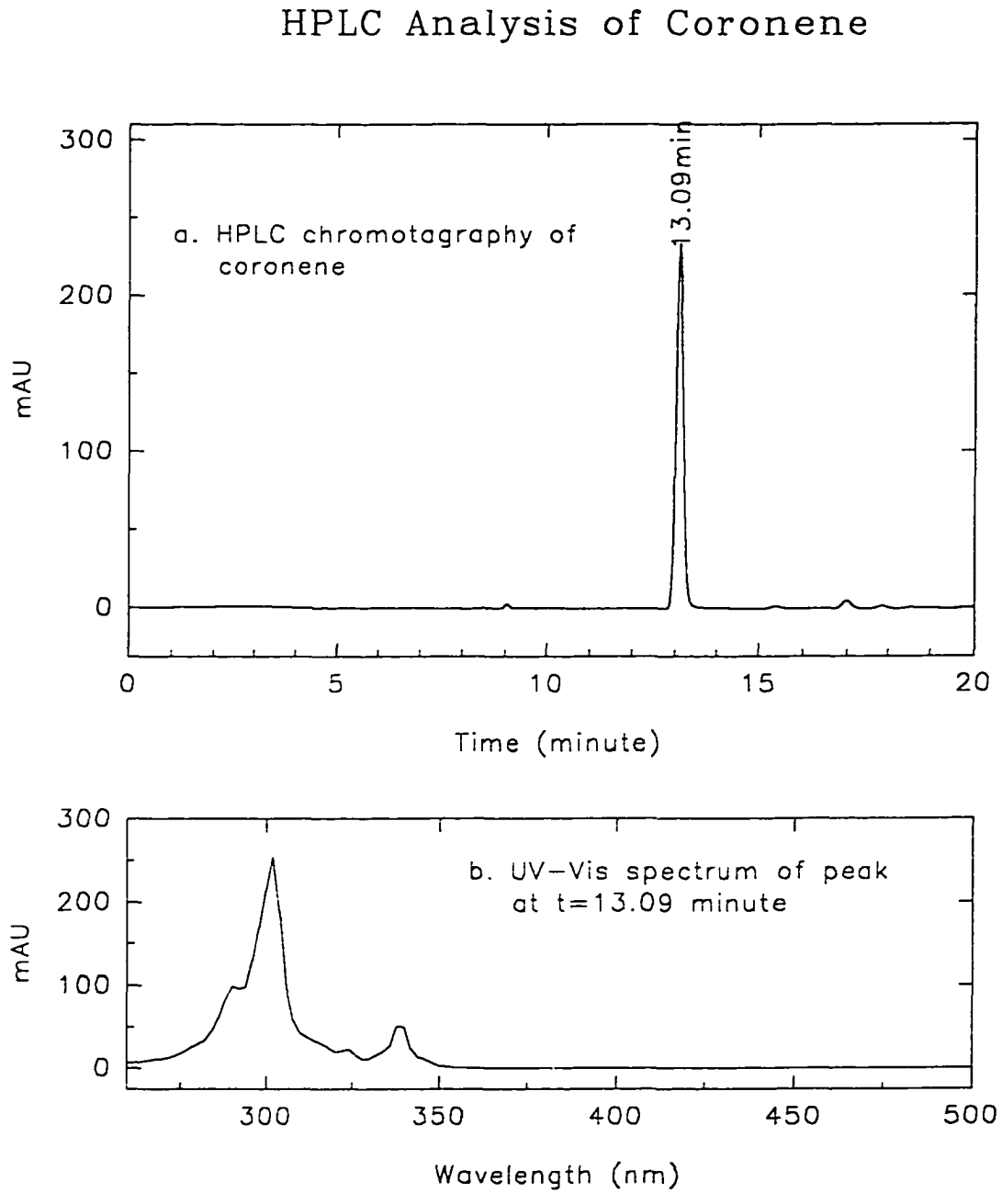

Figure 12. a). Reversed-phase HPLC analysis of coronene using a C-18 column. The absorbance of the eluant was monitored at 308 nm. The mobile phase was acetonitrile with a flow rate of 1 mL/minute. b). UV-visible absorption spectrum of the eluted coronene HPLC peak.

3.2. Spectroscopic Properties of Cor-PC and Coronene

3.2.1. Steady-State Spectral Studies

As shown (Figures 11b and 12b), the absorption properties for both Cor-PC and coronene are similar, revealing two strong absorption bands. For vesicles labeled with Cor-PC these absorptions are centered at 308 nm (strong, $S_0 \rightarrow S_3$ allowed transition) and 344 nm (less strong, $S_0 \rightarrow S_2$ forbidden transition) [70]. For coronene labeled DMPC SUVs, the absorption bands are located at 306 nm and 342 nm (Figures 11b and 12b, respectively).

Steady-state fluorescence excitation and emission spectra for Cor-PC and coronene embedded within DMPC SUVs are shown in Figures 13 and 14, respectively. While the fluorescence excitation spectra for coronene and Cor-PC are identical (and correspond to their absorption spectra), the vibrational peaks of the fluorescence emission spectra are significantly different, although both probes demonstrate fluorescence emission maxima at 448 nm. The vibrational structure of the emission spectrum for coronene is better resolved than for Cor-PC. This result is perhaps not surprising in light of the reduced symmetry (C_s) of the coronene moiety of Cor-PC after conjugation with phosphatidylcholine compared to 'free' coronene (D_{6h}). The symmetry difference between the two chromophores leads to different selection rules governing the vibrational transitions resulting in the observed differing emission spectral features of the coronene and Cor-PC fluorescence spectra.

Due to the high symmetrical nature of coronene, the lowest electronic transition from the singlet ground state to the first singlet excited state ($S_0 \rightarrow S_1$) is forbidden [70]. The strong absorption bands observed at 308 nm for Cor-PC, and 306 nm for coronene originate from the singlet ground state to the third singlet excited state ($S_0 \rightarrow S_3$) electronic transition,

whereas the absorption bands at 344 nm for Cor-PC and 342 nm for coronene, may be assigned to the $S_0 \rightarrow S_1$ electronic transition [70]. The fluorescence signal traditionally originates from deactivation of the first singlet excited state to the singlet ground state ($S_1 \rightarrow S_0$) coupled with different vibrational modes. However, for coronene, the electronic transition ($S_1 \rightarrow S_0$) is symmetry-forbidden and only allowed through vibronic coupling [69]. Hence, the (0, 0) band of the $S_1 \rightarrow S_0$ electronic transition is not detected directly from measurement of the fluorescence spectra observed for Cor-PC and coronene. As a consequence, the excitation and emission bands of Cor-PC and coronene originate from different electronic transitions coupled with vibrational transitions, resulting in non mirror imaging of these spectra.

As the symmetry of the coronene molecule is broken for the Cor-PC molecule, as shown by the vibrational peaks of the fluorescence emission spectrum, we may expect that parameters describing the rotational motions of Cor-PC will also be altered compared with 'free' coronene. These differences can provide interesting and new information about the structure and dynamics of membrane lipids.

3.2.2. Steady-State Emission Anisotropy Studies

Steady state emission anisotropies (<r>) were measured at 4°C as a function of excitation wavelength (λ_{exn}=448 nm) for Cor-PC embedded both within reference isotropic solvents (ethylene glycol and paraffin oil) and in a 'gel-phase' DMPC SUV preparation (Figure 15). Under these conditions (high viscosity and/or low temperature), it is expected that the rotational behavior of the coronenyl probe will be relatively hindered. In the wavelength range 295 to 360nm, the principal polarization data (Figure 15) reveal that for

Cor-PC, as previously observed for coronene [87], the emission anisotropy is relatively insensitive to excitation wavelength. The low emission anisotropy values for Cor-PC are not unexpected, since this probe in these solvents is not completely rotationally immobile, but does experience restricted rotational motions, with the effect being the greatest for Cor-PC in DMPC/SUV bilayers, below the gel-fluid transition temperature (T_c=23°C). For coronene, because of the high symmetry of the probe, in combination with its long fluorescence lifetime, the absorption and emission dipoles for $S_0 \rightarrow S_2$, $S_0 \rightarrow S_3$ and $S_1 \rightarrow S_0$ transitions are averaged over the surface of the planar disc. As a result, a theoretical value for the limiting anisotropy (r_0) of 0.1 is expected (see Figure 5 and Equation 9). For Cor-PC, it is expected that the limiting anisotropy value will be greater than 0.1 as the fluorophore is now anchored to a phospholipid molecule giving rise to both in- and out-of-plane probe rotations. In-plane depolarizing rotations may originate from a swinging pendulum effect and from local rotations around the anchoring terminal methylene group of the lipid acyl chain. Similarly out-of-plane probe depolarizing motions can originate from rotations around the same two anchoring points. Similar restricted in-plane and out-of-plane rotational motions have previously been reported for anthroyloxy phospholipid adducts [88].

Steady state emission anisotropy values were measured for Cor-PC in ethylene glycol, paraffin oil, and when embedded within DMPC SUVs for the temperature range 4-40°C using fixed excitation and emission wavelength conditions (Figure 16b). Any background signals arising from the 'solvent' (contributing less than 2% to the polarized fluorescence components of the emission) were subtracted. At 25°C, the viscosity for ethylene glycol is about 17.0 cp, whereas paraffin oil is more viscous (155 cp at 25°C) [89]. As expected,

higher <r> values for Cor-PC were observed when embedded within the more viscous paraffin oil, providing a more restricted rotational environment for the fluorophore. For both isotropic solvents studied, the emission anisotropy decreases with increasing temperature and reduced solvent viscosity.

The rotational sensitivity of Cor-PC to the surrounding viscosity of its immediate environment, may be used to estimate the apparent 'microviscosity' of lipid bilayer systems. Plots of emission anisotropy values for Cor-PC as a function of the solvent macroviscosity (in centipoise) for isotropic solvents suggest a correlation (Figure 16a). Using the approach previously discussed by Schinitzky *et. al.* [90], the <r> value for Cor-PC embedded within phospholipid vesicles may now be converted using this calibration emission anisotropy-viscosity plot, and interpreted in terms of a 'microviscosity' for the hydrocarbon interior of the bilayer. At 25°C, we see that the <r> value for Cor-PC in paraffin oil and DMPC SUVs are similar, suggesting that the local viscosity of Cor-PC in bilayers is comparable with this isotropic solvent (155 cp) at this temperature. The validity of these determinations has been the subject of a great many studies [11, 62]. Since the bilayer is an anisotropic or heterogeneous solvent, comparison of viscosities using isotropic solvents is not strictly valid. However, measurement of the so-called 'membrane microviscosity' has been a useful parameter for clinical and/or comparative studies [91]. Additionally, Cor-PC has the advantage that it maybe used as a fluorescence probe for determination of bilayer microviscosity at a precise location within the bilayer.

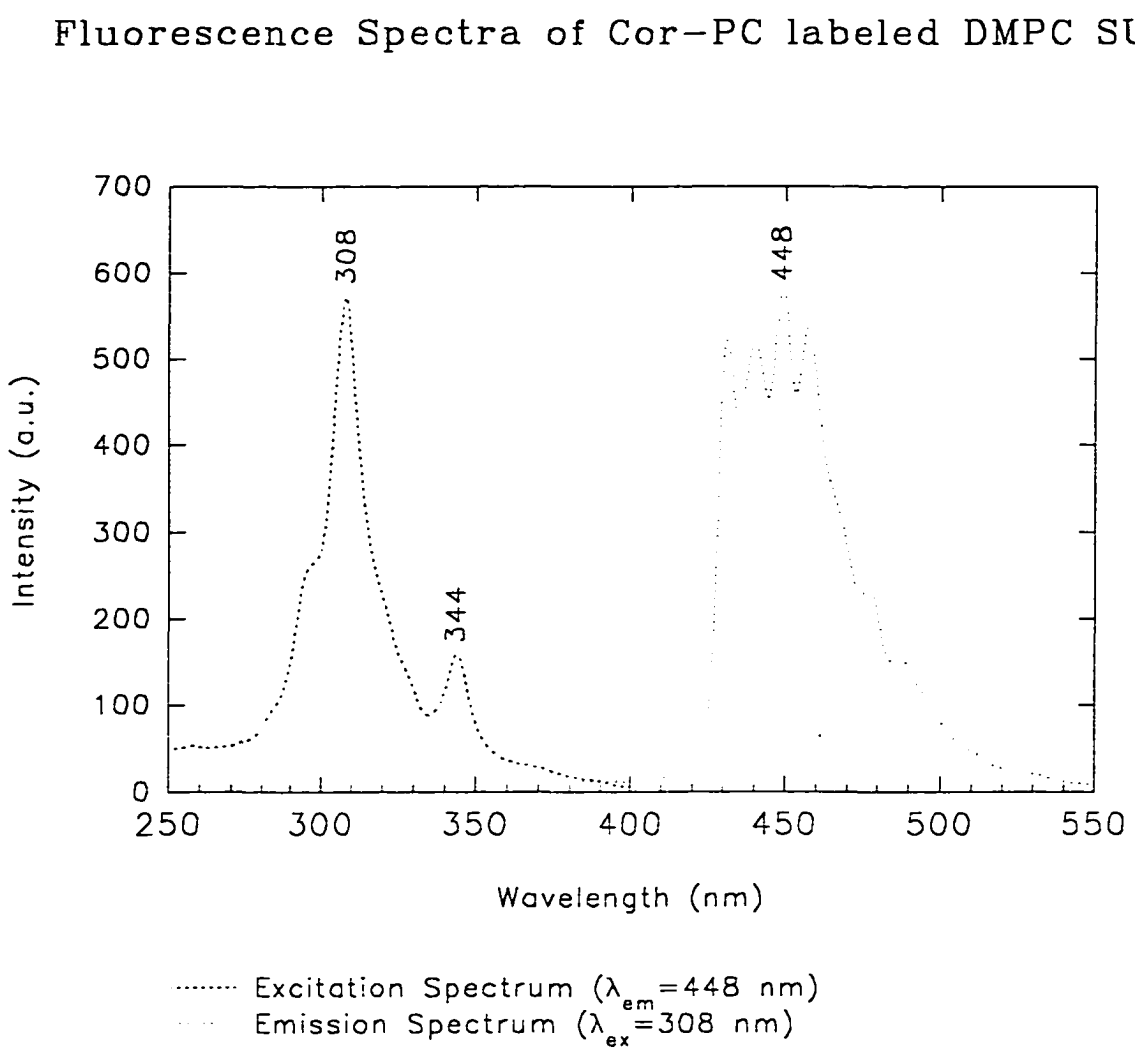

Figure 13. Fluorescence excitation and emission spectra of Cor-PC labeled DMPC SUVs. Excitation and emission wavelength: 308 nm and 448 nm. T = 14°C

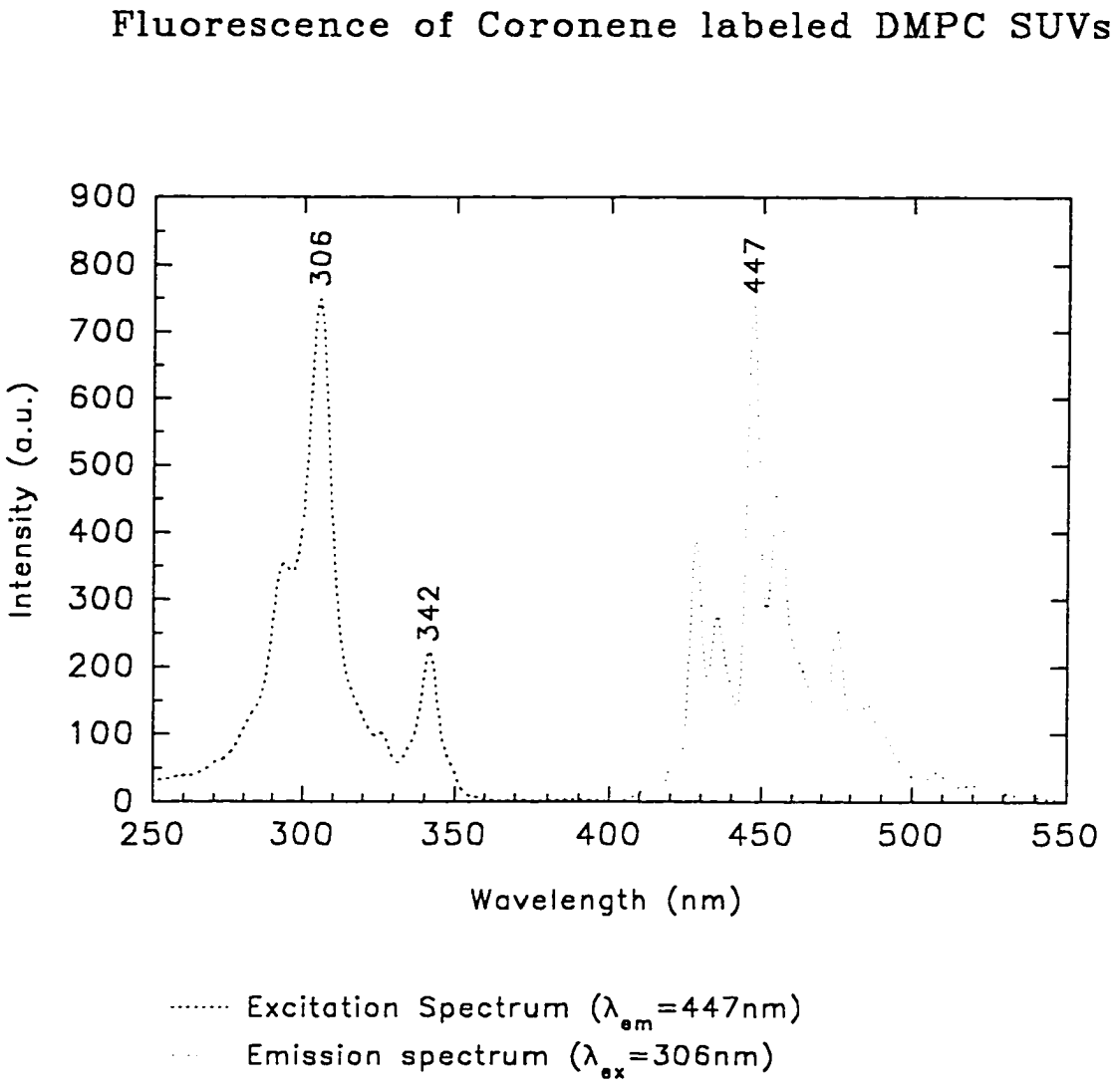

Figure 14. Fluorescence excitation and emission spectra of coronene labeled DMPC SUVs. Excitation and emission wavelength: 308 nm and 448 nm. T = 14°C

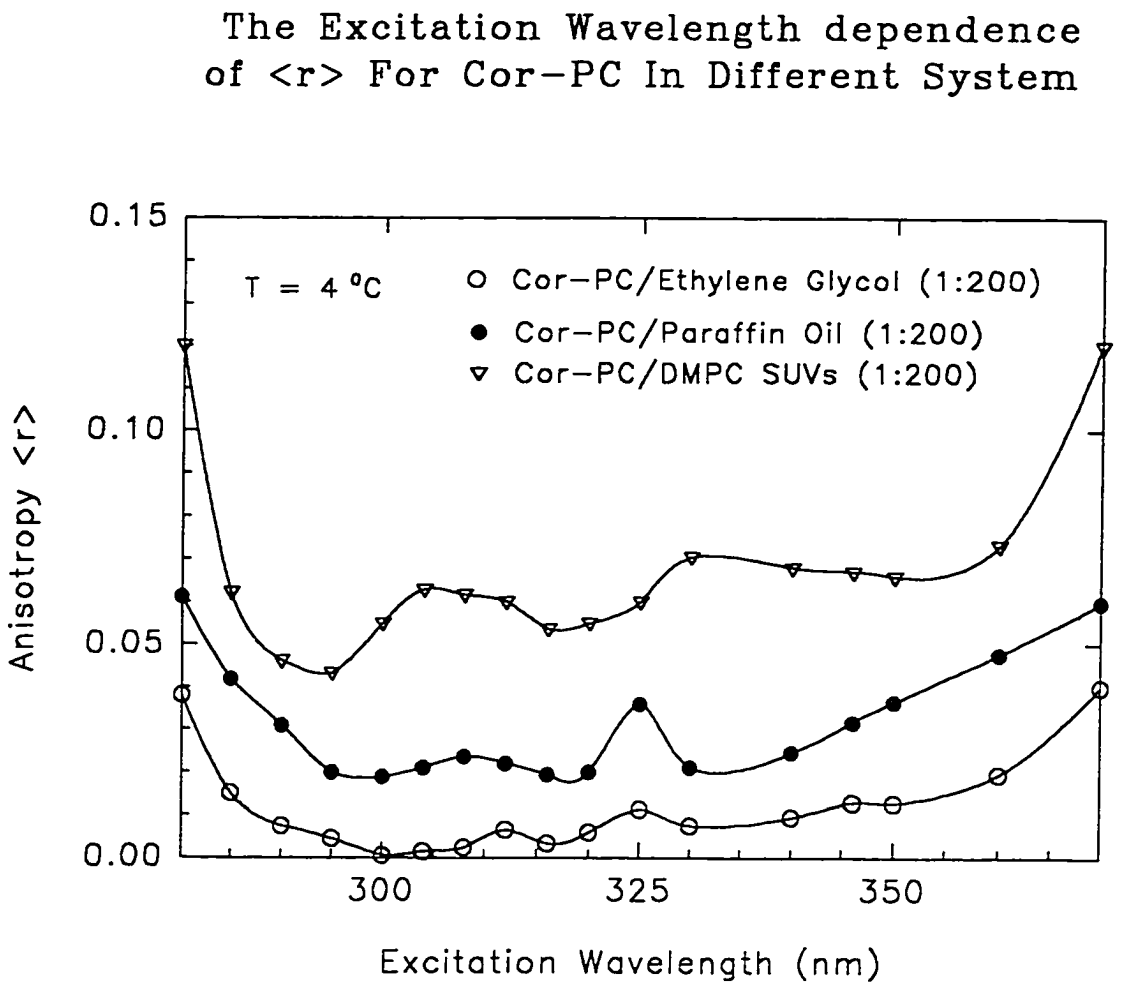

Figure 15. Dependence of the steady-state emission anisotropy (<r>) for Cor-PC in different solvents and DMPC phospholipid vesicles, on the excitation wavelength. The emission wavelength was 448 nm and the temperature was 4°C.

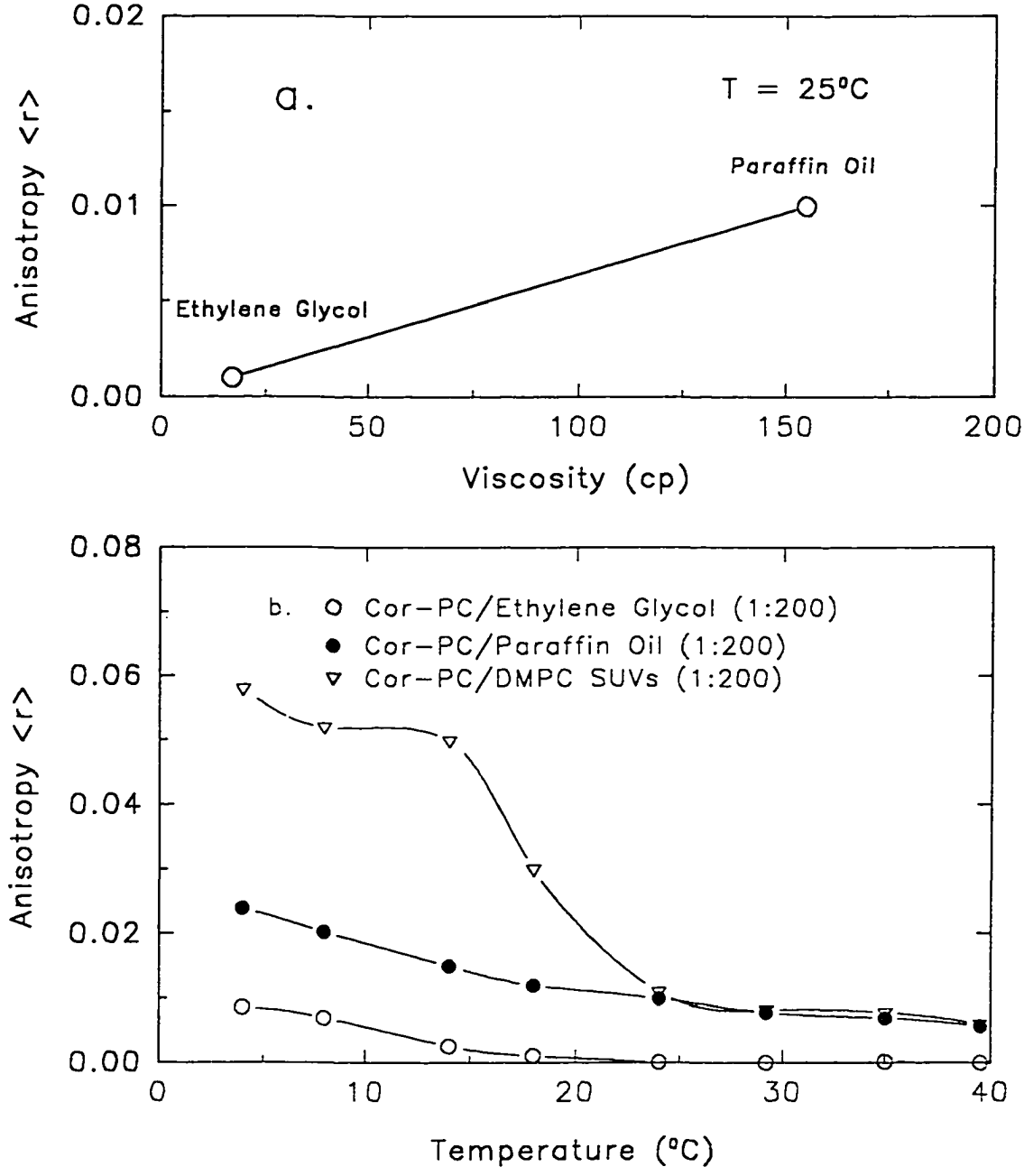

Figure 16. (a). The temperature dependence of the steady-state emission anisotropy (<r>) for Cor-PC in different isotropic solvent systems and DMPC phospholipid vesicles. The excitation wavelength used was 308 nm with an emission wavelength of 448 nm; (b). Relationship of the emission anisotropy (<r>) for Cor-PC on solvent macroviscosity.

3.2.3 Time-Resolved Fluorescence Studies in Paraffin Oil

Fluorescence lifetime decays for Cor-PC probe in paraffin oil were collected at 15 and 20°C. Paraffin oil was chosen as the solvent because although isotropic in nature, previous studies suggest that its macroviscosity is close to that of the lipid bilayer (see above), and as a consequence, serves as a model solvent for bilayer studies. Time-resolved data were analyzed using a Marquardt non-linear least squares fitting procedure as described in the Methods section 2.6. For both temperatures investigated the lifetime decay profiles were complex and best described using a multiexponential decay function with three fluorescence lifetime components (τ_i):

$$I(t) = \alpha_1 \cdot e^{-\frac{t}{\tau_1}} + \alpha_2 \cdot e^{-\frac{t}{\tau_2}} + \alpha_3 \cdot e^{-\frac{t}{\tau_3}} \qquad (43)$$

The results for the analyses of the fluorescence decays of Cor-PC in paraffin oil at each temperature are summarized in Table 1. Examination of the data shows that the fluorescence lifetime decay is dominated by a long-lived component (~80%). A lifetime centered around 20 ns contributes around 8.7% of the signal. The short component (1.6 ns) contributes around 9% to the decay. This short component may not be attributed to scattering of the excitation light by the sample, and reflects a true fluorescence component. With increasing temperature, a small quenching (~5%) of both the short and long lifetime components is observed, while the medium lifetime component appears relatively insensitive to the temperature change. Lifetime quenching may arise from thermal effects or altered oxygen permeability, correlated with decreased viscosity values, resulting in oxygen

quenching effects. In any event, the short and long-lived fluorescence components appear to demonstrate some sensitivity to the physical state of the solvent, although their contribution to the decay remain constant.

Origins for the multiexponential fluorescence decay of Cor-PC in paraffin oil are unclear. However, other fluorescence membrane probes, such as DPH and perylene in paraffin oil also demonstrate multiexponentiality.

The average fluorescence lifetime ($<\tau>$) for Cor-PC in paraffin oil may be defined as:

$$<\tau> = \frac{\sum_i \alpha_i \cdot \tau_i^2}{\sum_i \alpha_i \cdot \tau_i} \qquad (44)$$

As reported in Table 1, $<\tau>$ values confirm that Cor-PC provides a long-lived fluorescence probe.

Table 1

Summary of Fluorescence Lifetime Parameters for

Cor-PC in Paraffin Oil (0.0250mM) as a Function of Temperature.

(Excitation wavelength = 340nm; Emission wavelength = 448nm)

T (°C)	α_1 (f_1)[2]	τ_1 (ns)	α_2 (f_2)	τ_2 (ns)	α_3 (f_3)	τ_3 (ns)	$<\tau>$[1] (ns)	χ^2
15	0.3475 (0.03)	1.64	0.0818 (0.09)	20.37	0.1431 (0.88)	117.64	105.7	1.532
20	0.3605 (0.03)	1.56	0.0800 (0.09)	20.12	0.1453 (0.88)	111.99	100.6	1.599

[1]The average lifetime value, $<\tau>$, was determined according to Equation (44).

[2]The fractional fluorescence contribution (f_i) of each lifetime to the total intensity is defined as $f_i = \alpha_i\tau_i/\Sigma_i\alpha_i\tau_i$, where $\Sigma_i\alpha_i\tau_i=1$,. The values for α_i and τ_i were extracted from the fitting of the time-resolved fluorescence decay profile.

3.2.4 Time-Resolved Polarized Studies in Paraffin Oil.

Time-resolved fluorescence emission anisotropy decays for Cor-PC in paraffin oil were recorded at 15 and 20°C. Fits of rotational parameters to the data are summarized in Table 2a. The data were best resolved using two rotational correlation times, ϕ_1 and ϕ_2 according to the function:

$$r(t) = \beta_1 \cdot e^{\frac{-t}{\phi_1}} + \beta_2 \cdot e^{\frac{-t}{\phi_2}} \qquad (45)$$

In contrast to free coronene, where $r_0 = 0.1$, the limiting anisotropy for Cor-PC, $(\beta_1+\beta_2)$, is expected to be greater than 0.1 since this fluorophore represents an anisotropic rotor, exhibiting both in-plane and out-of-plane rotations as a consequence of the reduced molecular symmetry. For Cor-PC, r_0~0.2 (Table 2a). Hence Cor-PC, unlike coronene, is not a fluorescence probe of selective out-of-plane motion, but rather provides information about both in-plane and out-of-plane rotational motions of its anchored fluorophore.

In these studies, the data for Cor-PC were best analyzed using a simple biexponential rotational model, assuming that the transition dipoles lie within the plane of the coronene ring (ψ_{ac}=90°; Equation 11) and slipping boundary conditions (free diffusion about the symmetry axis, and alignment of dipoles with the principal diffusion axis). According to this model, the fast rotational correlation time (ϕ_1), reflects a combination of both in- and out-of-plane rotational motions [Equation 13; $\phi_1=1/(2D_\perp+4D_\parallel)$]. In contrast, ϕ_2 represents exclusively the slower out-of-plane rotations [$1/(6D_\perp)$] and the associated extracted preexponential term (β_2) is expected to tend towards the theoretical value of 0.1 in the absence of any rotational

depolarizing motions. In-plane rotational motions (ϕ_1) can presumably arise from both the in-plane swinging motion of the fluorophore tagged through the fatty acyl chain to the C-2 position of the phospholipid glycerol backbone, and local rotations around the anchoring methylene group as discussed above.

With increasing temperature, the rotational correlation times are expected to decrease, whereas the associated preexponential terms will remain constant. However, from Table 2a the combined in-plane and out-of-plane probe motions (ϕ_1) for Cor-PC appear to be relatively insensitive to the altered macroviscosity of the oil. Similarly, the out-of-plane rotational motions (ϕ_2) only exhibit a small enhanced rate of rotation, giving rise to the observed decreased rotational correlation times. From Equation 14, the rates of diffusion around the principal molecular axes of the molecule, $D_{\parallel}$ and $D_{\perp}$ can be determined (Table 2b). As expected, diffusion around the axis perpendicular to the excitation vector ($D_{\perp}$) increases with temperature. Interestingly, $D_{\parallel}$, while faster than $D_{\perp}$, appears to decrease with temperature. This seems physically unlikely, and most probably reflects either error in the value of the short correlation time extracted from polarized data with the experimental timing calibration (0.432ns/channel), or relative insensitivity of the in-plane rotations to the small temperature change (5°C) used in this study. The ratio of $D\parallel/D\perp$ decreases with temperature, which reflects the less hindered out-of-plane rotations for Cor-PC in paraffin oil with increasing temperature (Table 2b). The $D\parallel/D\perp$ ratio for free perylene in paraffin oil (D_{2h} symmetry) is 10:1. [62].

The preexponential terms show relative insensitivity to the temperature change, although application of global analysis methods [92], linking the preexponential terms across

the temperature isotherm, would enable better estimates of the β terms.

Table 2a.

Time Resolved Emission Anisotropy Decays for

Cor-PC in Paraffin Oil (0.025mM)

(Excitation wavelength = 340 nm; Emission wavelength = 448 nm)

T (°C)	β_1	ϕ_1 (ns)	β_2	ϕ_2 (ns)	$r_0=(\beta_1+\beta_2)$	χ^2
15.0	0.1517	1.56	0.0629	41.72	0.2146	1.268
20.0	0.1379	1.76	0.0549	32.34	0.1928	1.296

Table 2b.

Rotational Diffusion Constants for Cor-PC in Paraffin Oil (0.025mM)

(Excitation wavelength = 340 nm; Emission wavelength = 448 nm)

T (°C)	$D_\perp$ (MHz)	$D_\parallel$ (MHz)	$D_\parallel/D_\perp$
15.0	3.99	158.26	40
20.0	5.15	139.47	27

3.3. Pure Lipid Bilayer Studies

Steady-state fluorescence spectra and emission anisotropy values for DPH (a short-lived fluorescence probe; $<\tau>$ = ~10 ns), coronene and Cor-PC embedded within DMPC SUVs were measured as a function of different variables, e.g. temperature, bilayer probe labeling ratios, etc. The effect of melittin on these parameters is discussed below (Section 3.4). The location of the probes across the bilayer width was assessed using iodide quenching of the fluorescence (see Section 3.5). In general, the following studies were performed with the intention of assessing potential probe perturbation effects, and characterizing measured fluorescence signals before addition of peptide to the Cor-PC labeled DMPC SUVs.

3.3.1. Effect of Probe Labeling Ratio on Steady-State Emission Anisotropy Values

The effect of varying the Cor-PC labeling ratio on the bilayer architecture was determined by measurement of the steady-state fluorescence emission anisotropy ($<r>$) for Cor-PC as a function of the probe to lipid labeling ratio at 4 °C (Figure 17). As Cor-PC is a fluorescence probe that reports specifically on gel-phase lipid dynamics, the temperature chosen was below the reported gel-to-fluid transition (23.5 °C) [93] for DMPC SUVs. The results shown in Figure 17, reveal that the measured emission anisotropy ($<r>$) is independent of the molar labeling ratio up to as high as 1 Cor-PC molecule per 50 DMPC phospholipid molecules. This result suggests that any micro-perturbation of the DMPC bilayer architecture arising from the presence of Cor-PC under normal labeling conditions is minimal and most likely non-existent. Differential scanning calorimetry studies can only provide evidence for macro-perturbation, and were not performed. The probe to lipid labeling ratio used for all

future experiments was fixed at [DMPC]/[Cor-PC] = 100/1 or [DMPC]/[Cor-PC] = 200/1, where no significant perturbation of DMPC bilayer structure is anticipated. The measured phase transition temperature for DMPC SUVs. with different Cor-PC labeling ratio (up to Cor-PC:DMPC = 1:50) was also invariant to the labeling ratio providing further indication of minimal bilayer perturbation and unlikely preferential probe partitioning.

For studies using coronene and DPH labeled vesicles, previous studies have shown that a labeling ratio of 1:200 for coronene [94] and 1:500 for DPH [94] are nonperturbing, while still providing data with good signal to noise characteristic (Figure 17).

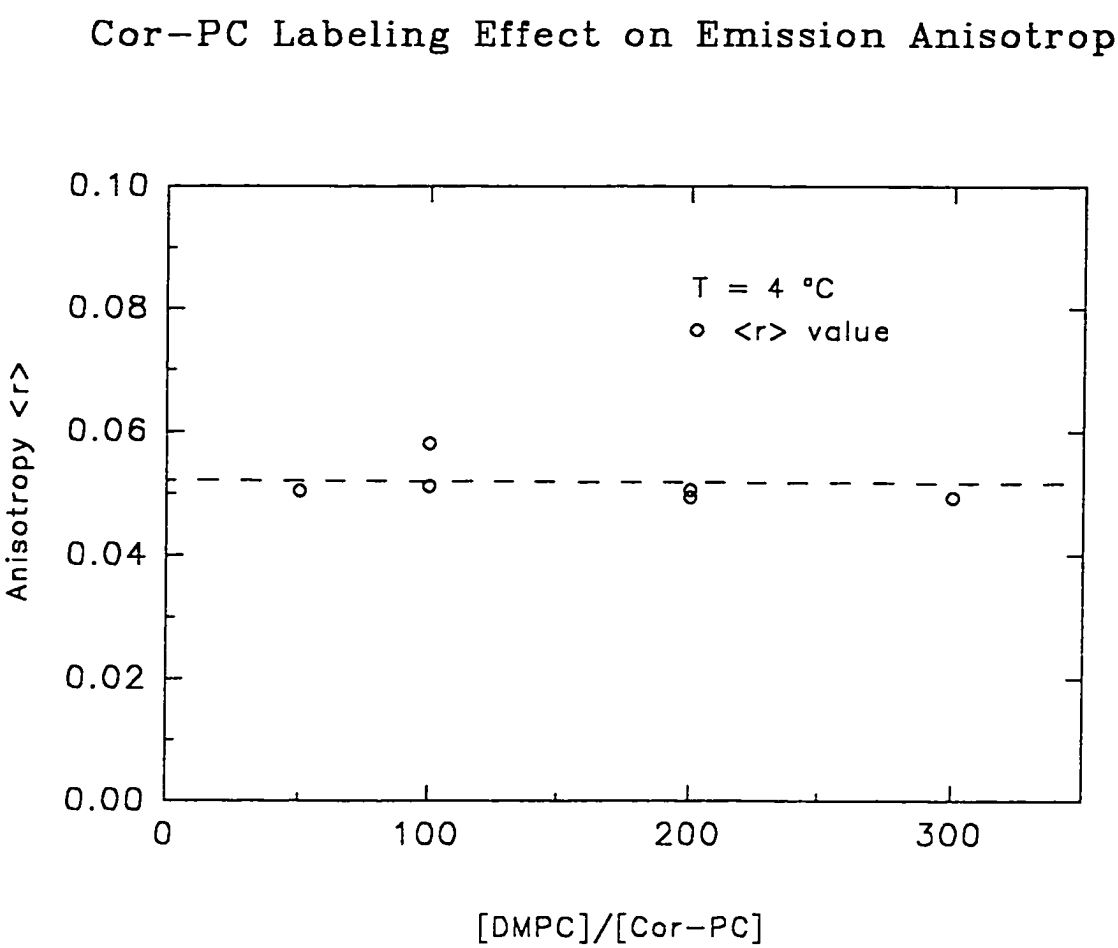

Figure 17. Effect of labeling using Cor-PC on DMPC SUVS, at 4°C. The excitation wavelength was 308 nm and the emission wavelength was 448 nm. T = 4°C

3.3.2. Emission Anisotropy versus Temperature: Lipid 'Melt' Profiles

DMPC SUVs were labeled with DPH (1:500), coronene (1:200) or Cor-PC (1:200). The steady-state fluorescence emission anisotropy (<r>) for each probe was recorded as a function of increasing temperature. For rotationally sensitive fluorescence probes, steady-state emission anisotropy values (<r>) are dramatically reduced when the surrounding lipid undergoes a phase or gel-fluid transition, giving rise to increased bilayer fluidity, or reduced membrane microviscosity [95].

Steady-state emission anisotropy values were measured for DPH (<τ>~10ns) labeled DMPC SUVs in the temperature range 5-45°C (Figure 18). As usual, any background fluorescence signal arising from an unlabeled vesicle suspension was always subtracted. A sharp discontinuity in the temperature dependence of the emission anisotropy for DPH was observed with a mid-point at about 23°C, which corresponds with the gel-to-lipid phase transition temperature (T_c) for DMPC lipid [93]. The anisotropy value for DPH is relatively high (0.3) at cold temperatures in gel phase lipid where the rotational motions of this rod-like molecule are severely hindered. In contrast, above T_c, increased rotational motion of the fluorescence probe occurs, resulting in significant depolarization and hence low <r> values (<r>=0.08) when the lipid is in the liquid-crystalline (L_α) phase. These results agree well with previously reported DPH/DMPC melt transition curves [95].

Steady-state fluorescence emission anisotropy values (<r>) were also measured as a function of temperature for coronene embedded inside DMPC SUVs. Unlike DPH, however, the phase transition curve for DMPC/SUVs as reported by the rotational motions of coronene (Figure 19) is a broader and shifted to lower temperatures. Previous studies have shown that

coronene, due to its long fluorescence lifetime (<τ>=~200ns in the gel phase) and D_{6h} planar symmetry (r_0=0.1), is a probe sensitive to long-lived out-of-plane rotational motions (<r_{op}>) exclusively. In DMPC gel-phase SUVs, the emission anisotropy value for coronene is about 0.06 (approaching the theoretical value of 0.1), and 0.005 in the liquid crystalline state. However, as has been discussed previously for coronene labeled DPPC SUVs, this broadening and shift to lower temperatures (apparent T_c is around 19°C) of the melt profile reflects the influence of submicrosecond lipid dynamics or slow lipid relaxations occurring within the gel phase well below the normally reported T_c for the phospholipid [96] on the rotational motions of Cor-PC, and not preferential partitioning of the probe into gel phase lipid (partition coefficient for coronene, K_P^{gf}=1). Broad and low temperature shifted 'melt' curves have been observed for other long-lived fluorescence probes [96]. Short-lived fluorescence probes, such as DPH, are not sensitive to such submicrosecond lipid dynamics occurring prior to the main gel-fluid phase transition. Consequently, the lipid 'melt' profile is well defined, and reflects the main pseudo first order [28] gel-fluid lipid phase transition (given that K_p^{gf}=1 for DPH).

In the case of Cor-PC, the rotational motions of this probe are influenced by both in-plane and out-of-plane rotational motions. Hence a limiting value of r_0=0.1 at temperatures below the lipid phase transition for Cor-PC labeled SUVs is not expected. The steady-state emission anisotropy data for Cor-PC, measured as a function of temperature (Figure 20) revealed in analogy with coronene the characteristic broad and shifted 'melt' profiles observed previously for a long-lived fluorescence probes demonstrating rotational sensitivity to gel-phase submicrosecond lipid dynamics or slow lipid relaxations occurring within the

submicrosecond 'time window' and well below T_c. For Cor-PC the average fluorescence lifetime is around 120ns (see section 3.7.1 for a complete discussion). In the gel phase the observed emission anisotropy for Cor-PC is about 0.055-0.06, similar to values recorded for coronene. However, this average <r> value represents both restricted in-plane and out-of-plane rotational motions (see below, Section 3.7.2). As expected, above T_c the observed experimental <r> value is low (0.002) where the phospholipid bilayer is essentially isotropic in character, and hindrance to the rotational motions of Cor-PC thus arises exclusively from the effect of anchoring the probe to an integral membrane lipid component.

The use of long-lived fluorescence probes for studying membrane lipid dynamics presents some unique challenges. Rotational depolarization effects for probes with long lifetimes may arise not only from the melting of lipid surrounding the probe, but from more general effects such as global rotation of the SUV during the lifetime of the probe, and/or lipid lateral diffusion effects. These important artifacts have been discussed fully for coronene [96] and it was concluded that anisotropy values were not contaminated by these secondary effects in this case. In analogy with the arguments proposed for coronene, the effect of lateral diffusion on the rotational motions of Cor-PC are not expected to influence the measured emission anisotropy values. However, to examine the effect of whole vesicle rotations on <r> values measured for Cor-PC, DMPC large unilamellar vesicles (LUVs) were prepared and labeled using Cor-PC. Since the diameter for the LUVs used here was 1000Å, the effect of vesicle size on the measured lipid 'melt' profile as reported by Cor-PC may be estimated. Steady-state emission anisotropy values for Cor-PC labeled DMPC LUVs measured as a function of increasing temperature are also shown in Figure 20. Clearly the phase transition

curve measured using DMPC LUVs shows the same shift and broadening to that of DMPC SUVs. Hence steady-state <r> values for Cor-PC labeled vesicles appear not to be contaminated by whole vesicle rotation.

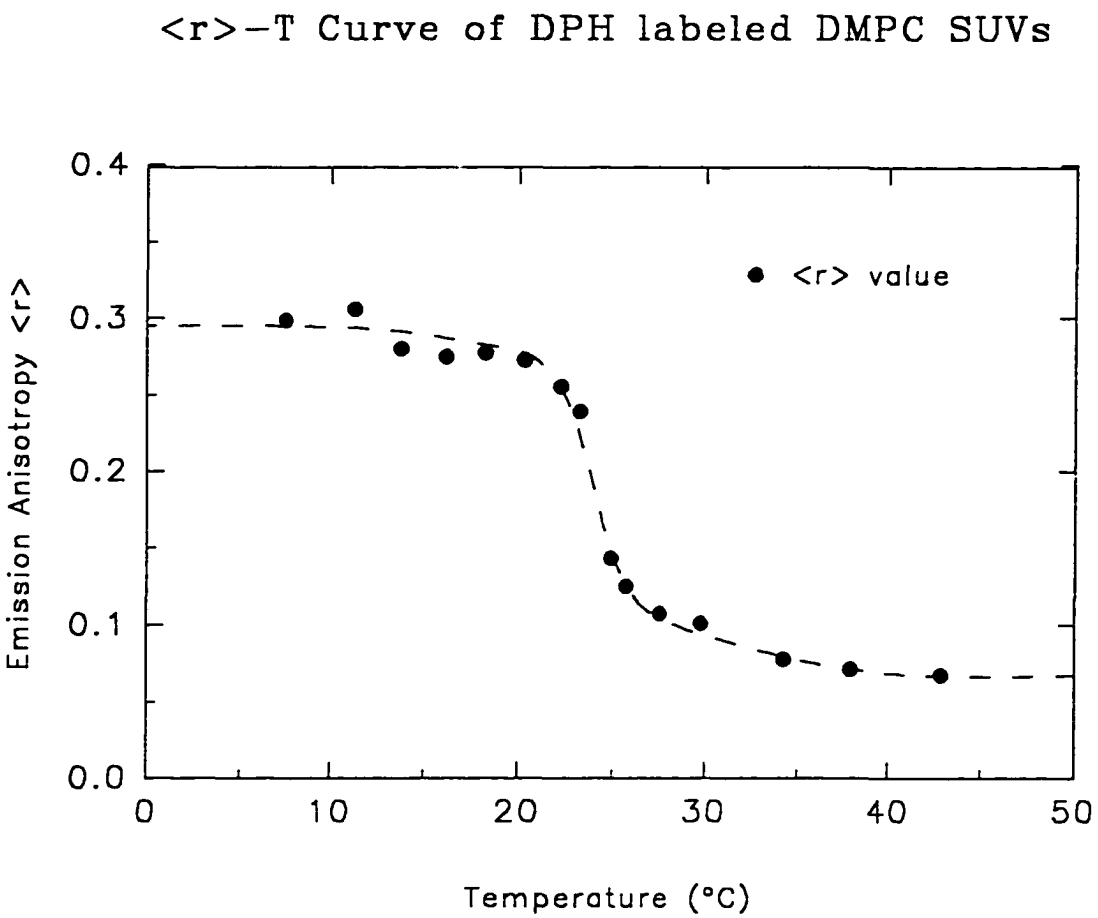

Figure 18. Steady-state emission anisotropy (<r>) for DPH labeled DMPC SUVs as a function of increasing temperature. The DPH to DMPC labeling ratio employed was 1:500. The excitation and emission wavelengths used were 355 nm and 430 nm, respectively.

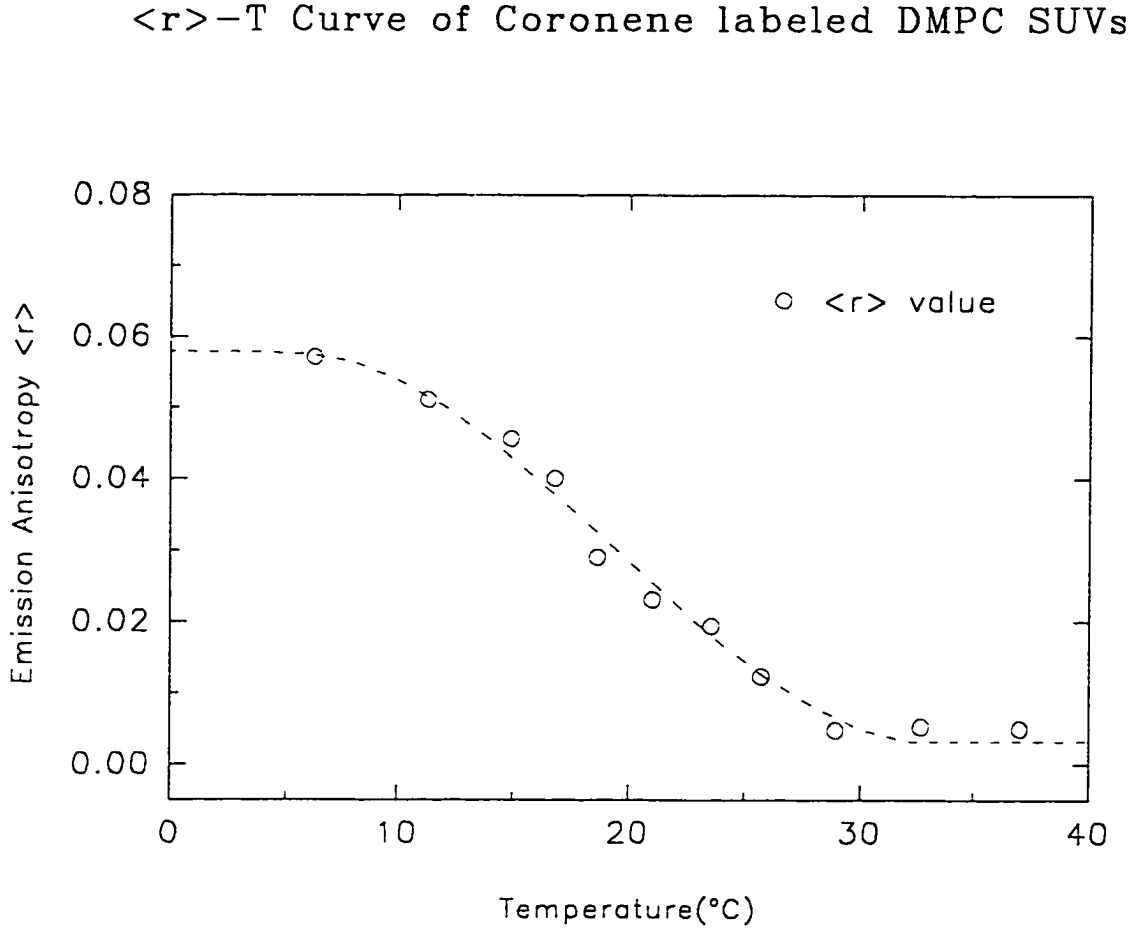

Figure 19. Steady-state emission anisotropy (<r>) for coronene labeled DMPC SUVs as a function of increasing temperature. The coronene to DMPC labeling ratio employed was 1:200. The excitation and emission wavelengths used were 306 nm and 447 nm, respectively.

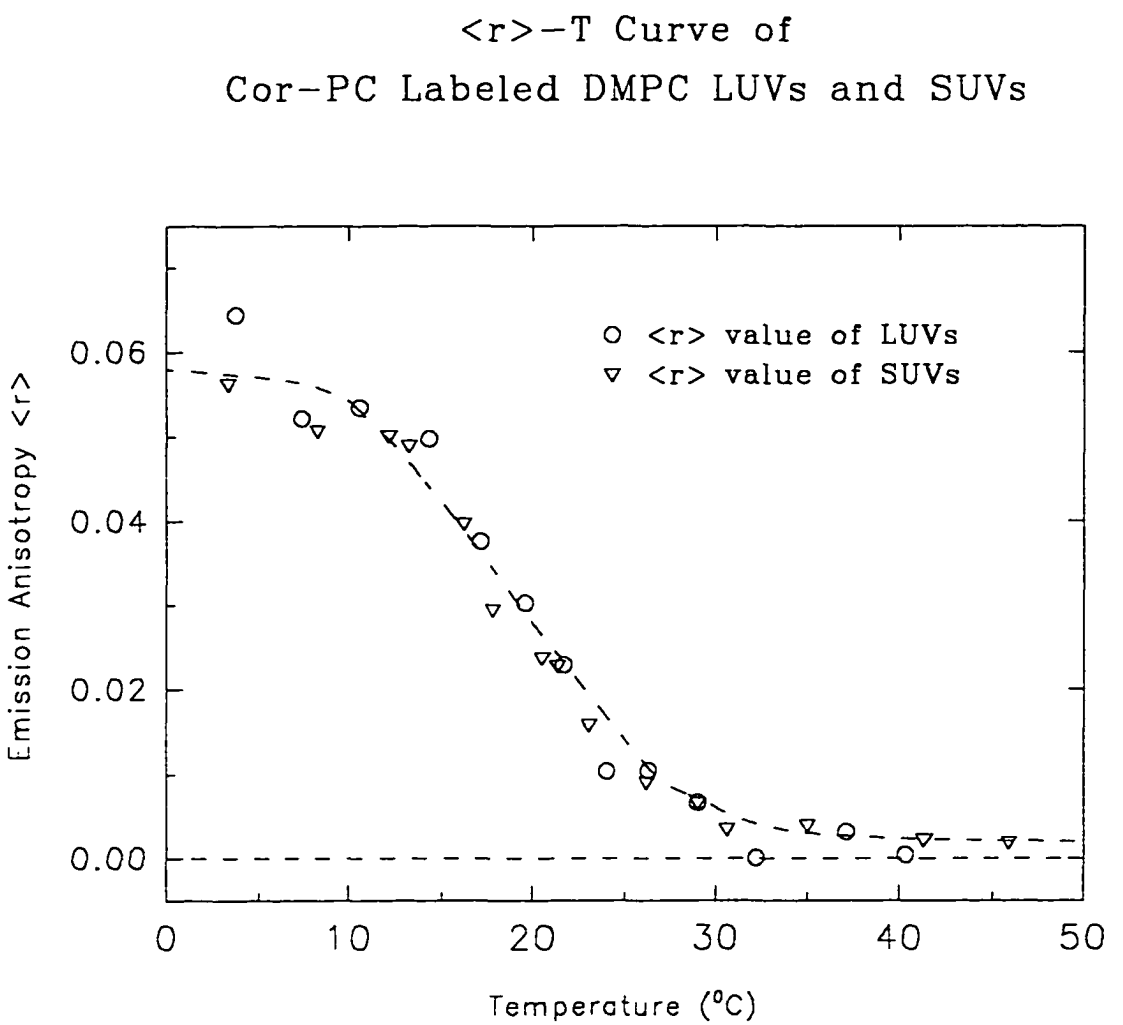

Figure 20. Steady-state emission anisotropy (<r>) for Cor-PC labeled DMPC SUVs and LUVs as a function of increasing temperature. The Cor-PC to DMPC labeling ratio employed was 1:200. The excitation and emission wavelengths used were 308 nm and 448 nm, respectively.

3.4. Effects of Melittin on Submicrosecond Lipid Dynamics

3.4.1. Titration of Fluorescently Labeled DMPC SUVs with Melittin

The effect of melittin on lipid packing in the gel phase of DMPC SUVs was examined by measuring the emission anisotropy as a function of melittin concentration (up to 2 mole%), for DPH, coronene and Cor-PC labeled samples. Of relevance to these studies is the effect of melittin on the emission spectra of the fluorescently labeled vesicles. Since the fluorescence intensity (I) is proportional to the fluorescence lifetime [$I(t)=\alpha_i e^{-t/\tau_i}$], reduced fluorescence intensities of the probes on addition of melittin may arise from lifetime quenching, which can weight emission anisotropy values to artificially higher values. For all the fluorescence probes examined, no shift of emission spectra or decreased fluorescence intensity was observed, suggesting that quenching (either dynamic or static mechanisms) appears not to influence the measured <r> values described here.

Steady-state emission anisotropy values were measured as a function of increasing melittin to lipid molar ratio for gel-phase DMPC SUVs labeled with DPH, coronene and Cor-PC probes at 14°C, respectively. The results of the peptide titration are summarized in Figures 21, 22 and 23.

Figure 21 shows the dependence of the emission anisotropy determined for DPH labeled DMPC/SUVs with varying melittin concentration. The emission anisotropy (<r>) values appear relatively insensitive to the presence of increasing peptide to phospholipid molar ratio (in the range MLT/DMPC = 0 to 1:30). Thus within the nanosecond time window, melittin appears to demonstrate little or no effect on the steady state rotational properties of DPH residing within the ordered gel phase of the bilayer. As a consequence of the relatively

short average fluorescence lifetime for DPH in bilayers (~10 ns) this probe does not provide sensitivity to any possible effects of melittin on gel-phase lipid dynamic events occurring on a slower time-scale (submicrosecond).

In contrast, when coronene labeled gel phase DMPC SUVs are titrated with melittin (MLT:DMPC = 1:10), the steady-state emission anisotropy ($<r>_{op}$) of the probe is increased slightly (22%; Figure 22), suggesting decreased out-of-plane rotational motions. While coronene provides sensitivity to effects on submicrosecond lipid dynamics, the rather weak response to the presence of melittin may arise from the position of the fluorophore within the acyl chain region of the bilayer. Since this probe is free to distribute within the acyl chain region of the membrane, it may be expected that on addition of melittin, if the bilayer is consequently made more rigid resulting in reduction of the free bilayer volume, then coronene may change its location and preferentially orient itself away from the more ordering effects imposed by the peptide. Thus the average emission anisotropy that is measured reflects a narrower probe distribution centered more towards the mid-plane of the bilayer, with only a slight weighting of the signal toward those probes residing in the area of the peptide. Altered probe distributions, in response to the physical state of the bilayer, have previously been described for both DPH and perylene [97]. At very high concentrations of melittin, with increased ordering of the bilayer, arising from decreased gel-fluid fluctuations, the possibility of potential probe aggregation will increase, enhancing the likelihood of homotransfer between neighboring probe molecules. Hence this artifact must be considered as a possible explanation for the increased emission anisotropy values. However, for coronene, probe aggregation can be clearly detected from examination of the red edge of the emission

spectrum. Aggregates appear as a broad featureless emission band around 610 nm. No evidence of this spectral signature was observed in these studies and probe aggregation was excluded.

For Cor-PC embedded within the lipid bilayer (1:200), titration with increasing concentrations of melittin revealed dramatic increases in the measured emission anisotropy (Figure 23), with melittin/DMPC molar rations higher than 1:200. If the number of phospholipids per SUV are about 2,500 [6], then the labeling ratios discussed here correspond to 12-13 molecules each of Cor-PC and melittin per vesicle.

For Cor-PC, the fluorophore location within the bilayer may be estimated (see Figure 24), and hence the emission anisotropy of this probe provides sensitivity not only to the effects of melittin on submicrosecond lipid dynamics but also provides information regarding the localization of these effects. The increasing emission anisotropy values with the increasing melittin content in the lipid bilayer suggests an ordering effect of the peptide on lipid packing, which is detected only on the submicrosecond time scale. Presumably both in-plane and out-of-plane rotational motions are affected, although perhaps to different extents.

In summary, we see that two factors are important when considering peptide effects on bilayer architecture: a) the location of the probe molecules within the lipid bilayer, and, b) the fluorescence lifetime of the probe molecule employed. Both factors strongly influence the overall final interpretations. Fluorescence membrane probes with lifetimes of several tens of nanoseconds can provide new insights into the previously unexplored and biologically relevant submicrosecond time window of lipid dynamic events. The position of the reporter fluorophore is an important consideration also. As previously shown using nanosecond lipid-

adduct probes, the relative depth of the fluorophore in the bilayer provides sensitivity to effects at more defined locations across the bilayer width [71]. In the case of Cor-PC, the fluorophore is fixed within the acyl chain region of the bilayer, and consequently may reflect a greater sensitivity to the effects of melittin on this area of the bilayer architecture. Indeed, at 20 °C, the bilayer thickness of DMPC lipid membrane is about 54.9 Å and the thickness of polar region (i.e. head group plus glycerol region) of DMPC lipid bilayer is about 10.4 Å [93]. Based on the structure of Cor-PC (see earlier), we estimate that the chromophore of Cor-PC is located at a depth of 11-12 Å from the bilayer surface (Figure 24).

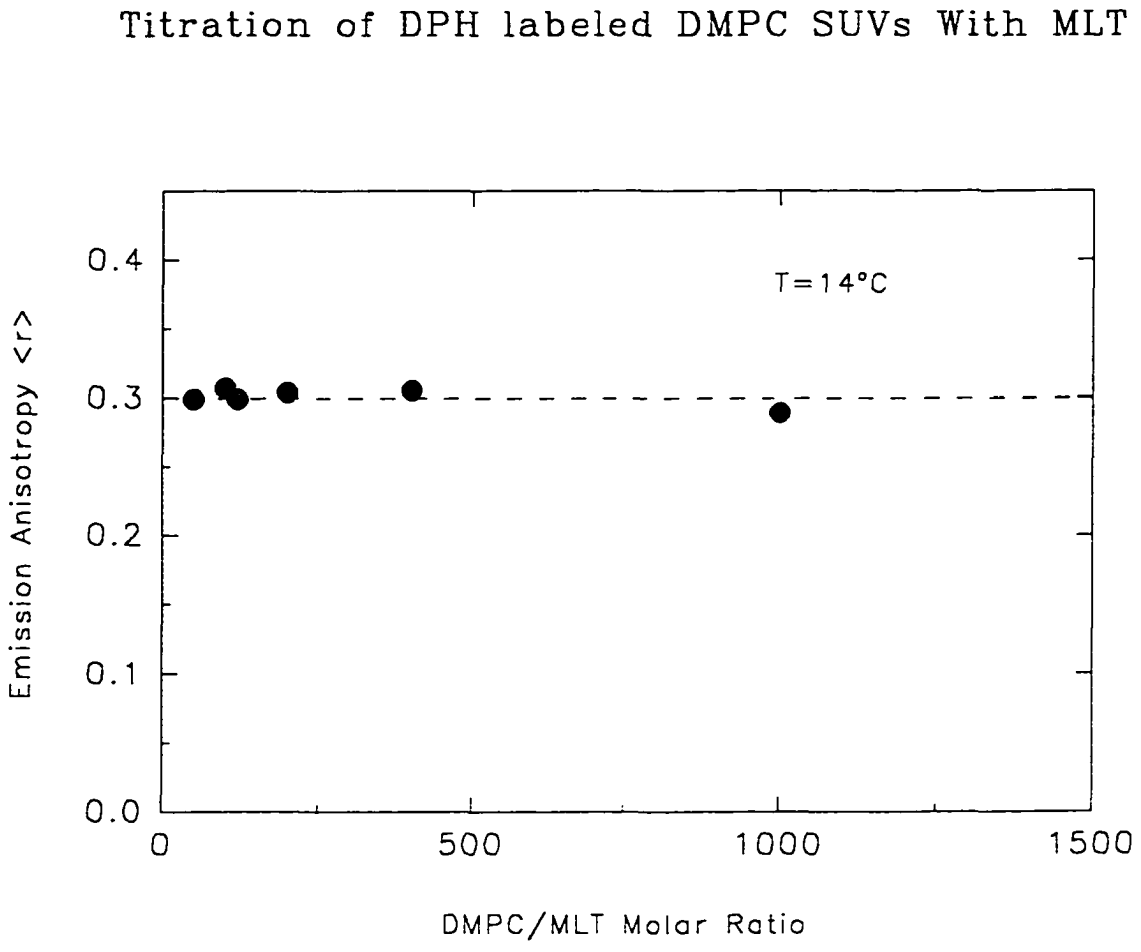

Figure 21. Steady state emission anisotropy for DPH labeled DMPC SUVs as a function of increasing melittin concentration. The excitation and emission wavelengths were 355 nm and 430 nm, respectively. The molar labeling ratio employed was DMPC:DPH = 500:1.

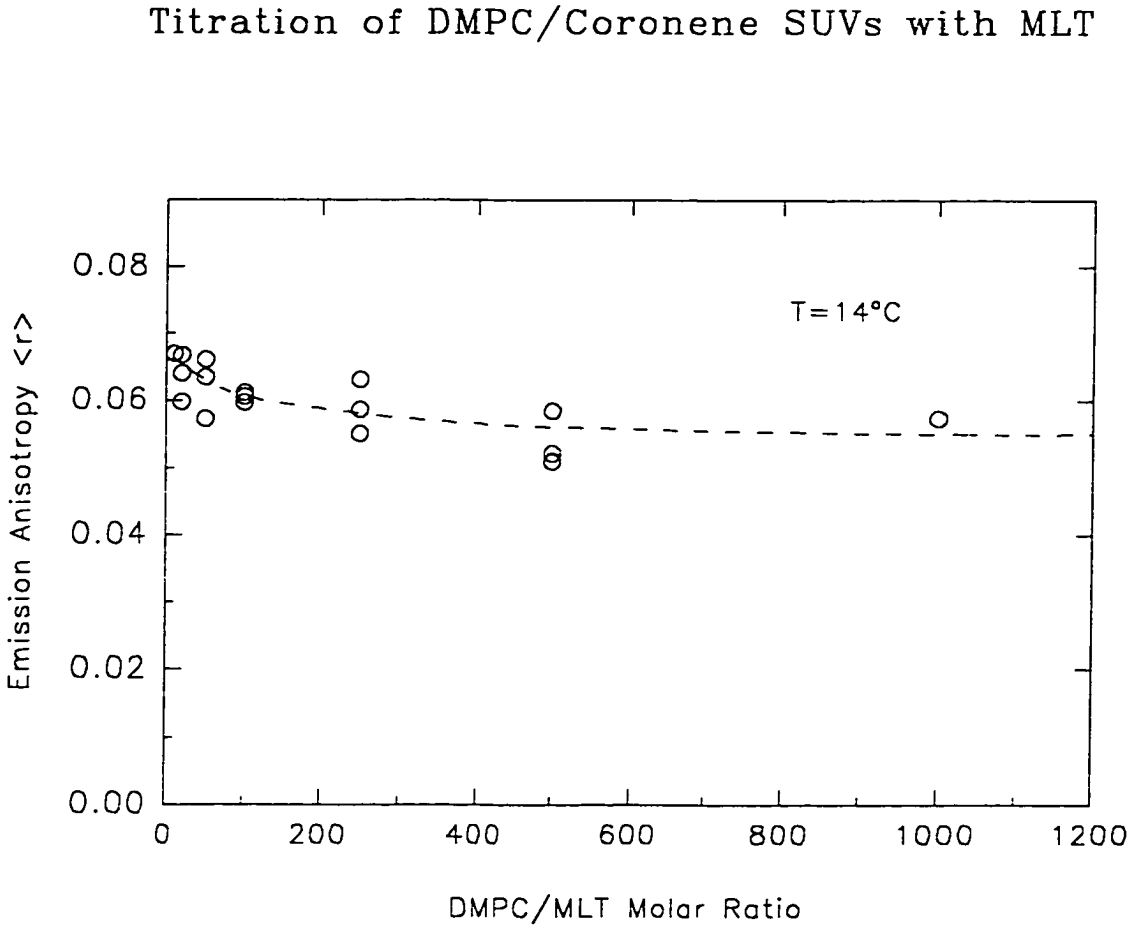

Figure 22. Steady-state emission anisotropy for coronene labeled DMPC SUVs as a function of increasing melittin concentration. The excitation and emission wavelengths were 306 nm and 446 nm, respectively. The molar labeling ratio employed was DMPC:coronene = 200:1.

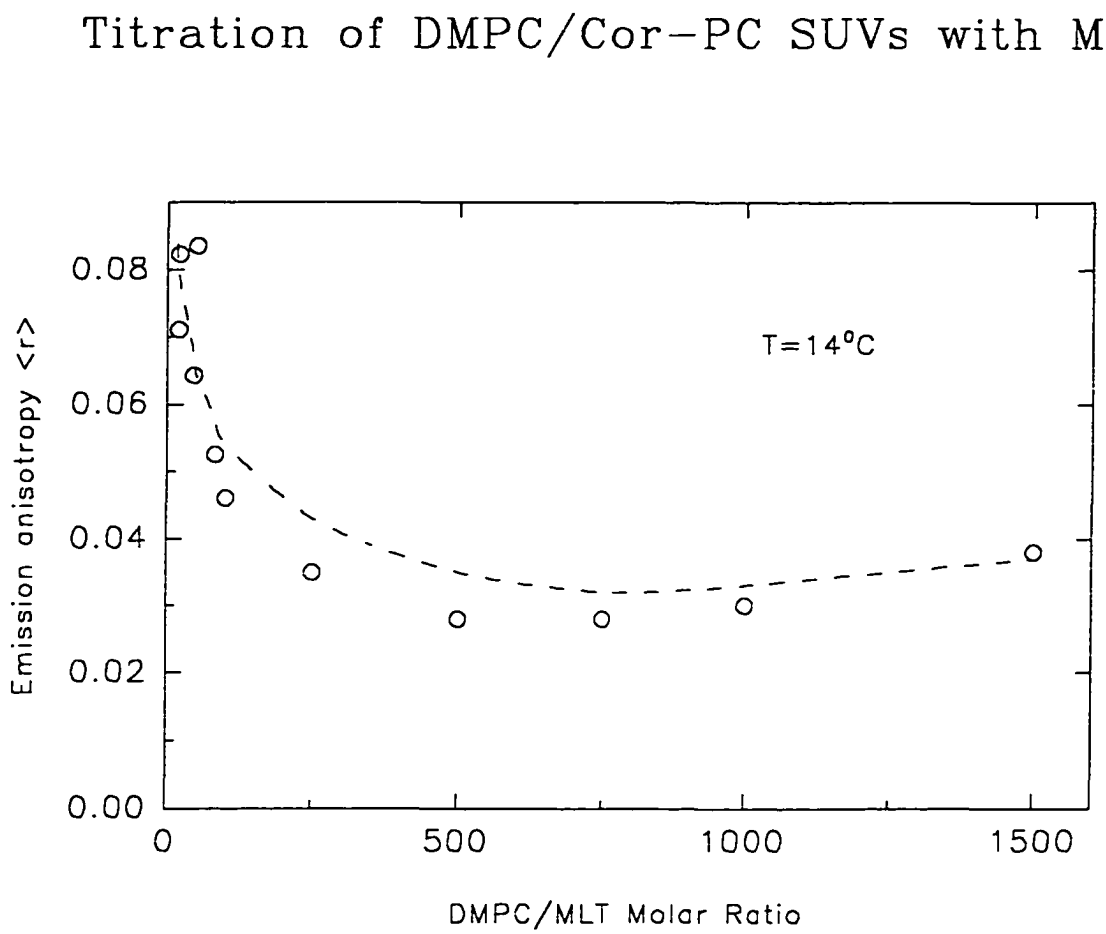

Figure 23. Steady state emission anisotropy for Cor-PC labeled DMPC SUVs as a function of increasing melittin concentration. The excitation and emission wavelengths were 308 nm and 448 nm, respectively. The molar labeling ratio employed was DMPC:Cor-PC = 200:1.

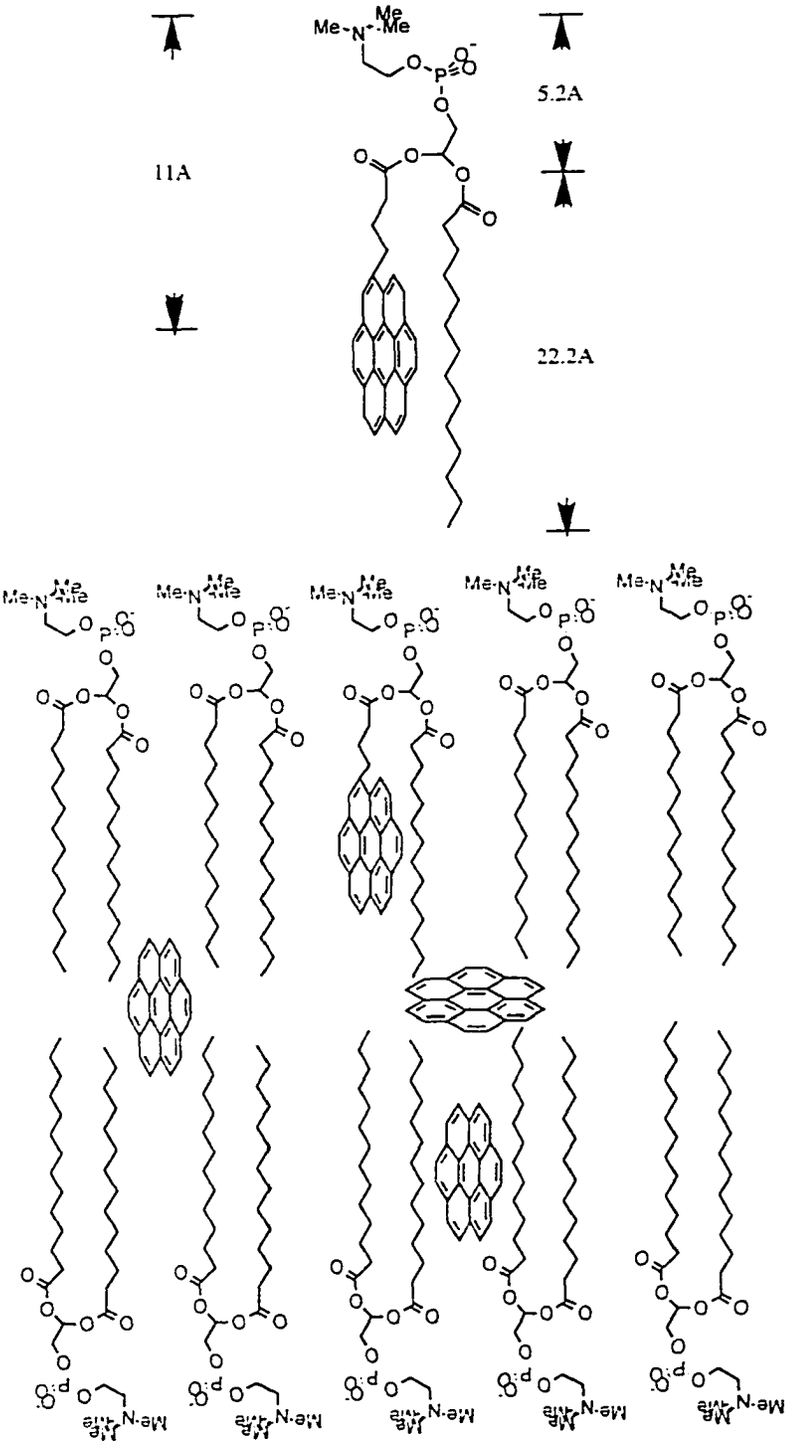

Figure 24. Cartoon showing the possible location and distances of the fluorescence probes (coronene and Cor-PC) inside the lipid bilayers.

3.4.2. Steady-State Emission Anisotropy

As predicted from the titration data (Section 3.4.1), the steady-state fluorescence emission anisotropy values measured as a function of temperature for DPH/DMPC SUVs containing melittin (DMPC/MLT = 50/1 molar ratio) are essentially identical with those which have non-peptide containing bilayers (Figure 25), and compare favorably with previous reports [98]. Additionally, the phase transition temperature determined for DMPC as revealed by DPH remained unchanged with addition of melittin (T_c = 23.5°C). Thus, it appears that on the nanosecond time scale the steady-state rotational motions of DPH ($<\tau>$ is ~10 ns) are relatively insensitive to the presence of melittin up to labeling ratios of 1:50 (MLT/DMPC), as previously discussed [98].

In contrast, for coronene labeled DMPC/SUV systems, addition of melittin (1:50) resulted in increased out-of-plane rotations and enhanced steady state emission anisotropy values ($<r_{op}>$) by ~15% from ~0.054 to ~0.062, below the lipid phase transition temperature (T_c) (Figure 26). Interestingly, the *apparent* lipid phase transition temperature of DMPC (T_c^{app} = 18°C) is unaffected by addition of melittin, which suggests that probe partitioning is unaffected by addition of the peptide.

Previous studies using coronene in DPPC SUVs have shown [96] that because of the long fluorescence lifetime of this probe, out-of-plane rotational motions of the probe can uniquely reflect the dynamic gel-to-fluid lipid exchange rate:

$$G \underset{k_{GF}}{\overset{k_{FG}}{\rightleftarrows}} F \qquad (46)$$

Estimates of the fluctuation rate, k_{FG}, from the time-resolved rotational behavior of coronene have been presented elsewhere [5, 28], and compare favorably with gel-fluid lipid exchange rates determined using ultrasound spectroscopy [59]. It is expected that the presence of peptide will alter this gel-fluid equilibrium. Since coronene is a probe of gel phase dynamics, increased measured <r> values in the presence of melittin, suggests that an enhanced ordering of the gel-phase occurs arising from a reduced gel-fluid exchange rate. Quantification of these exchange rates may be determined from time-dependent emission anisotropy measurements [5, 28], and will be discussed later (Section 3.5.2). However, due to the unknown precise location of coronene within the bilayer (which is presumably best described by a distribution function across the bilayer width), the problem we face is, that though melittin affects the gel-phase lipid ordering, the distribution of coronene may also be affected, and possibly exclude the fluorescence reporter group from the bilayer region that we are interested in studying. As a consequence, coronene, while sensitive to submicrosecond dynamics, may not be the optimal long-lived membrane dynamic probe for lipid-peptide studies.

The steady state rotational sensitivity of Cor-PC (combined in- and out-of-plane rotations) to the presence of melittin suggests that it may provide a more appropriate fluorescence probe for the study of long-lived lipid dynamics where the location of the

fluorescence moiety inside the lipid bilayer is fixed. Indeed, upon addition of melittin (DMPC/MLT = 50/1, mole ratio) to Cor-PC labeled DMPC/SUVs, a dramatic effect on the measured emission anisotropy values in the gel phase (Figure 27) was observed. Below the apparent T_c for Cor-PC, emission anisotropy (<r>) values increased on the order of 47% from ~0.053 to ~0.078. Above T_c, only a small increase in emission anisotropy (<r>) values was observed. The apparent detected lipid phase transition temperature (T_c^{app}~19-20°C), as measured by Cor-PC embedded within DMPC SUVs, however, remains constant on addition of melittin to the bilayer, suggesting no change in probe partitioning on addition of melittin. Melittin appears to have a significant ordering effect on the gel-phase of phospholipid bilayers observed within the submicrosecond time 'window' reported by Cor-PC, and in the region of the bilayer located toward the head group region. Possible specific interactions of the coronene moiety with melittin, resulting from aggregation, were assessed from lifetime determinations (see Section 3.5.1). Our time-resolved data suggest that such peptide/probe interactions do not play a role under the conditions used here.

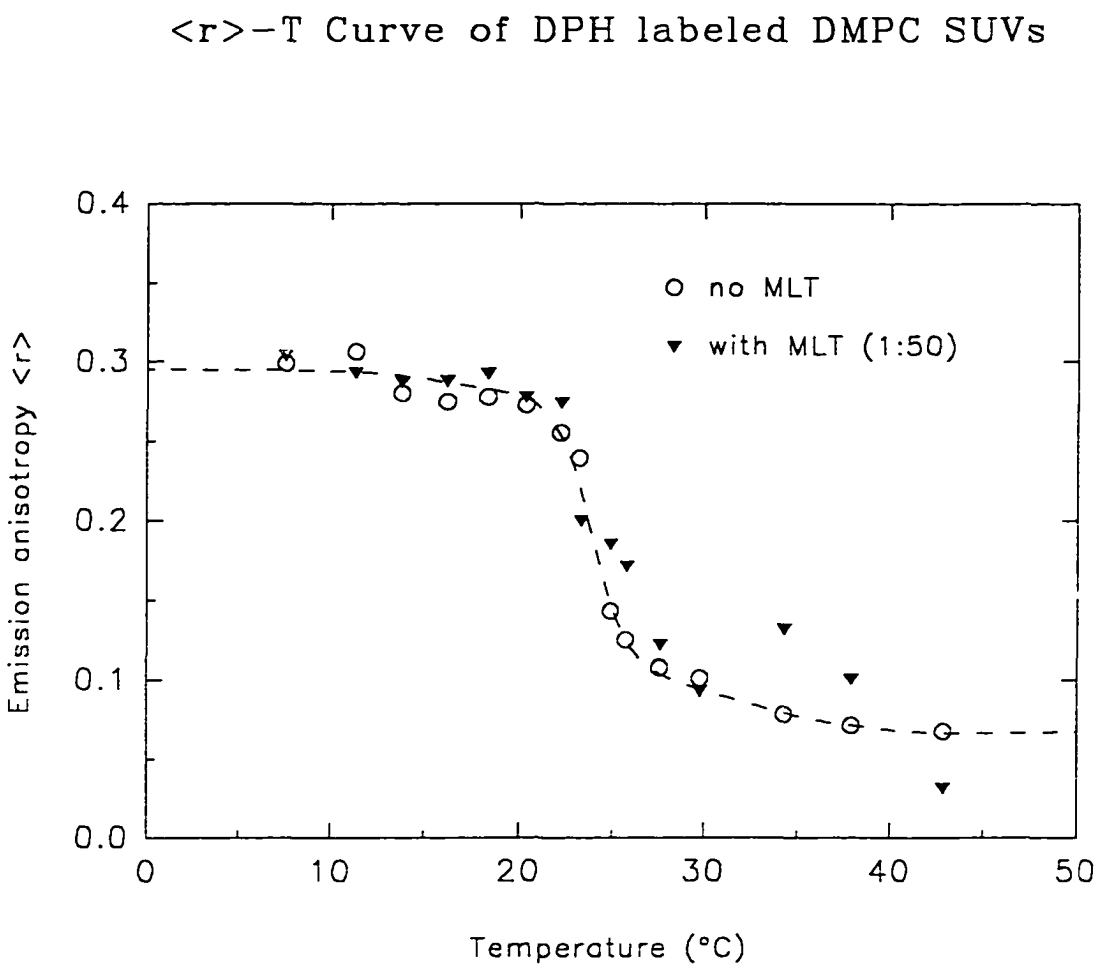

Figure 25. Steady state emission anisotropy of DPH labeled DMPC SUVs in the presence and absence of melittin (1:50; peptide-to-phospholipid molar labeling ratio), as a function of temperature. Excitation and emission wavelength were 355 nm and 430 nm, respectively. The DPH to DMPC molar labeling ratio used was 500:1.

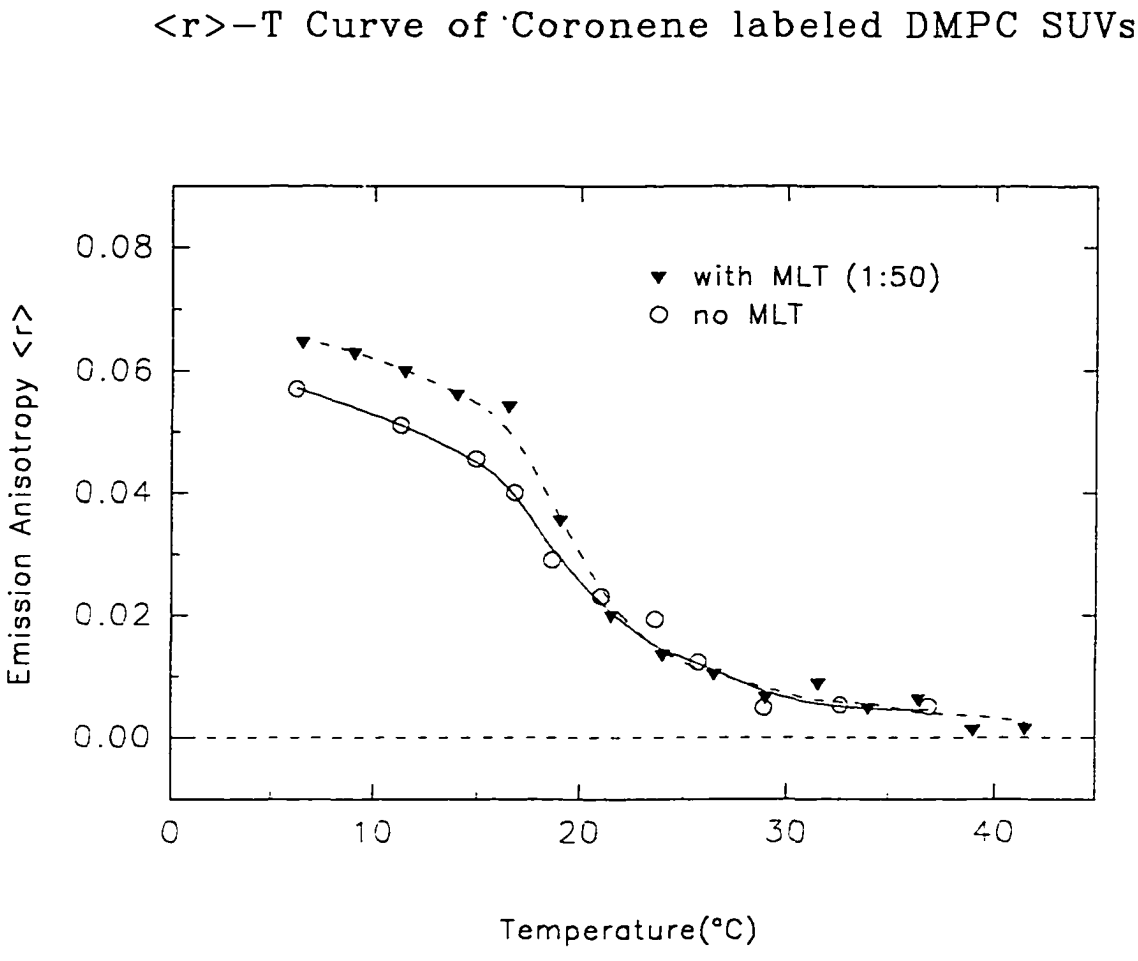

Figure 26. Steady state emission anisotropy (<r>) of coronene labeled DMPC SUVs with and without melittin as a function of temperature: the excitation and emission wavelength were 306 nm and 446 nm respectively. The labeling ratio was DMPC:Cor-PC = 200:1.

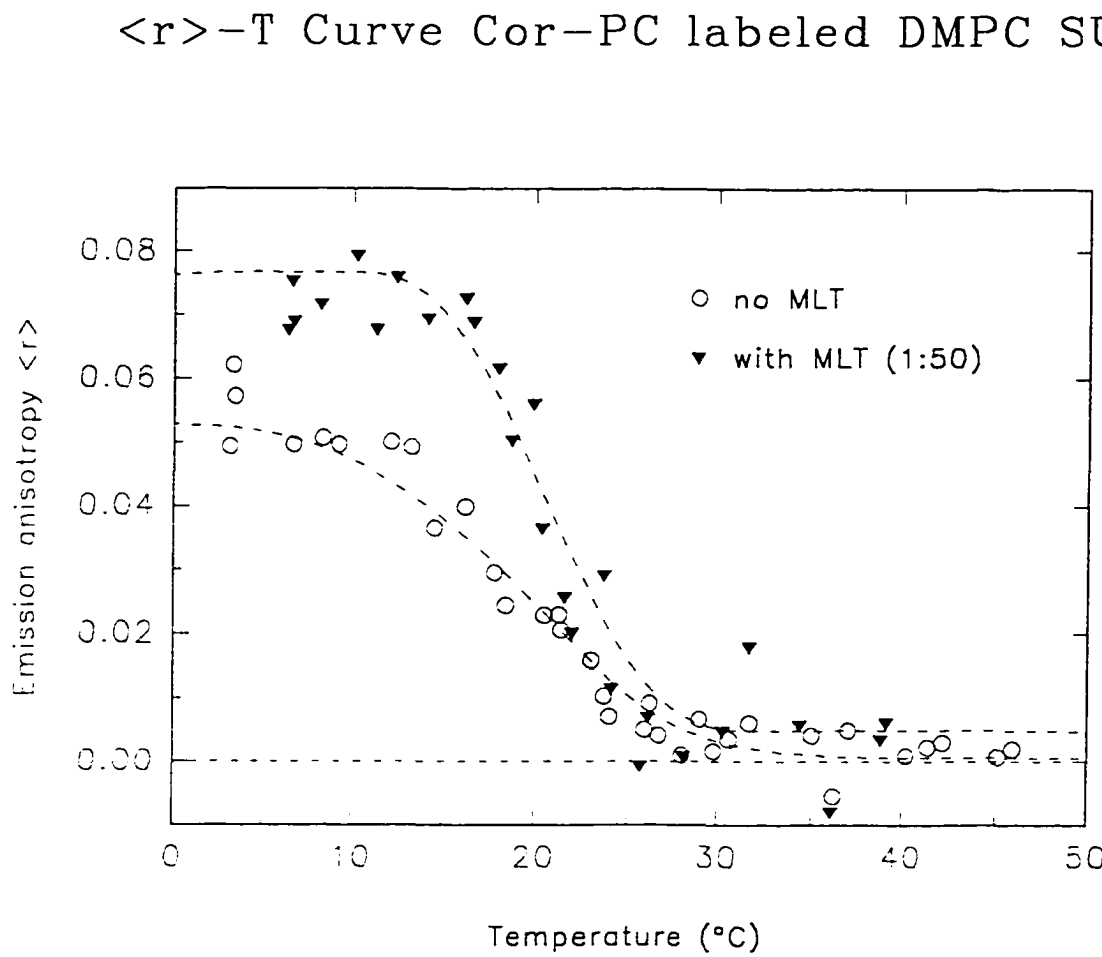

Figure 27. Steady-state emission anisotropy (<r>) of Cor-PC labeled DMPC SUVs with and without melittin as a function of temperature: the excitation and emission wavelength were 308 nm and 448 nm, respectively. The labeling ratio was DMPC:Coronene = 200:1.

3.5. Quenching Experiments to Determine Fluorescence Probe Location

While estimates of the location of the fluorescence moieties used in these studies can be derived from molecular geometries (Figure 24), we performed fluorescence quenching experiments using a heavy anion quencher to provide useful information about the location of a fluorophore within a lipid bilayer [65]. A fluorophore that is located at the surface of the lipid bilayer will be relatively accessible to a charged membrane impermeable solute quencher dissolved in the aqueous phase. In contrast, a fluorophore that is buried within the lipid bilayer is less accessible (depending on its bilayer width distribution) and hence will be quenched to a lesser degree by the added extrinsic quencher, and only fully quenched as a result of disruption of the bilayer, or use of a lipid soluble quencher, *e.g.*, acrylamide (for a review, see[65]).

In this study, we used the iodide anion as a membrane impermeable heavy anion quencher to determine the location of the coronene fluorophore in DMPC/Cor-PC and DMPC/Coronene SUVs at a fixed temperature of 14°C, below T_c. The effect of a quencher species on the steady state fluorescence intensity of a sample can be described by the Stern-Völmer equation [65]:

$$\frac{I_0}{I} = 1 + K_{sv}[Q] \qquad (47)$$

where:

$$K_{sv} = k_q \cdot \tau_0 \qquad (48)$$

and I_0, τ_0, and I, τ_q are the fluorescence intensities and lifetimes in the absence and presence of quencher Q, respectively. K_{sv} is the dynamic Stern-Völmer quenching constant which is the product of the quenching rate constant, k_q, and the fluorescence lifetime, τ_0, in the absence of quencher. If the quenching mechanism is dynamic, then the ratio of the lifetimes, τ_0/τ_q, will also be equal to $1 + K_{sv}[Q]$.

The quenching rate constant, k_q, is the product of the quenching efficiency, γ, and the diffusion-limited bimolecular rate constant for collision, k. k can be calculated from Smoluchowski equation:

$$\begin{aligned} k_q &= \gamma \cdot k \\ k &= 4\pi D R_0 N' \end{aligned} \qquad (49)$$

where D is the sum of the combined diffusion coefficients for the quencher and fluorophore, R_0 is the collision radius, equal to the sum of the molecular radii of the fluorophore and quencher, and N' is Avogadro's number divided by 1000. The diffusion coefficient for each species can be calculated using the Stokes-Einstein equation:

$$D_i = \frac{k_B \cdot T}{6\pi R\eta} \qquad (50)$$

where η is the solvent viscosity, k_B is the Boltzmann constant, T is the absolute temperature, and R is the radius of the species. Since k_q is expected to be a function of T/η, the Stern-Völmer constant, K_{SV}, is related to the solvent viscosity and the more viscous the solvent, the smaller is the expected value for K_{SV}.

3.5.1. Pure Lipid Systems

The decrease of fluorescence intensity as a function of added quencher concentration ([KI]) for both Cor-PC and coronene are shown as Stern-Völmer plots in Figure 28a. For both probes, at low concentration of KI, the decrease in fluorescence intensity is linear, reaching a plateau intensity value at higher quencher concentration. This characteristic quenching plot is representative of a heterogeneous population of fluorophores, where a population of fluorescence probes is inaccessible to the quencher [25, 99]. Since iodide may not permeate significantly into the lipid membrane [99], the quenching data suggest that a proportion of Cor-PC and coronene are buried within the lipid membrane, where the iodide anions are excluded. A second population of membrane bound fluorophores is however accessible to quencher.

On closer examination of the quenching plots, it is clear that the fluorescence of Cor-PC is more readily affected by iodide anions, when compared to coronene. These results may be rationalized when the location of the probes within the bilayer are considered. Coronene is free to distribute across the bilayer width, but due to its hydrophobicity is expected to reside deep within the acyl chain region of the lipid bilayer, where iodide anions will be excluded. In contrast, due to the short acyl chain lipid anchor, Cor-PC is expected to be located more towards the surface of the lipid bilayer (see Figures 7 and 24), and demonstrate a greater accessibility to extrinsically added quencher.

Quenching of two populations of fluorophores (accessible and inaccessible) may be quantified using a Lehrer plot which is a modified form of the Stern-Völmer equation [61]. If we assume that for a mixture of two fluorophore populations, one population 'a' is

accessible to quenching, and the other population 'i' is inaccessible, then the total fluorescence intensity in the absence of quencher (I_0) is given by:

$$I_0 = I_{0a} + I_{0i} \tag{51}$$

In the presence of quencher the fluorescence intensity of the accessible fraction (f_a) is affected according to Stern-Völmer equation (see Equation 47), and the inaccessible fraction is shielded from quencher. Therefore:

$$I = \frac{I_{0a}}{(1 + K_{SV}[Q])} + I_{0i} \tag{52}$$

where K_{SV} is the Stern-Völmer quenching constant for the accessible fraction. Subtraction of Equation 52 from Equation 51 yields:

$$\Delta I = I_0 - I = \frac{I_{0a} K_{SV}[Q]}{(1 + K_{SV}[Q])} \tag{53}$$

Inversion of Equation 53 followed by division into Equation 51 yields

$$\frac{I_0}{\Delta I} = \frac{1}{f_a K_{SV}[Q]} + \frac{1}{f_a} \tag{54}$$

where:

$$f_a = \frac{I_{0a}}{(I_{0a} + I_{0i})} \tag{55}$$

A linear plot of $I_0/\Delta I$ versus 1/[Q] now yields estimates of the inaccessible fraction (f_a^{-1}) as the intercept at infinite quencher concentration, and $(f_a K_{SV})^{-1}$ as the slope.

Lehrer plots for coronene and Cor-PC DMPC SUVs are represented in Figures 28b. The intercept on the $F/\Delta F$ axis, corresponding to $1/f_a$, is 3.76 for coronene and 1.76 for Cor-PC, representing 26.6% and 56.8% of the total fluorescence signal accessible for quenching by iodide anion for coronene and Cor-PC labeled DMPC SUVs, respectively. These data suggest that Cor-PC has greater exposure to the polar head group region than the hydrophobic coronene molecule, which is perhaps not surprising when considering the forced and more polar location for the fluorophore of Cor-PC in the bilayer.

Interestingly, the high percentage of accessible Cor-PC fraction can be correlated with the ratio of surface areas ($4\pi r^2$) for the inner versus outer leaflets of the bilayer. If an average bilayer width (50Å) is assumed [93], and given that the diameter of DMPC SUVs is 250-300Å [6], then the ratio of outer to inner bilayer surface areas is expected to be on the order of 1.5:1. From the quenching data, assuming that the Cor-PC distributes randomly across the inner and outer leaflets (which is justified for these studies, since the phospholipid probe was added during vesicle preparation and not post-preparatively), the outer to inner ratio may be represented by the accessible to nonaccessible probe fractions (56.8/43.2) = 1.32, and compares favorably with the theoretically expected value of 1.5.

Values for the Stern-Völmer quenching constant (K_{SV}), determined from the slope of the Lehrer plots, are 22.12 M^{-1} and 10.98 M^{-1} for coronene and Cor-PC labeled SUVs, respectively. Given that the average fluorescence lifetimes ($<\tau>$) for coronene and Cor-PC imbedded within SUVs are 216.6 ns and Cor-PC 111.9 ns at 14°C (see Section 3.7.1), the

bimolecular quenching constant (k_q) associated with the accessible probe fraction, determined according to Equation 48, yields values of 1.021×10^{8} $M^{-1}s^{-1}$ and $9.812x10^{7}$ M^{+} s^{+} for coronene and Cor-PC labeled DMPC SUVs, respectively, which compare favorably ($\sim10^{8}$ $M^{-1}s^{-1}$) with previous values determined for the bimolecular quenching constant of iodine [65].

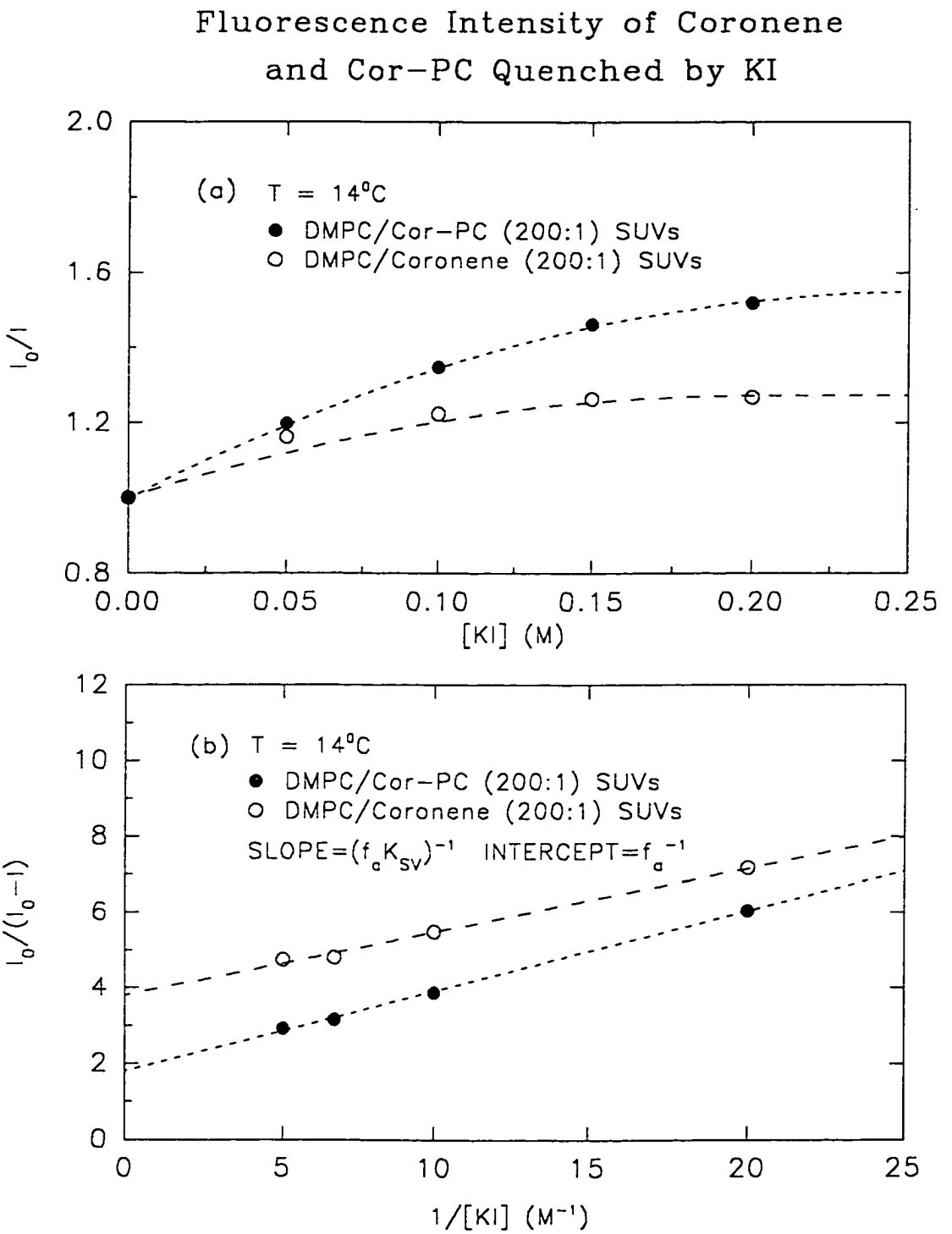

Figure 28. Fluorescence of Cor-PC and coronene labeled DMPC SUVs as a function of KI concentration represented as: (a) Stern-Völmer and (b) Lehrer plots. The excitation and emission wavelengths were 308 nm and 448 nm, respectively, for Cor-PC, and 306 nm and 446 nm, respectively, for coronene.

3.5.2. Effects of Melittin

The effect of melittin (1:75; peptide to phospholipid molar labeling ratio) on the extrinsic quenching of Cor-PC in DMPC SUVs was determined. Again a non-linear Stern-Völmer plot was observed (Figure 29a), however, there appears to be marginally less efficient quenching of the fluorescence of Cor-PC in the presence of peptide. Intepretations of these data are twofold. In the first model, the presence of peptide may result in a more inaccessible location for the coronenyl probe (*e.g.* buried deeper within the bilayer). Alternatively, the lipid bilayers may now exist in a more ordered or rigid state as a direct consequence of the peptide, and hence it is more difficult for the quencher molecule to penetrate and approach the probe molecules in a diffusion dependent mechanism. As the coronene chromophore is attached to the acyl chain of a phospholipid molecule, and hence located in essentially a fixed position within the bilayer, it appears unlikely that the chromophore will be buried deeper in the bilayer on addition of melittin to DMPC. Thus an increased lipid ordering appears to be a more appropriate explanation of the quenching results, and is in agreement with emission anisotropy data obtained previously for Cor-PC in the presence of melittin (see Section 3.4.2), suggesting a reduced k_{FG} and enhanced lipid ordering (see Equation 46).

Replotting the Cor-PC/Melittin/DMPC SUV quenching data as a Lehrer plot (Figure 29b), the resultant linear plot yields an intercept (f_a^{-1}) on the intensity axis of 1.98, which indicates a 51% accessibilty of the total Cor-PC fluorescence to extrinsic membrane impermeable iodide anion quenching. This represents a non significant 5% decrease in the accessible fluorophore population compared to non-melittin containing SUVs (see Section 3.4.1). Additionally, the biomolecular quenching rate constant (k_q) for Cor-PC labeled

DMPC/MLT SUVs is 7.345×10^{7} $M^{-1}s^{-1}$, determined from the slope of the Lehrer plot, and the average fluorescence lifetime of 106.0 ns for Cor-PC in labeled DMPC/MLT SUVs (see Section 3.8.1). The quenching constant (k_q) for Cor-PC labeled DMPC/MLT SUVs is less than nonmelittin containing systems ($9.812x10^{7}$ $M^{-1}s^{-1}$) and supports the model that the presence of melittin does have an ordering effect on lipid bilayers which reduces the accessibility of iodide ions to the coronene moiety of Cor-PC.

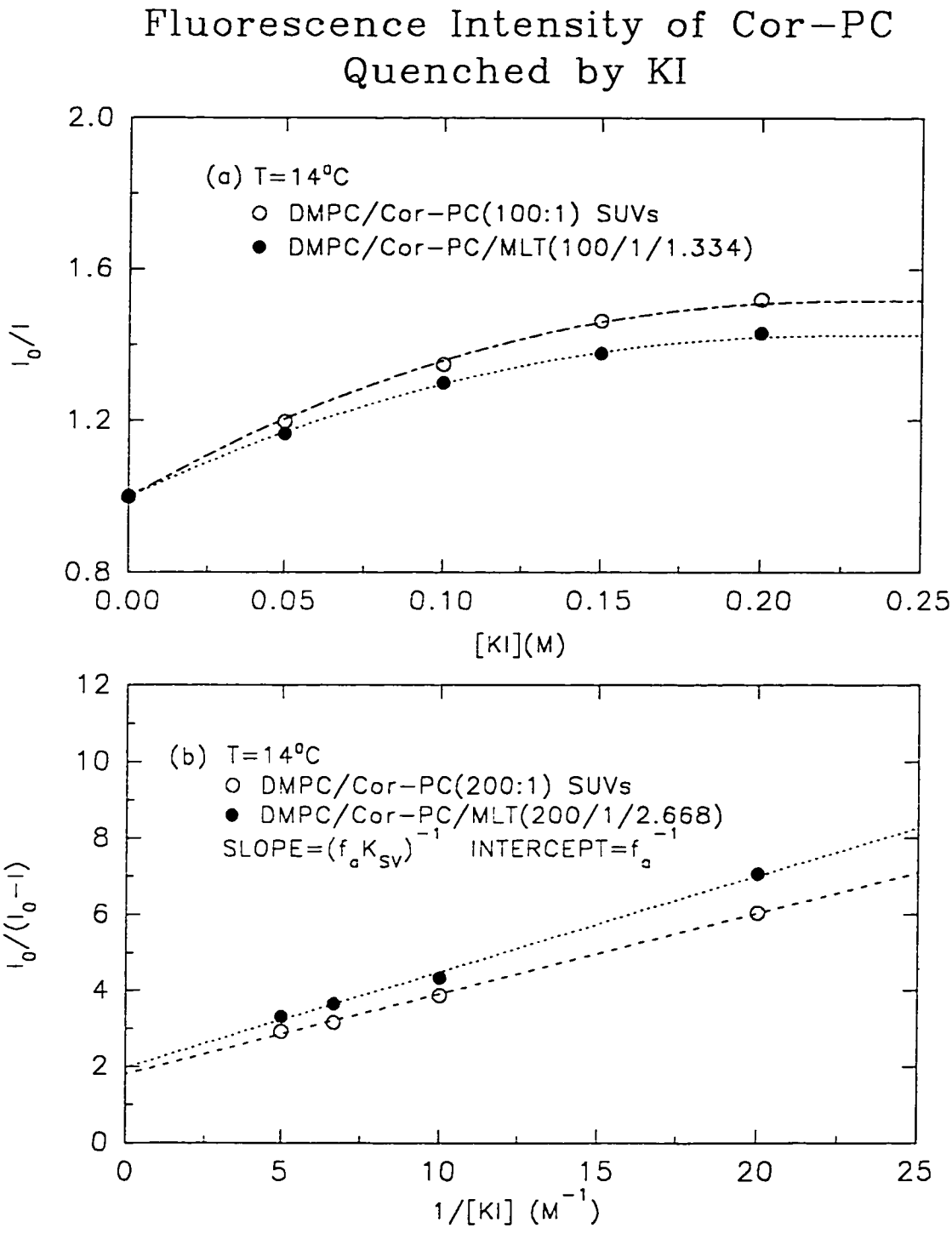

Figure 29. The fluorescence of Cor-PC labeled DMPC SUVs with and without melittin quenched by KI: (a). Stern-Völmer and (b). Lehrer plots for two populations of fluorophores, one of which is inaccessible to quencher. The excitation and emission wavelengths were 308 nm and 448 nm, respectively.

3.6. Using Excimer/Monomer (I_E/I_M) Measurements to Study Microfluidity of DMPC SUVs and the Effect of Melittin on DMPC Lipid Bilayers

Diffusion controlled intermolecular excimer (or dimer) formation by pyrene has been used extensively as a probe of changes in phospholipid mobility or 'microviscosity' occurring within the hydrocarbon interiors (acyl-chain region) of bilayers [50, 51, 100]. Such changes may be evaluated from the ratio of emission intensities of the pyrene excimer to monomer (I_E/I_M) species [50], and is based on the viscosity dependence of the translational diffusion rate for this fluorophore. The pyrene monomer emits around 390 nm, whereas the excimer species formed either in viscous solvents or isotropic solvents at high concentration, exhibits a broad and featureless emission spectrum which is shifted to longer wavelengths (475 nm) transition. Pyrene is a relatively long-lived fluorescence (τ_{AV} > 100 ns) probe, and the time-scale for excimer formation is on the order 10^{-10} - 10^{-7} s.

The photophysical details of pyrene excimer production and emission are as follows:

$$Py + h\nu \rightarrow Py^{*} \qquad \textit{Absorption}$$

$$Py^{*} \xrightarrow{k_f} Py + h\nu' \qquad \textit{Monomer fluorescence}$$

$$Py + Py^{*} \xrightarrow{k_a[Py]} Py_2^{*} \qquad \textit{Excimer formation} \qquad (56)$$

$$Py_2^{*} \xrightarrow{k_f'} 2Py + h\nu'' \qquad \textit{Excimer fluorescence}$$

where Py represents pyrene in its ground state; Py^*, pyrene in its first excited singlet state, and Py_2^* is pyrene in the excimer form (excimer is derived from *exci*ted di*mer*).

From the above equations, we can see that the intensity of monomer fluorescence (I_M) is proportional to $k_f[Py^*]$ (recorded at 390nm for pyrene). The intensity of excimer fluorescence (I_E) is proportional to $k_f[Py_2^*] \propto k_a[Py][Py^*]$ (recorded at 475 nm for pyrene), hence:

$$\frac{I_E}{I_M} \propto \frac{k_a[Py][Py*]}{k_f[Py*]} = \frac{k_a[Py]}{k_f} \qquad (57)$$

The rate constant (k_a) is given by the Einstein diffusion equation:

$$k_a = \frac{8RT}{3000\eta} \qquad (58)$$

where R is the ideal gas constant; T is the absolute temperature, and η is the viscosity (in centipoise, cP). Hence, the ratio of excimer to monomer fluorescence intensity, may be written:

$$\frac{I_E}{I_M} = \frac{KT[Py]}{\eta} \qquad (59)$$

where K equals to $8R/3000k_f$. Thus at constant temperature, the fluorescence emission intensity ratio, I_E/I_M, will increase as the viscosity decreases. Hence, measurement of I_E/I_M can provide information regarding the viscosity of the medium in which the probe is embedded [50]. Excimer formation of pyrene has been examined in this study to estimate any

possible microviscosity changes occurring within the bilayer of DMPC SUV's arising from the addition of melittin.

Initially the effect of pyrene labeling ratio ([Py]/[DMPC]) for DMPC SUV's at 14°C on the fluorescence intensity values measured at 475nm and at 390nm was assessed, and the intensity ratio (I_E/I_M) determined, in order to assess the optimal probe to phospholipid labeling ratio (a critical labeling ratio is required in order for excimers to be formed, but perturbation at higher probe labeling ratios must be minimized). This is depicted in Figure 30. At higher ratios, I_E/I_M increases linearly with increased pyrene concentration, suggesting that at molar labeling ratios ([Py]:[DMPC]) lower than 1:100, excimer formation does not appreciably exist. However, at [Py]:[DMPC] greater than 1:10 (0.1), excimer formation reaches a constant value presumably due to self-quenching and reabsorption of emitted light from high local probe concentrations. Hence, information regarding lipid bilayer microviscosity information may only be properly obtained from excimer formation using the labeling ratio [Py]:[DMPC]=1:50 or 1:25.

The temperature dependence of the excimer/monomer ratio for pyrene embedded within DMPC SUVs (1:50 and 1:25 probe to phospholipid molar labeling ratios) is shown in Figure 31, from which the phase transition temperature (T_c) of the phospholipid bilayer can be estimated. As expected, the I_E/I_M ratio increases linearly in the temperature range 5 to 20°C, as more excimer species is formed with increasing temperature. However, at T_c=23°C, the slope of the line changes, reflecting the phase change of the lipid bilayer which becomes more fluid and results in enhanced excimer formation. This result agrees with other reports [50].

Inclusion of melittin within DMPC SUVs decreases the excimer/monomer ratio over the entire temperature range (Figure 32).Indeed at 1/25 melittin to lipid ratios (Figure 32) the lipid phase transition is almost lost. Thus at any given temperature, addition of melittin appears to decreases the formation of excimer species within the lipid bilayer. Given that the probe labeling ratio is identical to the non-peptide containing vesicles, the peptide appears to reduces the probe diffusion rate in the bilayer, which results from the imposed lipid ordering. Additionally, the phase transition temperature (T_c) for DMPC is not well defined in the presence of melittin, suggesting an overall ordering of the bilayer in the presence of peptide, both above and below the phase transition. Melittin appears to decrease intermolecular excimer formation, by decreasing the lateral diffusion coefficient. This is further indicated from the titration of DMPC SUVs (at 14°C) with fixed pyrene labeling ratios (1:50 and 1:25). A reduction in the excimer/monomer ratio with increasing melittin concentration (Figure 33) suggests that the 'microviscosity' of phospholipid bilayer appears to increase on addition of peptide and the lipid bilayer becomes more rigid or ordered. This result compares favorably with our Cor-PC data obtained from fluorescence anisotropy and quenching experiments (see above).

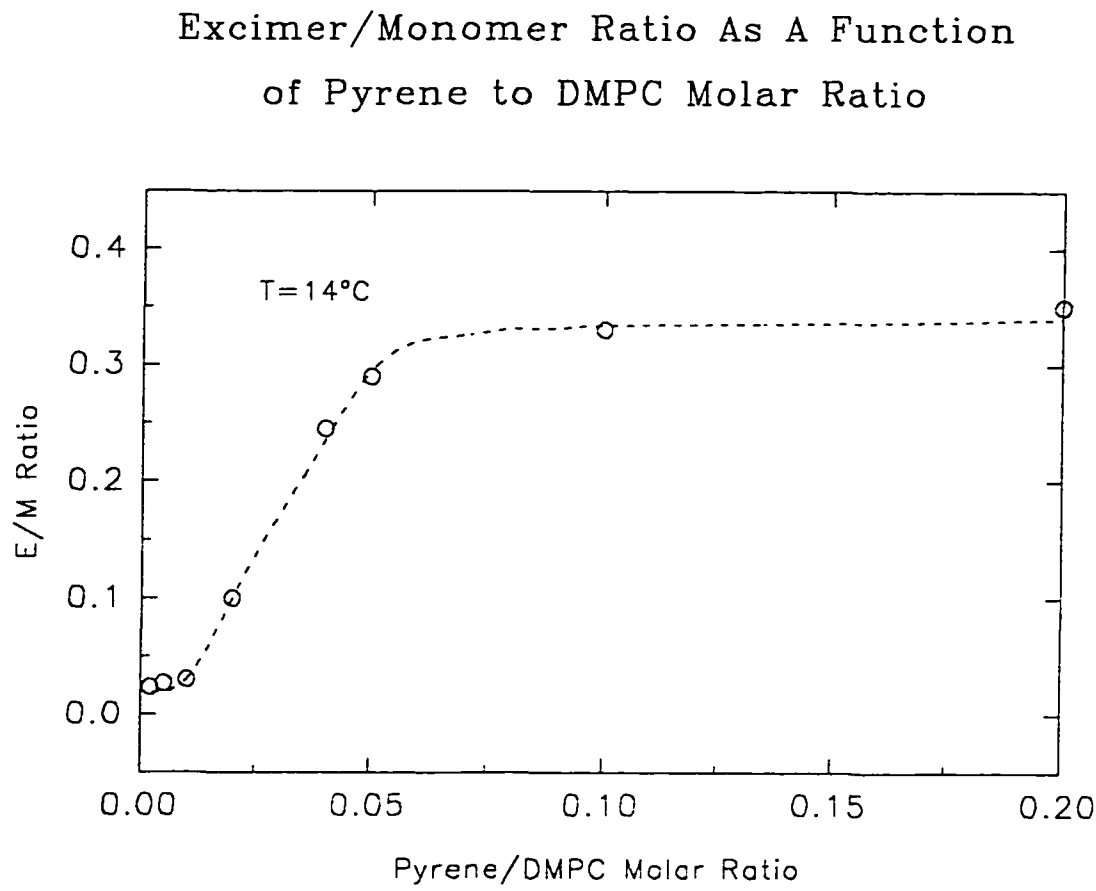

Figure 30. The excimer to monomer intensity ratio of pyrene as function of pyrene concentration for DMPC SUVs at 14 °C. The excitation wavelength was 340 nm. The emission wavelengths were 470 nm for the excimer and 390 nm for the monomer.

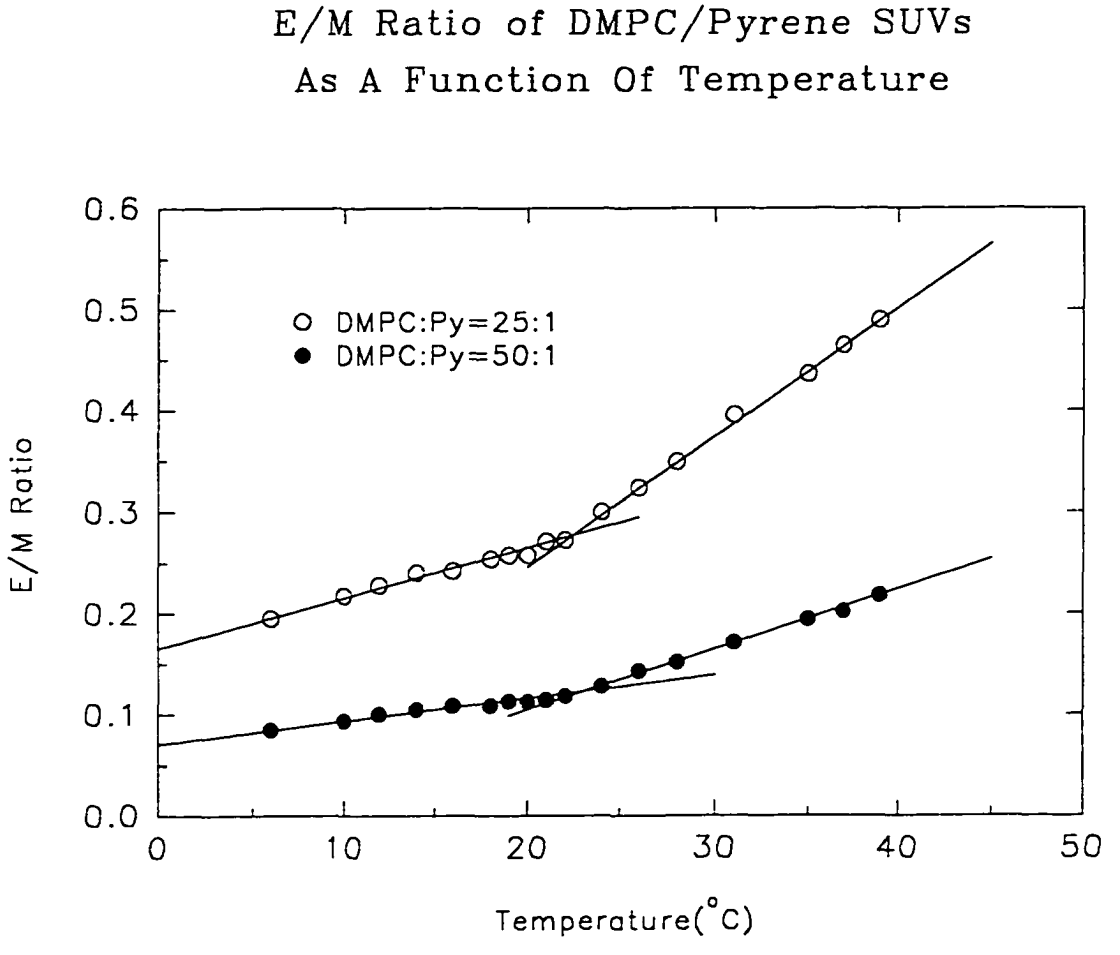

Figure 31. The excimer-to-monomer intensity ratio of pyrene labeled DMPC SUVs as a function of increasing temperature. The excitation wavelength was 340 nm. The emission wavelengths were 390nm for the monomer and 470 nm for the excimer.

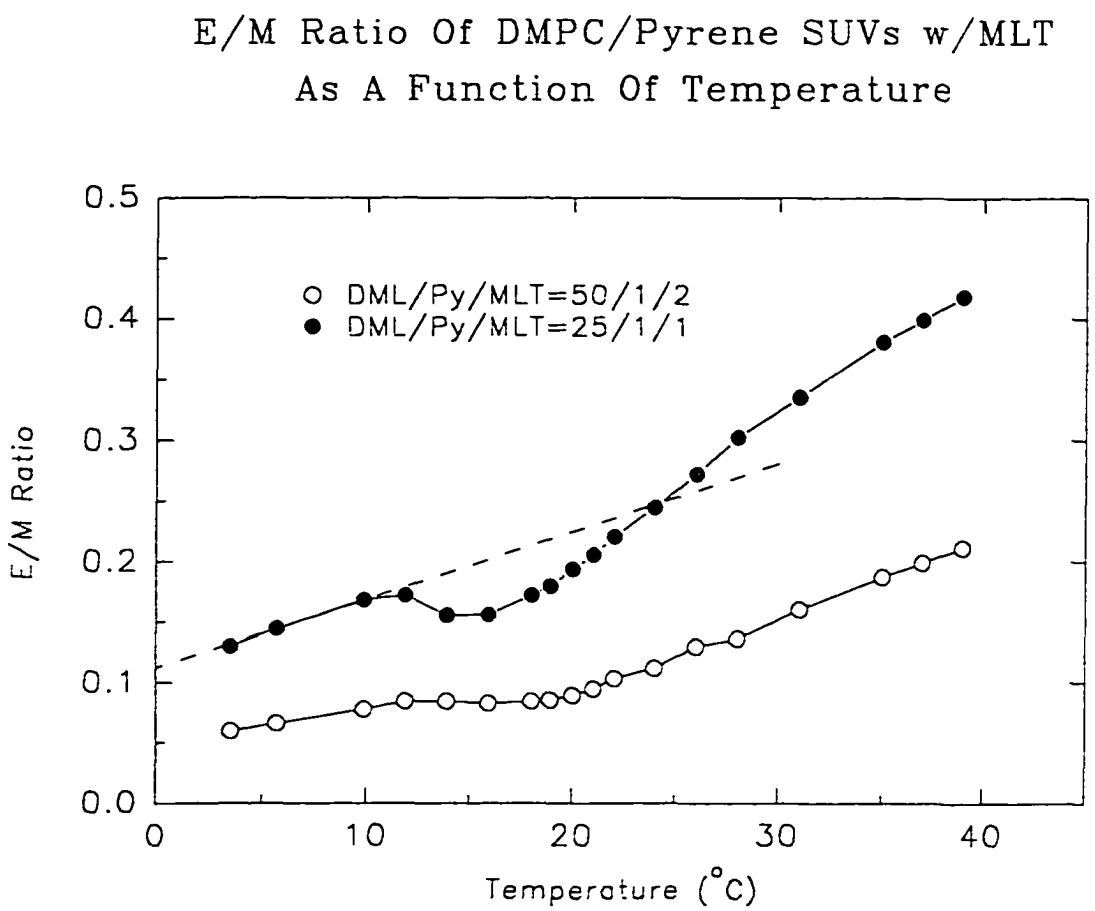

Figure 32. The excimer-to-monomer intensity ratio of pyrene labeled DMPC SUVs with and without melittin as a function of increasing temperature. The excitation wavelength was 340 nm. The emission wavelengths were 390 nm for the monomer and 470 nm for the excimer. The DMPC to melittin ratio was 25:1.

In a qualitative fashion, the interaction of melittin with DMPC SUVs was demonstrated via electronic energy transfer from the single tryptophan residue of melittin to pyrene, when embedded within the hydrocarbon layer of the phospholipid bilayer (Figure 34). The fluorescence emission spectrum of the tryptophan residue (λ_{max}~350 nm) of melittin shows good overlap with the absorption maxima of pyrene (λ_{max}~340 nm) as shown in Figure 34a.

On excitation of the single tryptophan residue of melittin (λ_{ex}~290 nm), increased pyrene monomer emission is observed (after correction for direct pyrene excitation) and suggests that these two fluorophores fall within the critical (10-100 Å) distance required for efficient energy transfer. Qualitatively, the transfer efficiency appears to increase with increasing melittin to lipid ratios (1:1000 to 1:100), which provides an additional indication of the penetration of melittin within the DMPC lipid bilayers, and interaction of the hydrophobic probe pyrene with the bilayer embedded tryptophan residue. These energy transfer experiments were not performed with the intention of calculating energy transfer distances in a quantitative fashion which would require estimates of donor and acceptor quantum yield Φ values, the orientation factor $\langle\kappa^2\rangle$, and the extinction coefficient for the acceptor, but merely to demonstrate that the peptide interacts with the bilayer for the labeling ratios studied in this work.

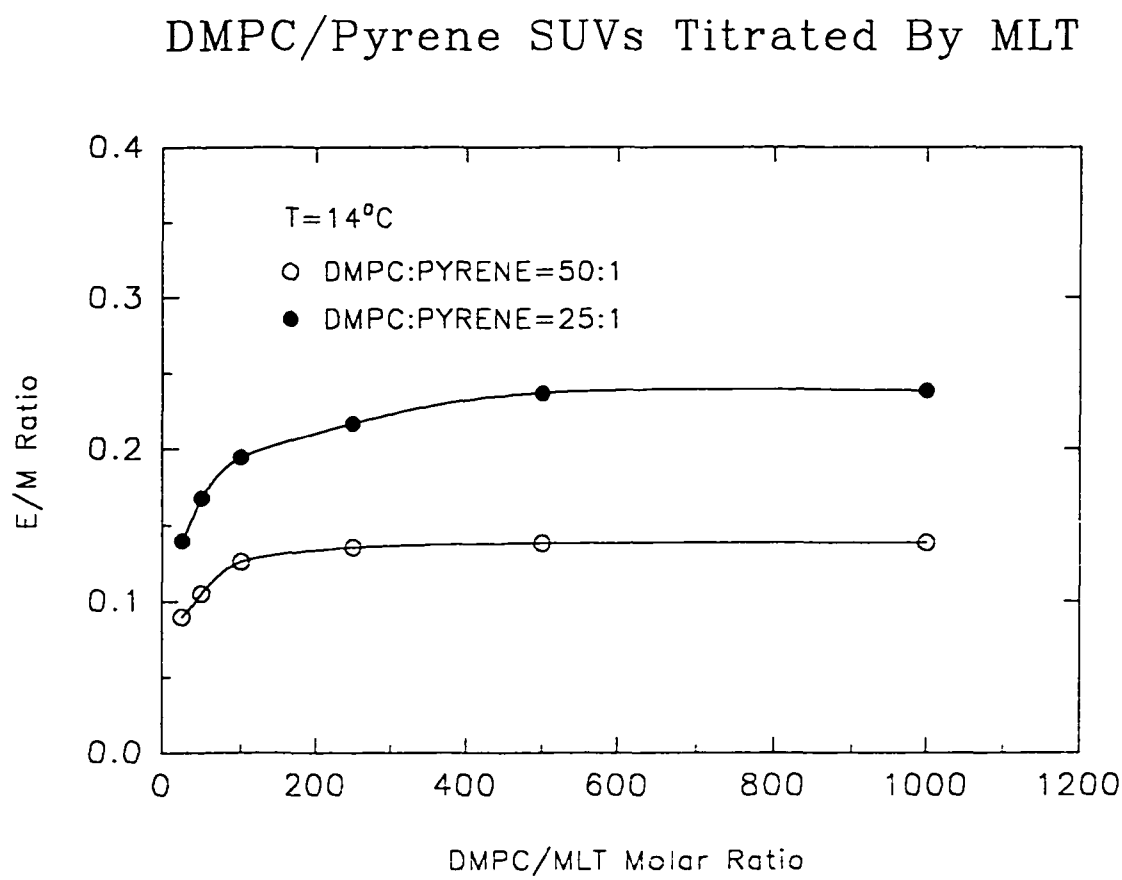

Figure 33. Excimer to monomer intensity ratio of pyrene labeled DMPC SUVs as a function of melittin concentration. The excitation wavelength was 340 nm. The emission wavelengths were 390 nm for monomer and 470 nm for excimer.

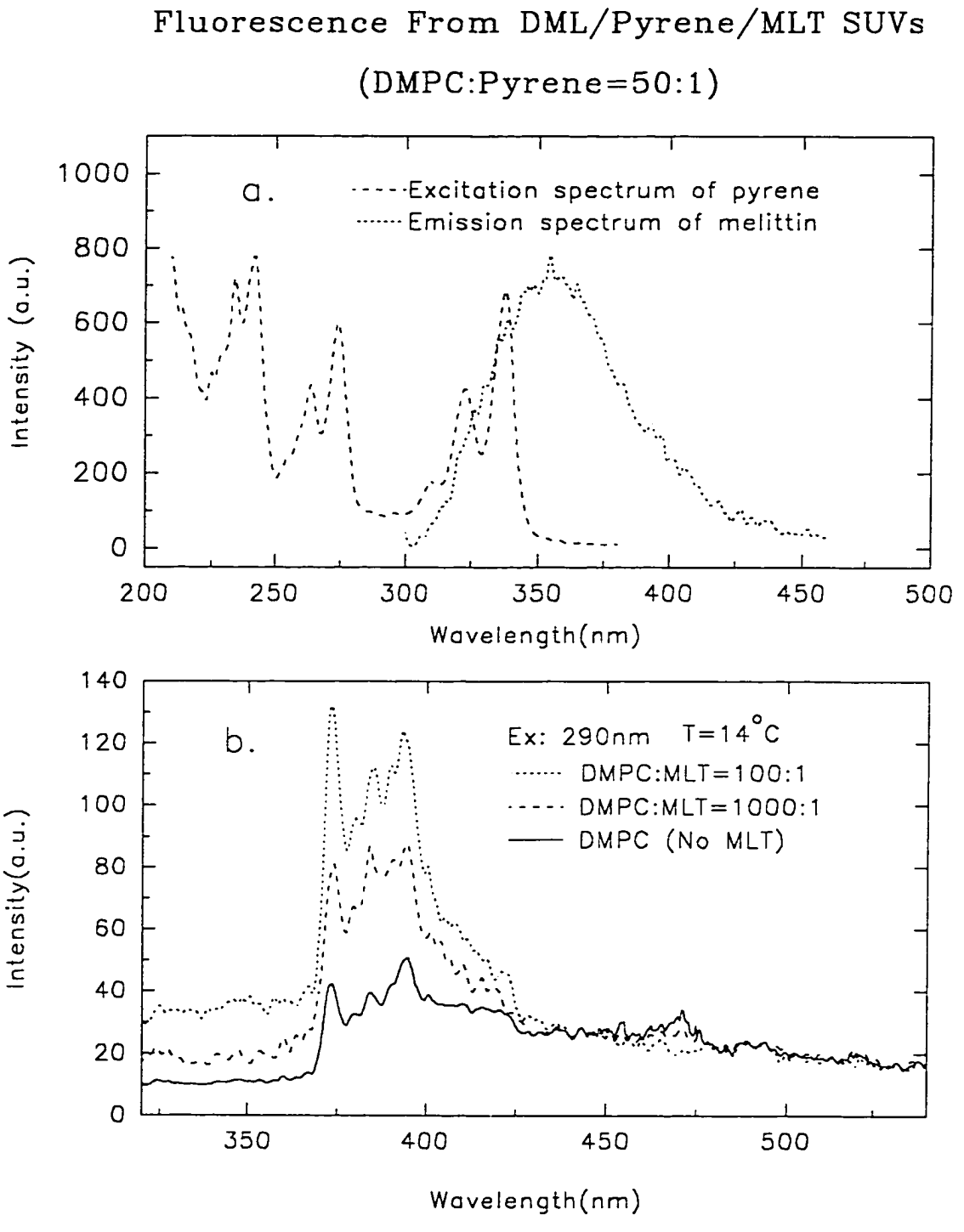

Figure 34. (a) The overlap of emission spectrum of melittin with the excitation spectrum of pyrene. (b) The emission spectra from pyrene labeled DMPC SUVs with varying melittin concentrations. The increased emission from pyrene is mainly due to the energy transfer between the tryptophan of the melittin and bilayer embedded pyrene.

3.7. Time-Resolved Studies of Coronene and Cor-PC in Pure Lipid Systems

3.7.1. Lifetime Analysis

Time-resolved fluorescence decay data were obtained for DMPC SUVs labeled with either Cor-PC or coronene as a function of temperature (8~30°C), below and above the phospholipid phase transition temperature (23°C). A representative fluorescence emission decay for DMPC SUVs labeled with coronene (1:200; probe to phospholipid molar labeling ratio) is shown in Figure 35 at 14°C (below T_c). Clearly the long lifetime dominates the decay profile and data truncation is evident at the timing calibration used for these experiments (0.432 ns/channel). This effect is not crucial for lifetime analyses, but is critical for determination of rotational parameters.

For both Cor-PC (1:100) and coronene (1:200) labeled samples, an iterative Marquardt non-linear least-squares fitting of the decay data provided the 'best' fit using a triple exponential decay function, as judged by chi-squared, residuals and autocorrelation functions (see Section 2.6):

$$I(t) = \alpha_1 \cdot e^{\frac{-t}{\tau_1}} + \alpha_2 \cdot e^{\frac{-t}{\tau_2}} + \alpha_3 \cdot e^{\frac{-t}{\tau_3}} \qquad (60)$$

In an attempt to unravel the origins of the lifetime heterogeneity for these probes, fluorescence decay profiles were collected at varying temperatures spanning the phospholipid phase transition. Tables 3 and 4 summarize the temperature dependent data for Cor-PC and coronene, respectively. For each temperature studied, the fluorescence data for both coronene and Cor-PC were best described using a triple exponential decay function dominated by a

long lifetime component (τ_3). However, the long lifetime component for Cor-PC [τ_3(14°C)~125 ns], while long-lived, is short relative to pure coronene [τ_3(14°C)~223ns] in bilayers. This lifetime difference most probably arises from differences in the position of the coronenyl moiety within the bilayer, as discussed previously (see Section 3.5.1). For Cor-PC, the fluorophore is attached to a PC chain and is expected to reside at a location closer to the bilayer surface. In contrast, free coronene, due to its hydrophobic nature, will locate more towards the center of the bilayer, residing in a less polar environment. Previous studies with DPH in bilayers by the groups of Gratton [101] and Stubbs [102] have suggested that a polarity gradient exists down the acyl chain length of the phospholipids and across the bilayer width. As a consequence, the lifetime for Cor-PC will be correspondingly quenched. In any event, it is clear that this new fluorescent phospholipid adduct can provide sensitivity to 'slow' (submicrosecond) lipid dynamics.

The magnitude of the short and medium lifetime components (τ_1 and τ_2) observed for both coronene and Cor-PC are very similar (Tables 3 and 4). However, their relative contribution (f_1) to the exponential lifetime decay are different. For example, at 14°C, the fractional contribution (f_1) of τ_1 for Cor-PC is 2.9%, in contrast to 0.7% for coronene at the same temperature. Similarly, τ_2 for Cor-PC, contributes around 9.5% to fluorescence decay profile in contrast to 2.4% for coronene. The contribution of τ_1, τ_2 and τ_3 to the decay of Cor-PC in paraffin oil (Table 1) compares favorably with those observed here for Cor-PC in vesicles. This may reflect a similarity in solvent polarities for these two systems examined. In any event, for Cor-PC, the total contribution of the short and medium lifetime components to the fluorescence lifetime decay at 14°C (f_1 and f_2) represents 11.4%, compared with 3.6%

for coronene, and represents a minor component of the decay profile.

Measured fluorescence lifetimes, for both Cor-PC and coronene (Figure 36 and 37, respectively) are relatively insensitive to temperature, and do not vary significantly through the main gel-fluid phospholipid phase transition. The small decrease in the long decay component with increasing temperature may be attributed to simple thermal quenching effects, possibly arising from increased bilayer oxygen permeability with increasing temperature [103]. The shorter lifetime components (τ_1 and τ_2) appear unaffected by temperature.

Additionally, no temperature or lipid phase sensitivity can be associated with the fractional contributions of each lifetime to the decay. Hence there appears to be no association of lifetime with a particular gel (L_β) or fluid (L_α) lipid environment. The origins of the complicated multiexponential decay profile are thus unclear. However, other well studied fluorescence membrane probes, such as DPH and perylene, also demonstrate multi-exponential fluorescence decay profiles when embedded within lipid bilayer systems. For these cases, probe heterogeneity (where is the probe residing in the bilayer?) or environmental lipid heterogeneity, either positional (different bilayer dielectric gradients) or packing considerations (gel or fluid lipid), have been implicated. In the case of Cor-PC, heterogeneity of probe location has been excluded. Additionally, since the probe location is fixed, it is expected that bilayer dielectric gradients (e.g. from dissolved oxygen [103] or water penetration [101, 102]) would not play a significant role in the lifetime multiexponentiality of Cor-PC. In addition, there appears to be no sensitivity of the lifetime to gel-fluid lipid (as demonstrated by the almost constant preexponential terms with changing temperature). Thus

the origins for the multiexponential decay remain unclear, but are most likely to arise from lipid rather than probe heterogeneity.

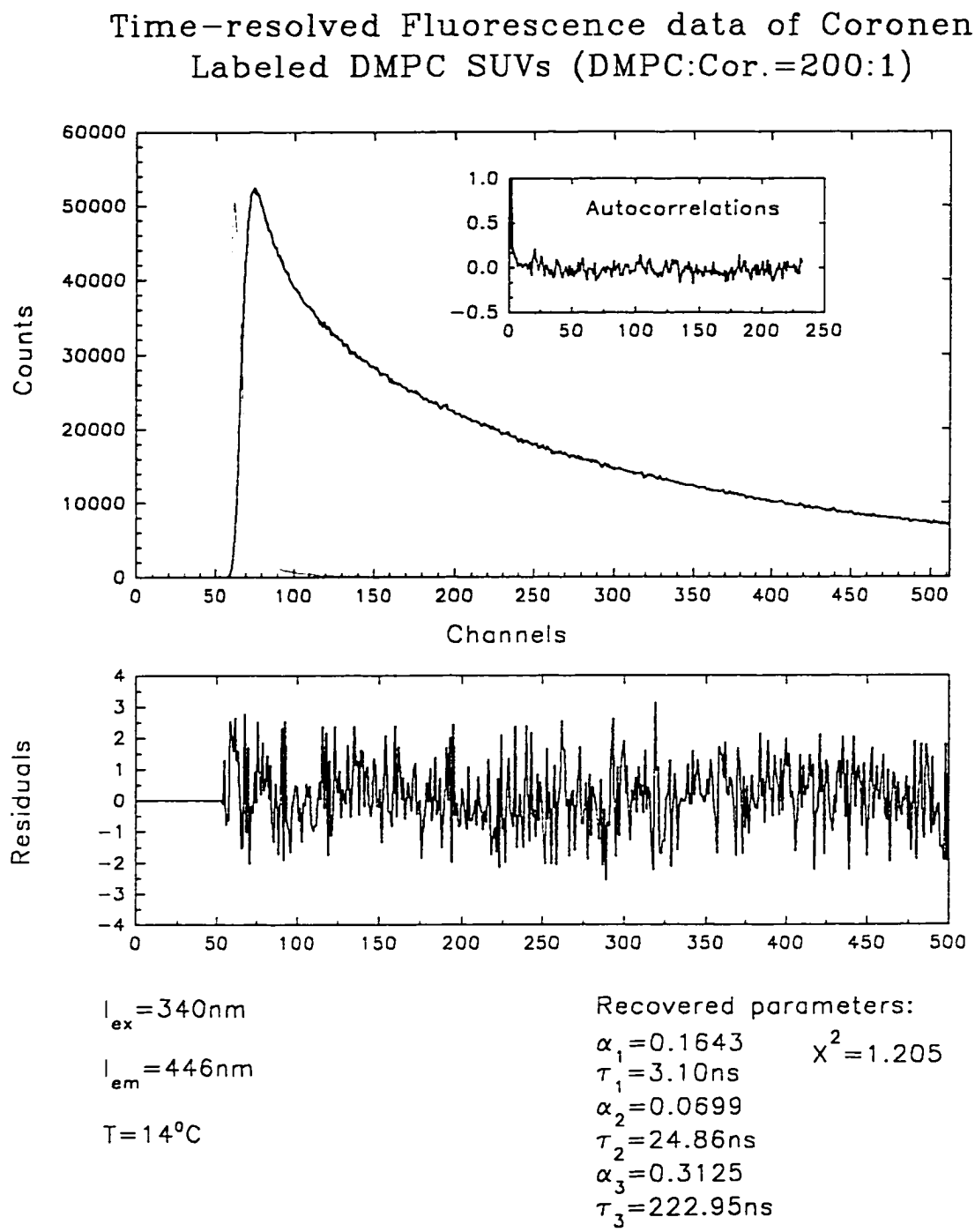

Figure 35. Fluorescence emission decay of coronene labeled DMPC SUVs. The excitation and emission wavelengths employed were 340 nm and 446 nm, respectively. The probe to phospholipid molar labeling ratio was 1:200 and the temperature was 14°C.

Table 3

Summary of Fluorescence Lifetime Analyses for Cor-PC labeled DMPC SUVs as a Function of Temperature

(DMPC:Cor-PC=100:1)

Temp. (°C)	[a]f_1	τ_1 (ns)	f_2	τ_2 (ns)	f_3	τ_3 (ns)	χ^2
8.0	0.0376	2.54	0.0892	22.99	0.8732	137.23	1.418
10.0	0.0296	2.47	0.0937	25.54	0.8768	126.83	1.209
14.0	0.0287	2.03	0.0954	26.23	0.8759	124.75	1.361
15.0	0.0383	2.47	0.0905	22.30	0.8712	130.39	1.268
17.5	0.0273	2.36	0.0974	27.15	0.8753	114.26	1.055
18.0	0.0301	2.19	0.0930	24.59	0.8769	114.93	1.304
20.0	0.0328	2.08	0.0972	23.56	0.8699	117.43	1.259
22.0	0.0322	2.06	0.0985	24.54	0.8693	110.15	1.190
25.0	0.0426	2.73	0.0990	23.68	0.8583	114.44	1.094
30.0	0.0368	2.06	0.1019	22.91	0.8616	106.67	1.485

[a]The fractional fluorescence contribution of each species to the total intensity is defined as $f_i = \alpha_i\tau_i/\Sigma_i\alpha_i\tau_i$, where $\Sigma_i\alpha_i\tau_i=1$. The values for α_i and τ_i were extracted from the fitting of the time-resolved fluorescence decay profile.

Table 4

Summary of Fluorescence Lifetime Analyses for Coronene Labeled DMPC SUVs as a Function of Temperature

(DMPC:Coronene = 200:1)

Temp. (°C)	f_1	τ_1 (ns)	f_2	τ_2 (ns)	f_3	τ_3 (ns)	χ^2
13.0	0.00327	3.22	0.01285	23.45	0.9839	228.62	1.101
14.0	0.00708	3.10	0.02416	24.86	0.9688	222.95	1.205
18.0	0.00734	2.82	0.02459	23.24	0.9681	203.59	1.454
22.0	0.00823	2.96	0.02583	23.30	0.9659	190.39	1.209
26.0	0.00850	2.82	0.02613	20.59	0.9653	171.07	1.268
30.0	0.00974	3.15	0.02791	22.17	0.9623	160.27	1.295

[a]The fractional fluorescence contribution of each species to the total intensity is defined as $f_i = \alpha_i\tau_i/\sum_i\alpha_i\tau_i$, where $\sum_i\alpha_i\tau_i=1$. The values for α_i and τ_i were extracted from the fitting of the time-resolved fluorescence decay profile.

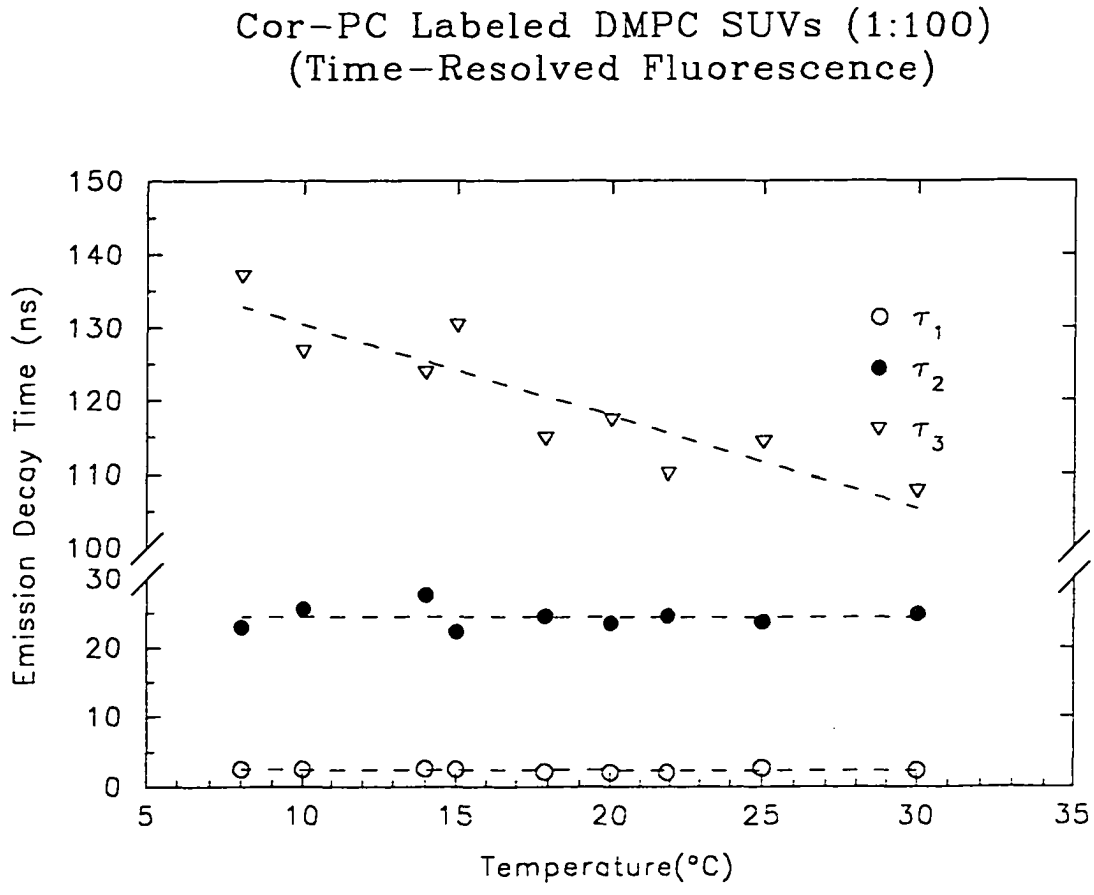

Figure 36. Fluorescence lifetimes of DMPC SUVs embedded Cor-PC, as a function of temperature. The excitation and emission wavelengths were 340 nm and 448 nm, respectively. The Cor-PC to DMPC molar labeling ratio was 1:100.

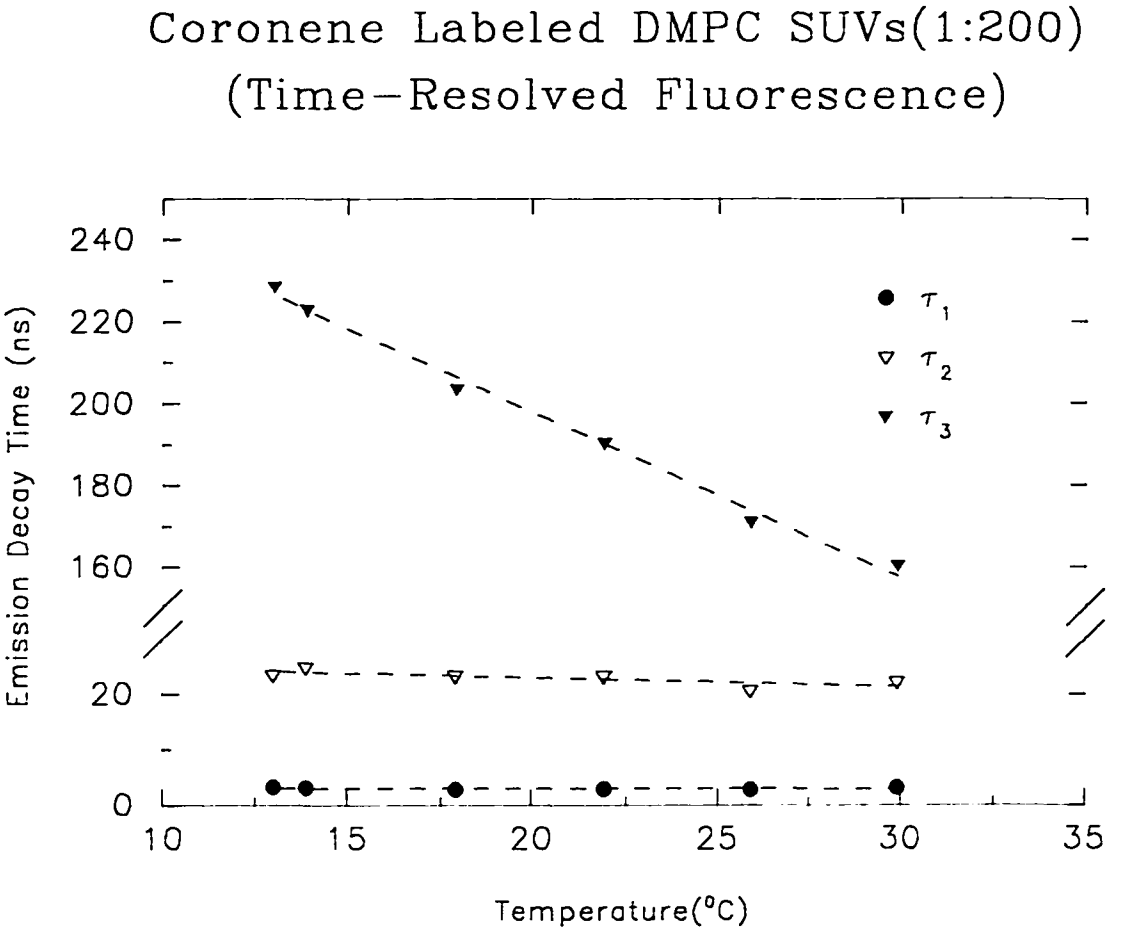

Figure 37. Fluorescence lifetimes of DMPC SUVs embedded coronene, as a function of temperature. The excitation and emission wavelengths were 340 nm and 448 nm, respectively. The coronene to DMPC molar labeling ratio was 1:200.

3.7.2. Fluorescence Emission Anisotropy Studies

Typical vertical and horizontal polarized decay profiles obtained for Cor-PC embedded within DMPC SUVs at 14°C, below the lipid T_c, are shown in Figure 38. Analysis of the difference decays $[I_{VV}(t) - I_{VH}(t)]$ as discussed previously (Section 2.6), revealed a biexponential anisotropy decay for both Cor-PC and coronene, with two rotational correlation times (ϕ_1 and ϕ_2) according to the expression:

$$r(t) = \beta_1 \cdot e^{\frac{-t}{\phi_1}} + \beta_2 \cdot e^{\frac{-t}{\phi_2}} \qquad (61)$$

where $\sum_j \beta_j = r_0$.

Time resolved emission anisotropy profiles for Cor-PC and coronene labeled DMPC SUVs were determined as a function of temperature. The results of the complete analyses are reported in Tables 5 and 6. The variations of the rotational correlation times with temperature are shown in Figures 39 and 40, respectively. For both probes, at all temperatures investigated (both above and below the phospholipid T_c), the TREA data were best fit using two discrete rotational correlation times, rather than a residual anisotropy term (r_∞). For short-lived probes embedded within anisotropic lipid bilayers, the rotational correlation times for the probe is longer than the measured fluorescence lifetime ($\phi >> \tau$). Hence equilibrium is not established, and a residual anisotropy term is expected.

The fast rotational correlation time, ϕ_1, for both coronene and Cor-PC appears relatively insensitive to the physical state of the bilayer (Figures 39 and 40). Origins of this fast rotational rate (ϕ^{-1}) are expected to be different for the two probes. For coronene, a long-

lived probe exclusively sensitive to out-of-plane depolarizing motions, the rotational behavior may be explained using a simple compartmental membrane model [5, 28] where the bilayer exists as a dynamic equilibrium of gel and fluid phase lipid. ϕ_1 may be assigned to those probes residing within the fluid phase lipid (F), and the associated preexponential term (β_1) now reflects the varying contribution of fluid phase lipid as a function of temperature. As expected, the contribution increases with increasing temperature (Table 6).

However, for Cor-PC, as previously suggested from paraffin oil studies (Section 3.2.2), because of the altered symmetry due to lipid anchoring, the probe is expected to demonstrate both in- and out-of-plane rotational motions with $r_0 \neq 0.1$, arising from rotations around the $-CH_2-$ bond to the butyric acid, and those associated with rotations of the coronene moiety anchor to the C_2 position on the glycerol backbone. Extraction of only two rotational rates suggests that certain rotational motions may either be very similar (reducing the system to the slipping boundary model, as used for the paraffin oil data, Section 3.2.2) or are not fully resolved due to widely disparate decay components, as suggested by non constant r_0 values (Table 5). Beechem, *et al.* [92, 104] have discussed the advantages of using two different instrument timing calibrations in combination with global analysis methods for overcoming this problem. Alternatively, use of other polyaromatic probes, such as benz-[ghi]-perylene, where the D_{6h} symmetry is also broken, or more restrictive tagging to the phospholipid through a vinyl group where probe rotation around the methylene group attached to the ring structure is excluded, would assist with in unraveling this complex rotational decay.

From Table 5 and Figure 39, the fast rotational correlation time (ϕ_1) for Cor-PC

appears to be independent of the physical state of the bilayer. For a simple anisotropic rotor, this term represents a complex sum of the diffusion rates, $D_{\parallel}$ and $D_{\perp}$ (Section 1.6.5). If ϕ_1 is constant, and ϕ_2 (which is directly proportional to $D_{\perp}$) is decreasing (Table 5), this suggests that $D_{\parallel}$ is also decreasing with temperature, which is physically unsatisfactory. Furthermore, the preexponential term β_1 associated with ϕ_1 reveals temperature dependence, decreasing with increasing temperature (for a compartmental model, the preexponential term would increase, as more fluid embedded probes result). Since the peexponential terms are functions of the angle between the absorption and emission dipoles, they are expected to be constant for a given excitation wavelength, and independent of temperature. These results, combined with a varying r_0 value across the temperature isotherm, strongly suggest that our simple anisotropic in-plane and out-of-plane rotational model as described for Cor-PC in paraffin oil, does not fully explain the rotational properties of the Cor-PC/lipid system. Most likely the in- and out-of-plane rotations are hindered or restricted to some extent ($r_{\infty ip} + r_{\infty op}$, respectively), particularly at lower temperatures, where $T \ll T_c$. Global analysis [92, 104] of the data, linking the preexponential beta terms for a fixed excitation wavelength across the temperature axis, can assist in unraveling complex bilayer systems.

For both coronene and Cor-PC, the second rotational correlation time ϕ_2, reveals high sensitivity to the phase transition of the phospholipid (Figures 39 and 40). Previously, it has been reported that for coronene in DPPC SUVs that ϕ_2 reflects the gel-fluid lipid fluctuation rate (k_{FG}) (Equation 46), which decreases in an almost linear fashion with increasing temperature [105]. In contrast, for Cor-PC, ϕ_2 presumably reflects out-of-plane rotational probe motions, although it is complicated since the β_2 terms are also sensitive to the phase

transition. As discussed previously, for a simple anisotropic rotor, this term is expected to be independent of temperature, unlike coronene with D_{6h} symmetry.

The change in ϕ_2 values for Cor-PC correspond well with the changes observed in the measured steady-state emission anisotropy values (Figures 19 and 20), confirming that long lived rotational events dominate the steady-state measurements, and are associated with bilayer dynamics which occur prior to the main lipid phase transition temperature, on a time scale of several tens of nanoseconds. Thus ϕ_2 reflects slow packing fluctuations among the acyl chains of the gel phospholipid bilayer and appears highly sensitive to any alteration in the physical state of the lipid packing. Above T_c, values for ϕ_2 are slower for Cor-PC compared with coronene, and may reflect more hindered rotations due to anchoring of the fluorophore.

The long fluorescence lifetime of the probe is an important factor in these studies, in order for the embedded probe to detect the structure and dynamics of the bilayer occurring well after its excitation. This effect has been previously observed for fluorophores which have lifetimes that may be associated with two different rotational environments. Here the fluorescence emission anisotropy decay, as $t \rightarrow \infty$, is dominated by the rotations of the long-lived fluorescence species [25].

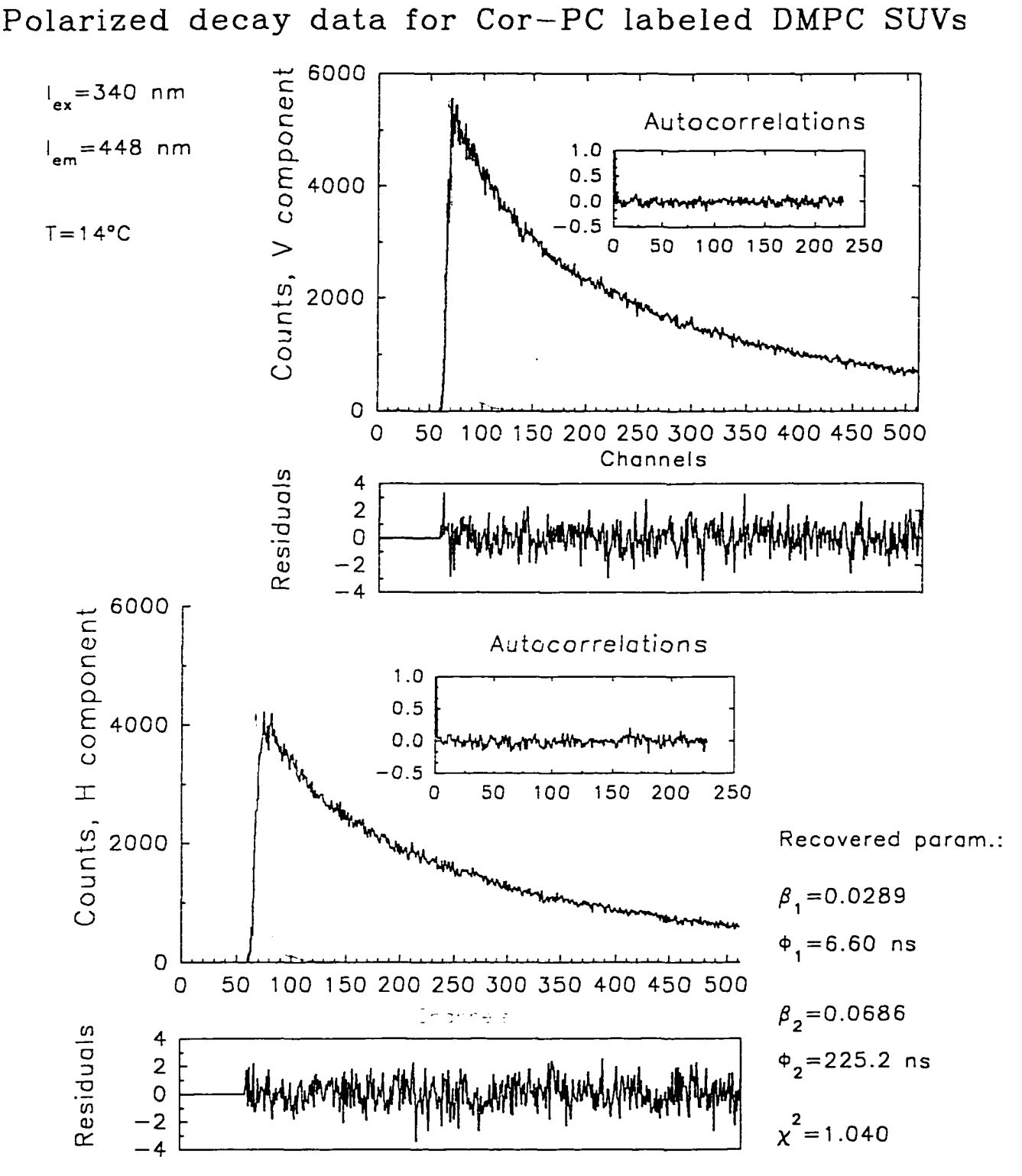

Figure 38. Vertical and horizontal components of the polarized emission decay from Cor-PC embedded inside the DMPC SUVs. The temperature was 14°C.

Table 5

Rotational Correlation Time of Cor-PC Labeled DMPC SUVs Measured at Different Temperatures.

Temp. (°C)	β_1	ϕ_1 (ns)	β_2	ϕ_2 (ns)	$r_0=\beta_1+\beta_2$	χ^2
8.0°C	0.1335	2.63	0.0706	299.39	0.2041	1.271
10.0°C	0.1496	1.66	0.0763	266.11	0.2259	1.070
12.5°C	0.1333	2.46	0.0673	242.05	0.2006	1.310
14.0°C	0.1370	2.02	0.0686	225.17	0.2056	1.420
15.0°C	0.1120	3.88	0.0520	193.25	0.1640	1.346
17.9°C	0.1052	3.79	0.0604	130.72	0.1656	1.194
20.0°C	0.1249	2.25	0.0544	44.02	0.1793	1.350
22.0°C	0.1096	2.01	0.0551	28.11	0.1647	1.030
25.0°C	0.1050	2.52	0.0460	23.77	0.1510	1.096
30.0°C	0.1656	2.38	0.0397	42.89	0.2053	1.508

Table 6

Rotational Correlation Time of Coronene Labeled DMPC SUVs Measured at Different Temperatures.

Temp. (°C)	β_1	ϕ_1 (ns)	β_2	ϕ_2 (ns)	$r_0=\beta_1+\beta_2$	χ^2
13.0°C	0.0709	1.23	0.0650	291.02	0.1359	1.036
14.0°C	0.0447	1.84	0.0624	229.42	0.1071	1.049
18.0°C	0.0775	1.85	0.0618	174.16	0.1393	1.337
22.0°C	0.0868	2.26	0.0446	80.08	0.1314	1.319
26.0°C	0.0859	1.53	0.0517	15.51	0.1346	1.150
30.0°C	0.0881	1.56	0.0508	7.71	0.1389	1.102

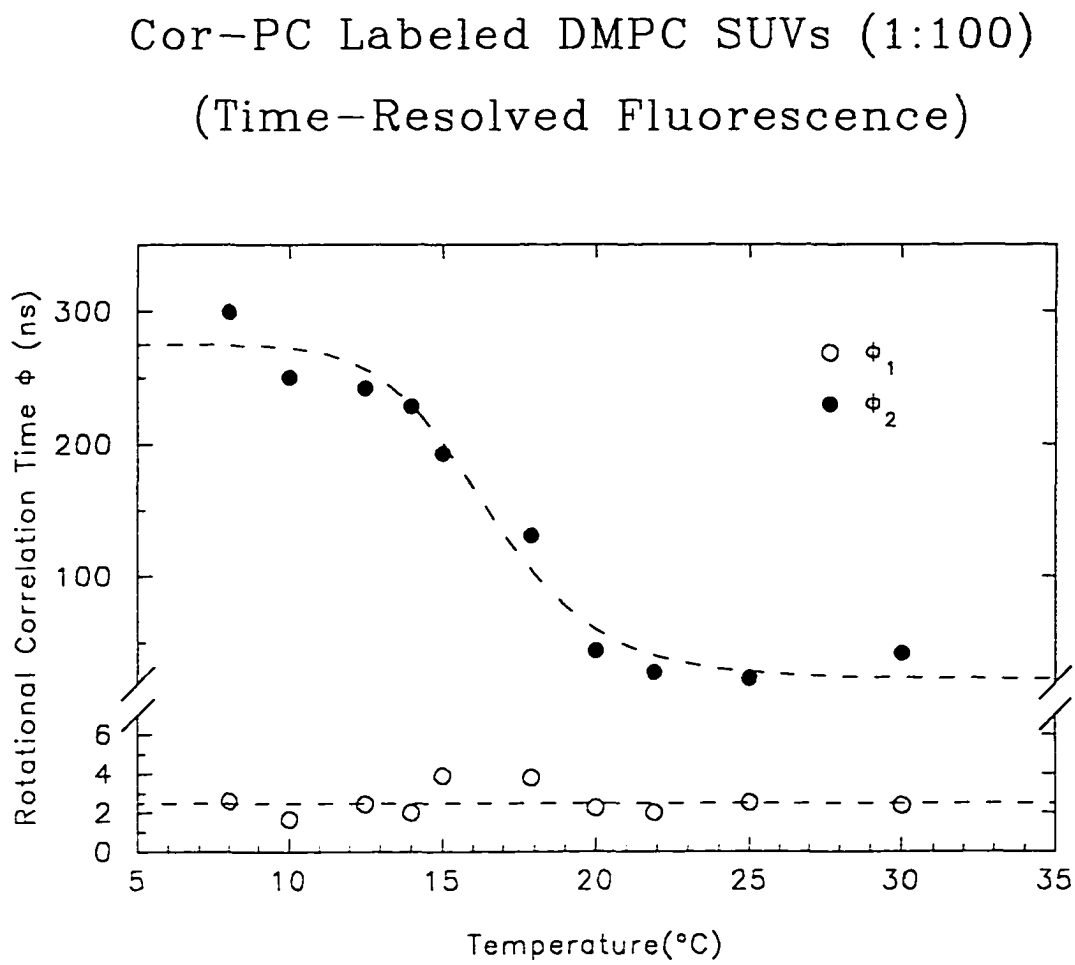

Figure 39. Rotational correlation times for Cor-PC labeled DMPC SUVs as a function of temperature: the excitation and emission wavelengths were 340 nm and 448 nm, respectively. Cor-PC to DMPC labeling ratio was 1:100.

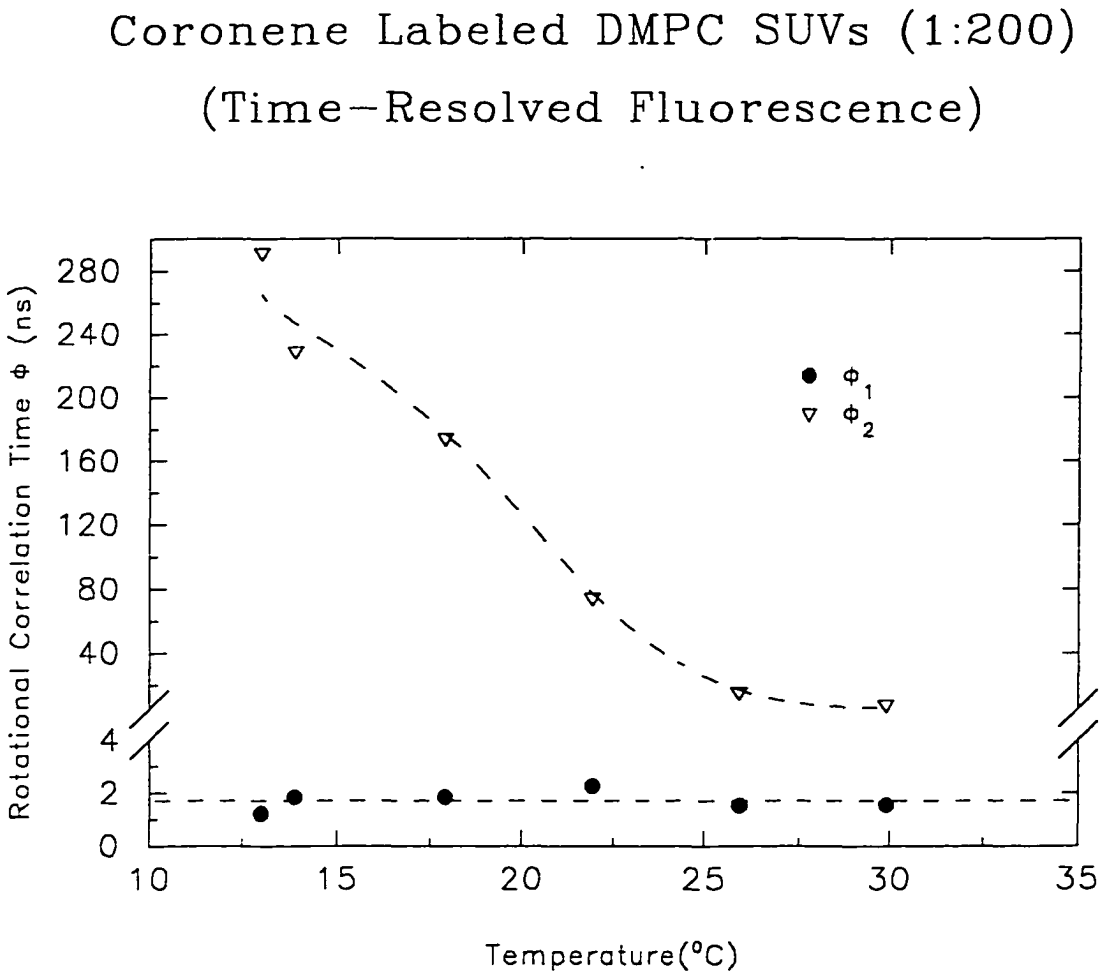

Figure 40. Rotational correlation times for coronene labeled DMPC SUVs as a function of temperature: the excitation and emission wavelengths were 340 nm and 448 nm respectively. Coronene to DMPC labeling ratio was 1:200.

3.7.3. DPH in Lipid Bilayers

As a comparison, time-resolved fluorescence decay and emission anisotropy decays of the short-lived probe DPH embedded within DMPC SUVs were also measured at temperatures of 14°C and 35°C. The intensity decay data were analyzed using a double exponential decay function:

$$I(t) = \alpha_1 \cdot e^{\frac{-t}{\tau_1}} + \alpha_2 \cdot e^{\frac{-t}{\tau_2}} \qquad (62)$$

The experimental difference decay data [$D(t) = I_{VV}(t)G - I_{HV}(t)$] were analyzed as a single rotational correlation time plus a residual anisotropy term (this was performed experimentally by fixing a rotational correlation time with ϕ=10000 nsecs):

$$r(t) = \beta_1 \cdot e^{\frac{-t}{\phi_1}} + \beta_2 \qquad (63)$$

The data are shown in Table 7, and reveal that the fluorescence lifetime for DPH is insensitive to the phase transition of DMPC lipid bilayer. In contrast, the rotational motions of this probe (β_1, β_2 and ϕ_2) are sensitive to the physical state and phase transition of DMPC lipid bilayers, as previously reported elsewhere [56, 91]. Thus, unlike coronene and Cor-PC, long-lived lipid dynamics occurring in the gel phase below T_c are hidden in the residual anisotropy term for DPH.

Table 7a

Fluorescence Lifetime of DPH Labeled DMPC SUVs

Measured at Different Temperatures

Temp (°C)	[a]f_1	τ_1 (ns)	f_2	τ_2 (ns)	$<\tau>$	χ^2
14.0°C	0.2222	6.611	0.7778	11.563	10.463	1.060
35.0°C	0.1124	4.594	0.8876	8.891	8.408	1.196

[a]The fractional fluorescence contribution of each species to the total intensity is defined as $f_i = \alpha_i\tau_i/\Sigma_i\alpha_i\tau_i$.

Table 7b

Fluorescence Rotational Correlation Time of DPH Labeled DMPC SUVs

Measured at Different Temperatures

Temp (°C)	β_1	ϕ_1 (ns)	β_2	ϕ_2 (ns)	$r_0=\beta_1+\beta_2$	χ^2
14.0°C	0.0860	5.262	0.2363	∞	0.3223	1.059
35.0°C	0.2620	1.386	0.0568	32.843	0.3188	1.149

3.8. Time-Resolved Studies of Melittin-Containing Lipid Samples

3.8.1. Cor-PC and Coronene Labeled Samples

The effects of the simple peptide melittin on the time-resolved fluorescence and emission anisotropy decays of Cor-PC and coronene labeled DMPC SUVs (14°C) were determined for varying melittin concentrations (0.1 to 2 mole%). Gel-phase lipid was chosen for these studies as both Cor-PC and coronene exhibit sensitivity to submicrosecond lipid dynamics occurring within this lipid phase.

Again, a complex three lifetime decay profile was resolved for both Cor-PC and coronene labeled SUV systems (compare Equation 60). The lifetime data are summarized in Tables 8 and 10a, respectively. Interestingly, comparison of the melittin/Cor-PC labeled systems with those containing no peptide (Table 5), reveals that the emission decay times for Cor-PC and their relative contribution to the decay, is apparently unaffected by the presence of melittin within the lipid bilayers (Figure 41). Similarly, no significant detectable effect was observed for the effect of melittin on the fluorescence decay profile of coronene. These results suggest that no energy transfer or quenching (dynamic or static) effects appear to arise from any direct peptide-probe interactions.

However, while the decay of the emission anisotropy for both Cor-PC and coronene in DMPC/SUVs at 14°C as a function of increasing melittin concentrations revealed a biexponential decay function (see Equation 61) as previously determined for non-peptide containing lipid systems, addition of melittin to the bilayer has significant consequences on the rotational behavior of both Cor-PC and coronene. The emission anisotropy data are shown in Tables 9 and 10b for Cor-PC and coronene, respectively.

For Cor-PC, with increasing mole ratios of melittin to lipid, the slower rotational correlation time (ϕ_2) increases dramatically (Figure 42), confirming that the addition of melittin to the bilayer results in a more rigid or ordered phospholipid structure, as detected by decreased submicrosecond out-of-plane rotations of the probe. For Cor-PC, the magnitude of the fast rotational correlation time (ϕ_1), as previously observed in the non-peptide vesicles cases (Table 5), is invariant to the presence of peptide.

Careful examination of the preexponential terms associated with the two measured rotational motions observed for Cor-PC in the presence of peptide suggest that preexponential terms β_1 and β_2 are relatively independent of melittin concentration. As discussed previously, for a fixed excitation wavelength, the preexponential terms, which are related to the angles between the excitation and emission oscillators, are expected to be independent of peptide concentration (or temperature). However, as discussed above (Section 3.5.2), the fluctuating r_0 terms (which additionally are different from non peptide containing bilayer samples) suggest that the rotational behavior of Cor-PC may not be a simple anisotropic rotor as for perylene [62] and pyrene [100], and rotational hindrance is likely to exist.

Interpretation of the rotational data for coronene is somewhat simpler due to the symmetry of this planar molecule which results in out-of-plane rotational motions only. According to the compartmental model previously described [105], the fast rotational time (ϕ_1) may be attributed to the fluid phase lipid, and the associated preexponential term (β_1) represents the contribution of probes to the decay which reside in the fluid phase. With increasing melittin concentration, this preexponential term is expected to decrease as the

bilayer becomes more ordered or 'gel'-like with addition of melittin. For the rather limited melittin range (Table 10b) covered in this coronene study (1:1000 to 1:200), the value for β_1 suggests a decrease with increasing melittin concentration.

In accordance with a simple gel-fluid compartmental model which defines a discrete gel-fluid fluctuation rate, k_{GF} (denoted by ϕ_2^{-1}), the observed small decrease in this rotational rate implies a rather weak sensitivity of this rotational motion to the presence of peptide, although the bilayer must now exist in a more rigid or ordered state as the preexponential term associated with ϕ_2, reveals a slight increase with increasing melittin concentration.

The relative insensitivity of ϕ_2 for coronene over Cor-PC to the presence of melittin may arise for two reasons. In the first, addition of peptide may result in distribution of coronene in the bilayer changing and becoming more localized away from the effects of the peptide. Alternatively, if the probe distribution is unaltered (and no changes in lifetime are observed with melittin), the small changes in ϕ_2 may reflect that the magnitude of k_{FG} is only marginally affected by the presence of peptide, which implies that k_{GF} increases, leading to a higher mole fraction of gel lipid (Equation 46). This important finding suggests that peptides can significantly affect or modulate bilayer dynamics and their effect may only be observed on the submicrosecond time scale. Further, out-of-plane rotational motions for both Cor-PC and coronene appear to be exquisitely sensitive to the physical state of the bilayer.

Here, once again, the 'time window' of the fluorescence probe is critical for the investigation packing or dynamics of lipid bilayers. Since lipid relaxation times or bilayer fluctuations (gel-fluid exchange) are reported to be on the scale of 10^{-7} second [96, 105], the long mean fluorescence lifetime of both coronene and/or Cor-PC ensures that the rotational

motions of these probes can be exploited for lipid fluctuation studies, with Cor-PC having the added advantage that its reports on a more localized bilayer environment. Our studies show that submicrosecond lipid fluctuations are significantly affected by incorporation of peptide into the lipid bilayers, reflected by large changes in the rotational properties of Cor-PC embedded in DMPC SUVs. Cor-PC provides an ideal new and sensitive localized fluorescent probe for investigating submicrosecond lipid dynamics and their modulation, which may have profound biological importance for controlled passive or active membrane transport processes.

Table 8

Fluorescence Emission Decay Times of Cor-PC Labeled DMPC SUVs at Different Concentrations of Melittin

(DMPC:Cor-PC = 100:1, T = 14°C)

[DMPC]/ [MLT]	[a]f_1	τ_1 (ns)	f_2	τ_2 (ns)	f_3	τ_3 (ns)	χ^2
1000:1	0.0321	1.92	0.1266	22.52	0.8413	115.37	1.096
500:1	0.0329	2.22	0.0911	23.38	0.8760	116.54	1.349
300:1	0.0366	2.32	0.0891	21.90	0.8743	118.10	1.793
200:1	0.0361	2.59	0.0850	21.11	0.8789	115.63	1.300
100:1	0.0288	1.53	0.0792	21.41	0.8919	114.22	1.256
50:1	0.0240	1.74	0.0972	26.15	0.8788	117.52	1.072

[a]The fractional fluorescence contribution is defined as $f_i = \alpha_i\tau_i/\Sigma_i\alpha_i\tau_i$.

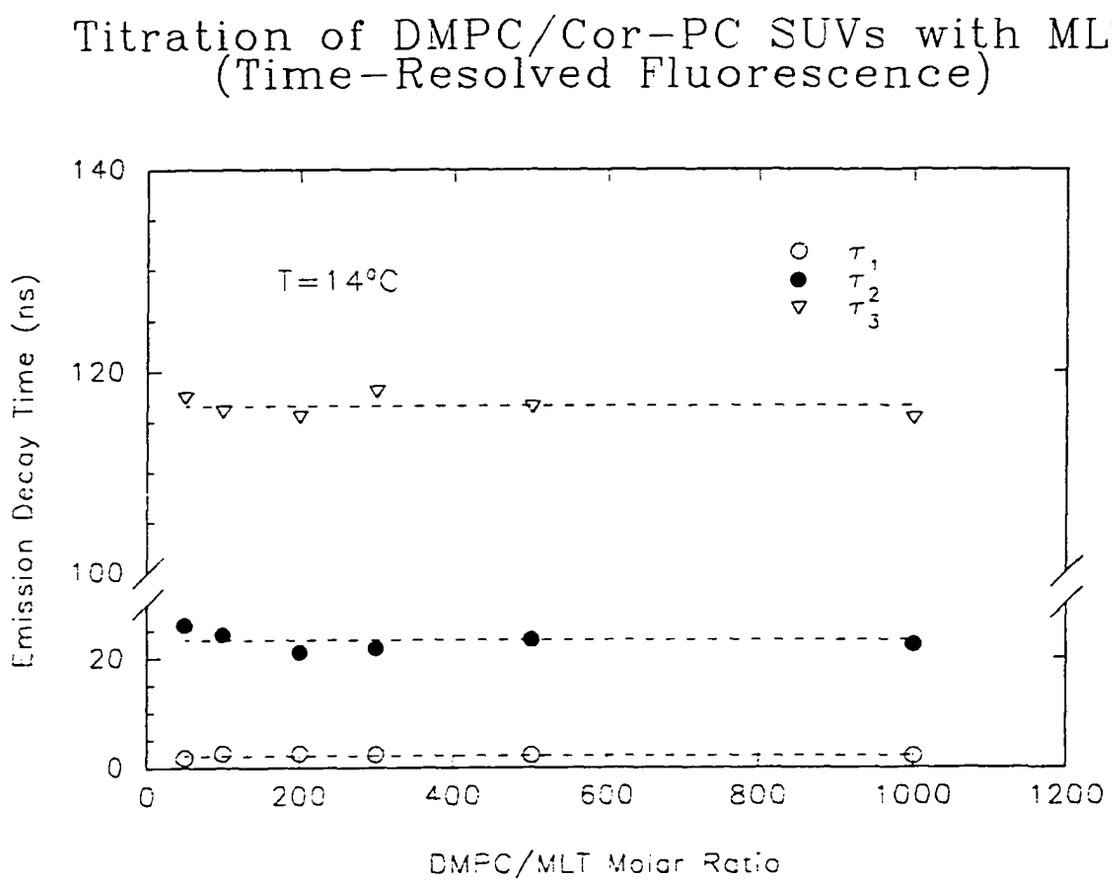

Figure 41. The emission decay time for Cor-PC labeled DMPC SUVs as a function of melittin concentration. The excitation and emission wavelengths were 340 nm and 448 nm, respectively. The Cor-PC to DMPC labeling ratio was 1:100.

Table 9

Rotational Correlation Times of Cor-PC Labeled DMPC SUVs

at Different Concentrations of Melittin

(DMPC:Cor-PC = 100:1; T = 14°C)

[DMPC]/ [MLT]	β_1	ϕ_1 (ns)	β_2	ϕ_2 (ns)	$\beta_1+\beta_2$	χ^2
1000:1	0.0715	2.80	0.0700	157.12	0.1415	1.128
500:1	0.0960	1.68	0.0665	136.91	0.1625	1.225
300:1	0.0421	0.85	0.0713	352.56	0.1134	1.077
200:1	0.0775	2.01	0.0828	419.43	0.1603	1.307
100:1	0.1005	1.85	0.0882	460.96	0.1887	1.089
50:1	0.1103	1.97	0.0736	520.90	0.1839	0.970

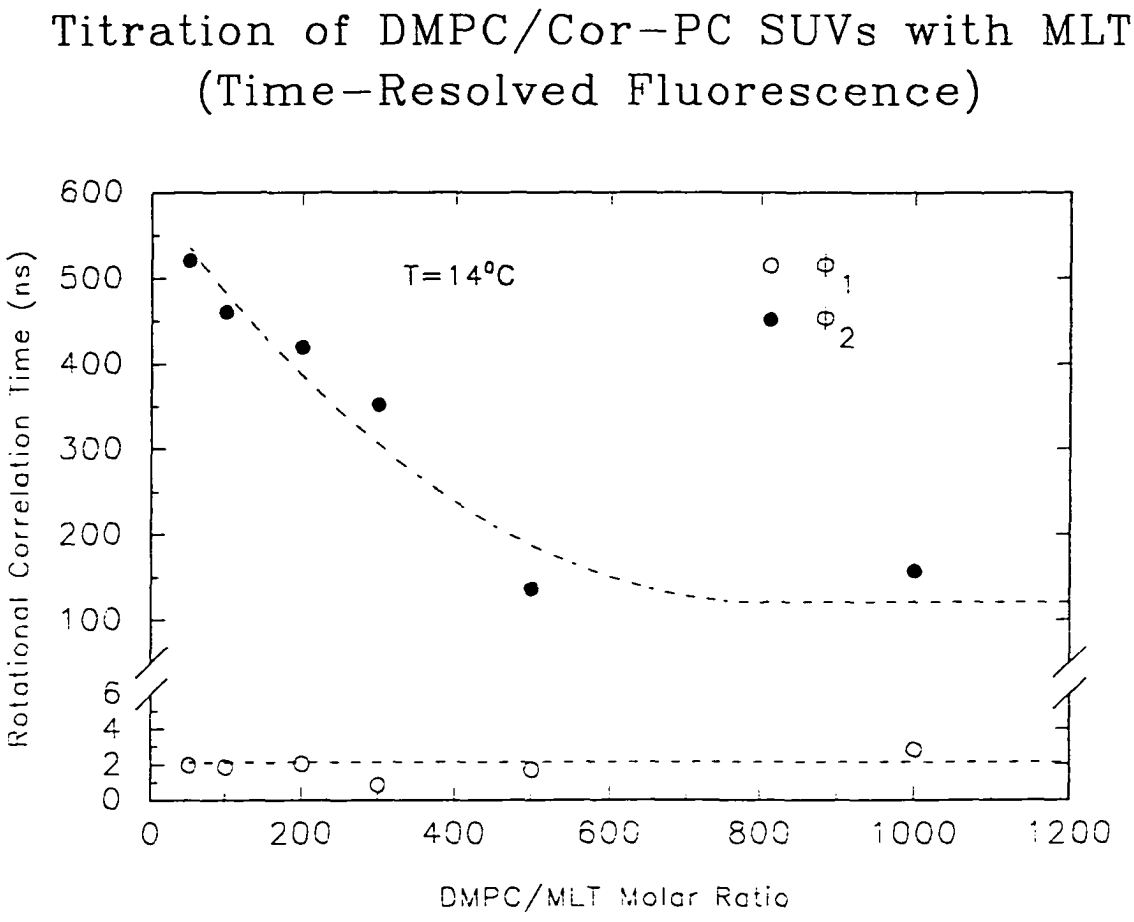

Figure 42. Rotational correlation times for Cor-PC labeled DMPC SUVs as a function of melittin concentration. The excitation and emission wavelengths were 340 nm and 448 nm, respectively. The Cor-PC to DMPC labeling ratio was 1:100.

Table 10a

Fluorescence Lifetimes for Coronene Labeled DMPC SUVs with Varying Melittin Concentration

(DMPC:Coronene = 200:1; T = 14°C)

[DMPC]/ [MLT]	[a]f_1	τ_1 (ns)	f_2	τ_2 (ns)	f_3	τ_3 (ns)	χ^2
1000:1	0.0082	2.279	0.0191	29.739	0.9727	234.62	1.078
750:1	0.0059	2.010	0.0198	24.692	0.9743	234.08	1.113
200:1	0.0056	2.340	0.0242	30.701	0.9702	243.78	1.140

[a]The fractional fluorescence contribution is defined as $f_i = \alpha_i\tau_i/\sum_i\alpha_i\tau_i$.

Table 10b

Rotational Correlation Times for Coronene Labeled DMPC SUVs with Varying Melittin Concentration

(DMPC:Coronene = 200:1; T = 14°C)

[DMPC]/ [MLT]	β_1	ϕ_1 (ns)	β_2	ϕ_2 (ns)	$r_0=\beta_1+\beta_2$	χ^2
1000:1	0.0117	4.41	0.0669	236.46	0.0786	1.092
750:1	0.0197	8.06	0.0682	247.82	0.0879	0.977
200:1	0.0107	6.01	0.0712	294.03	0.0819	0.983

3.8.2. DPH and Melittin in Bilayers

The fluorescence lifetime and emission anisotropy decay behavior of DPH labeled DMPC vesicles has been previously studied by many authors [86, 91]. Our interest here is focused on the effects of melittin on these decay parameters, and to determine to what extent a shorter-lived fluorescence probe reveals sensitivity to the effect of this peptide within the bilayer.

Experimental time-resolved emission decay and emission anisotropy decay data were obtained for DPH labeled DMPC SUVs in the presence of varying melittin concentrations. The intensity decay data were analyzed (as before, Section 3.4.2) using a double exponential decay function:

$$I(t) = \alpha_1 \cdot e^{\frac{-t}{\tau_1}} + \alpha_2 \cdot e^{\frac{-t}{\tau_2}} \qquad (64)$$

And the experimental difference decay data [$D(t) = I_{VV}(t)G - I_{HV}(t)$] were analyzed as a single rotational correlation time plus a residual anisotropy term ($r_\infty \equiv \beta_\infty$):

$$r(t) = \beta_1 \cdot e^{\frac{-t}{\Phi_1}} + \beta_\infty \qquad (65)$$

The results obtained for the experiments are summarized in Tables 11 and 12.

Table 11

Fluorescence Emission Decay Times for DPH Labeled DMPC SUVs at Different Melittin Concentrations

(DMPC:DPH = 500:1, 14°C)

[DMPC] /[MLT]	[a]f_1	τ_1(ns)	f_2	τ_2(ns)	[b]$\langle\tau\rangle$	χ^2
No MLT	0.2155	6.562	0.7845	11.527	10.457	1.050
No MLT	0.2289	6.660	0.7711	11.600	10.461	1.060
1000:1	0.0586	4.535	0.9414	11.193	10.803	1.052
600:1	0.0741	4.416	0.9259	11.603	11.071	1.212
300:1	0.0741	4.292	0.9259	11.403	10.998	1.129
120:1	0.0457	4.176	0.9543	11.117	10.800	1.070
30:1	0.0492	3.776	0.9508	10.813	10.466	1.012

[a]The fractional fluorescence contribution is defined as $f_i = \alpha_i\tau_i/\Sigma_i\alpha_i\tau_i$.

[b]The average lifetime $\langle\tau\rangle$ is defined $\Sigma_i(\alpha_i\tau_i^2)/\Sigma_i(\alpha_i\tau_i)$.

Table 12

Rotational Correlation Times for DPH Labeled DMPC SUVs

at Different Melittin Concentration

(DMPC:DPH = 500:1, 14°C)

DMPC:MLT	β_1	ϕ_1(ns)	β_∞	ϕ_2(ns)	$r_0=\beta_1+\beta_\infty$
No MLT	0.0860	5.262	0.2363	∞	0.3223
No MLT	0.0978	4.128	0.2344	∞	0.3322
1000:1	0.0977	4.124	0.2345	∞	0.3322
600:1	0.0550	3.892	0.2814	∞	0.3364
300:1	0.0288	2.996	0.2920	∞	0.3201
120:1	0.0209	2.990	0.3006	∞	0.3215
30:1	0.0188	4.178	0.3110	∞	0.3298

The fluorescence emission decay of DPH embedded within the DMPC bilayers can adequately be described in terms of double exponential. The fluorescence lifetime of DPH is essentially unaffected by the addition of melittin to DMPC/DPH SUVs (Figure 43). Only at high melittin concentrations is the fluorescence lifetime of DPH quenched a little by the presence of melittin.

The emission anisotropy decay was fitted using a single correlation time plus a constant (r_∞) term. At 14°C, the emission anisotropy of DPH initially decays rapidly to an r(t) value around 0.235 for DMPC SUVs without melittin. The rotational correlation time ϕ_1 remains constant with increasing melittin concentration (Figure 44). However, β_1 decreased and β_∞ increased with addition of melittin, although $\beta_1 + \beta_\infty$ ($\equiv r_0$) remained constant (Figure 45). Thus melittin does impact on the time-dependent rotational properties of DPH, resulting in increased hindered rotations, indicating a more ordered bilayer system.

The rotational motions of DPH embedded in the membrane bilayer can be approximated using a 'wobbling-in-a-cone' model in which the major axis of the probe is assumed to wobble freely within a cone of semiangle θ_c around the normal of the bilayer, with a wobbling diffusion constant D_w [106, 107]. The motion of DPH may now be described by two experimentally determined parameters, D_w (rate) and θ_c (range), which reflect the motion of neighboring lipid hydrocarbon chains and their barrier to probe rotations (or ordering). The cone angle θ_c is calculated from β_∞ by using the following equation [106, 107].

$$\frac{\beta_\infty}{(\beta_1 + \beta_\infty)} = \frac{\cos^2\theta_c(1+\cos\theta_c)^2}{4} \qquad \textbf{(66)}$$

We can see that β_a increases with increasing melittin concentration at 14°C (Figure 45), and the corresponding values for θ_c decrease. Table 13 shows the calculated $_c\theta$ at different melittin concentrations. The decrease in θ_c values reflects the restricted motion of DPH with increasing melittin concentration. This can be rationalized in terms of a more ordered lipid bilayer in the presence of peptide.

By comparison of TREA data for coronene and Cor-PC labeled DMPC SUVs *versus* DPH labeled DMPC SUVs titrated with melittin, we see that the rotational correlation times ϕ_1 and ϕ_2 of DPH are not sensitive to the submicrosecond dynamic changes within the lipid bilayer induced by melittin, whereas the rotational correlation time ϕ_2 for coronene and Cor-PC are very sensitive to submicrosecond dynamic events of the lipid bilayer.

For Cor-PC and coronene labeled DMPC SUVs, the fluorescence lifetimes (τ_1, τ_2 and τ_3) of these probes are not affected by titration with melittin (Table 8 and 10a). The rotational correlation time ϕ_2 is sensitive to peptide induced submicrosecond dynamic fluctuations within lipid bilayers (Table 9 and 10b). However, coronene may be less sensitive to the structure and dynamic change of lipid bilayer than Cor-PC due to its unfixed position within the lipid bilayer.

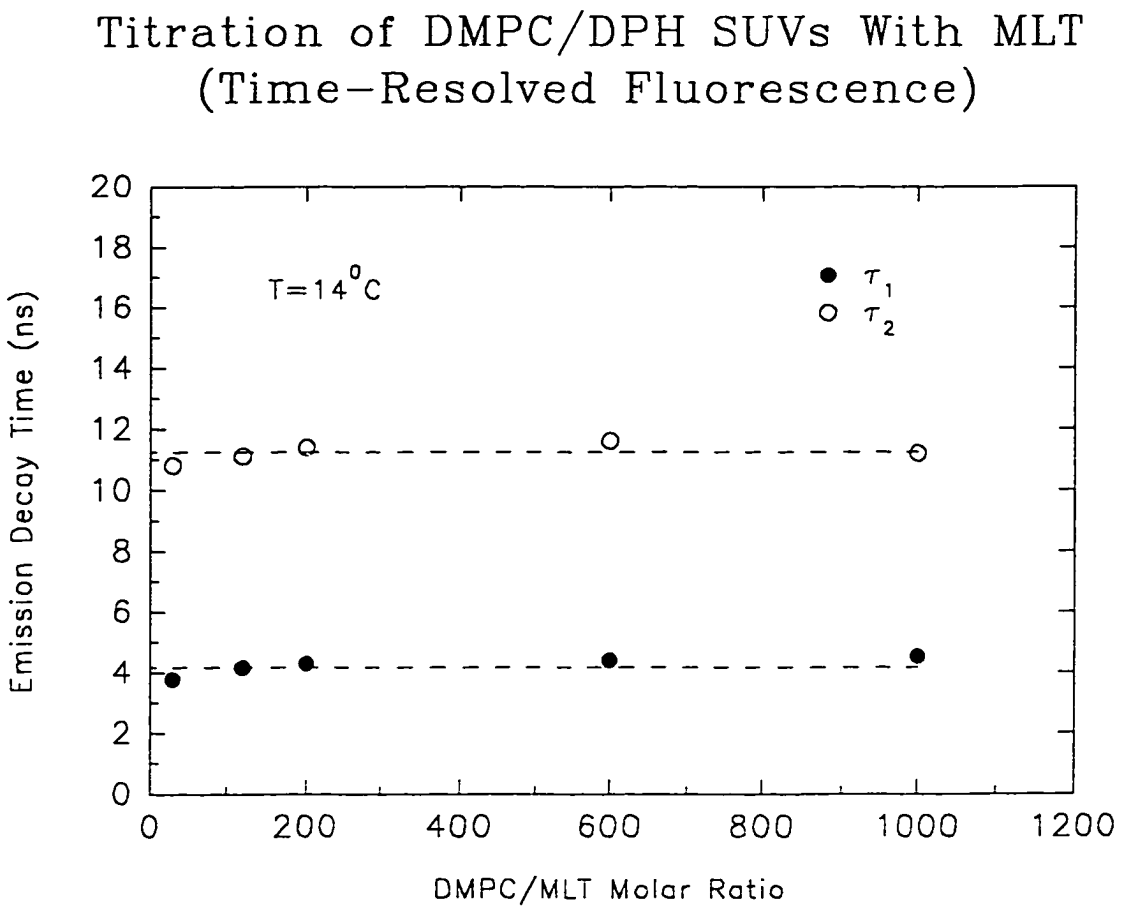

Figure 43. Fluorescence emission decay times for DPH labeled DMPC SUVs as a function melittin concentration. The excitation and emission wavelengths were 340 nm and 430 nm, respectively. DPH to DMPC labeling ratio was 1:500.

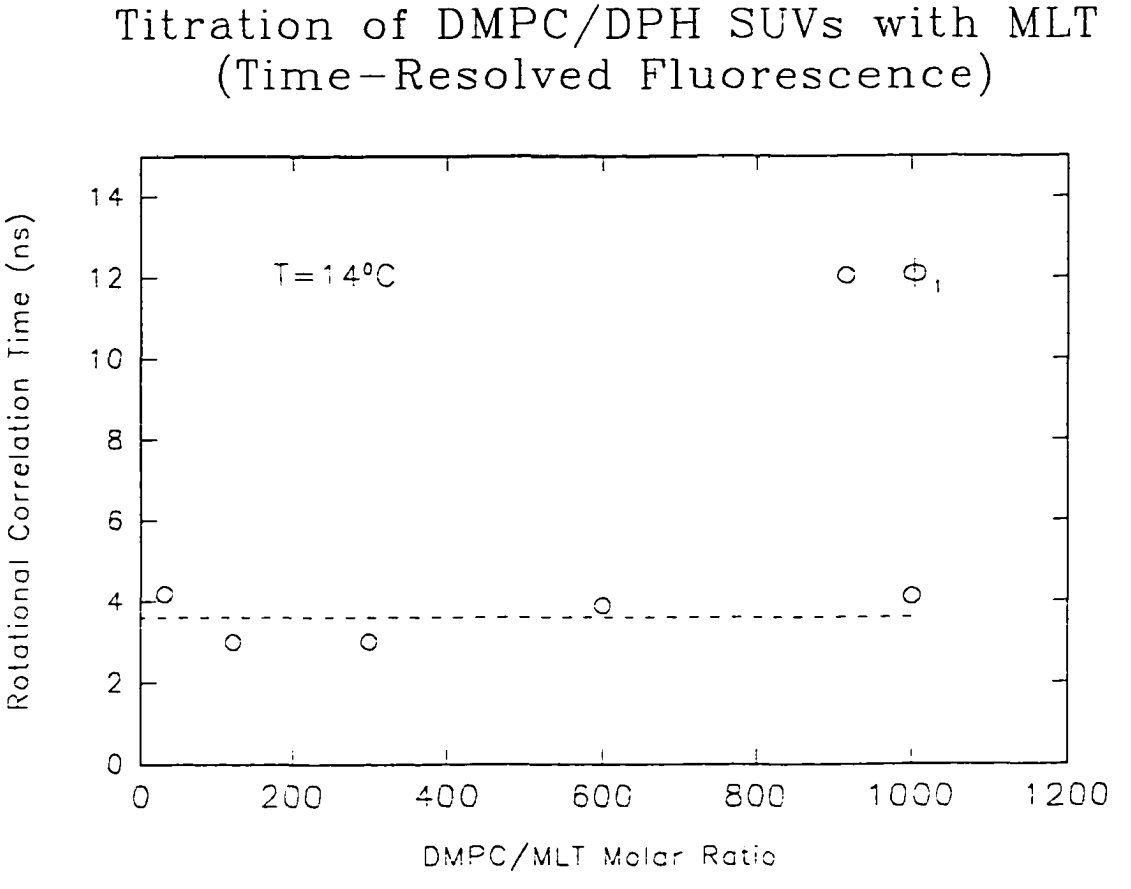

Figure 44. The rotational correlation time (ϕ_1) of DPH labeled DMPC SUVs as a function of melittin concentration: the excitation and emission wavelengths were 340 nm and 430 nm, respectively. DPH to DMPC labeling ratio was 1:500.

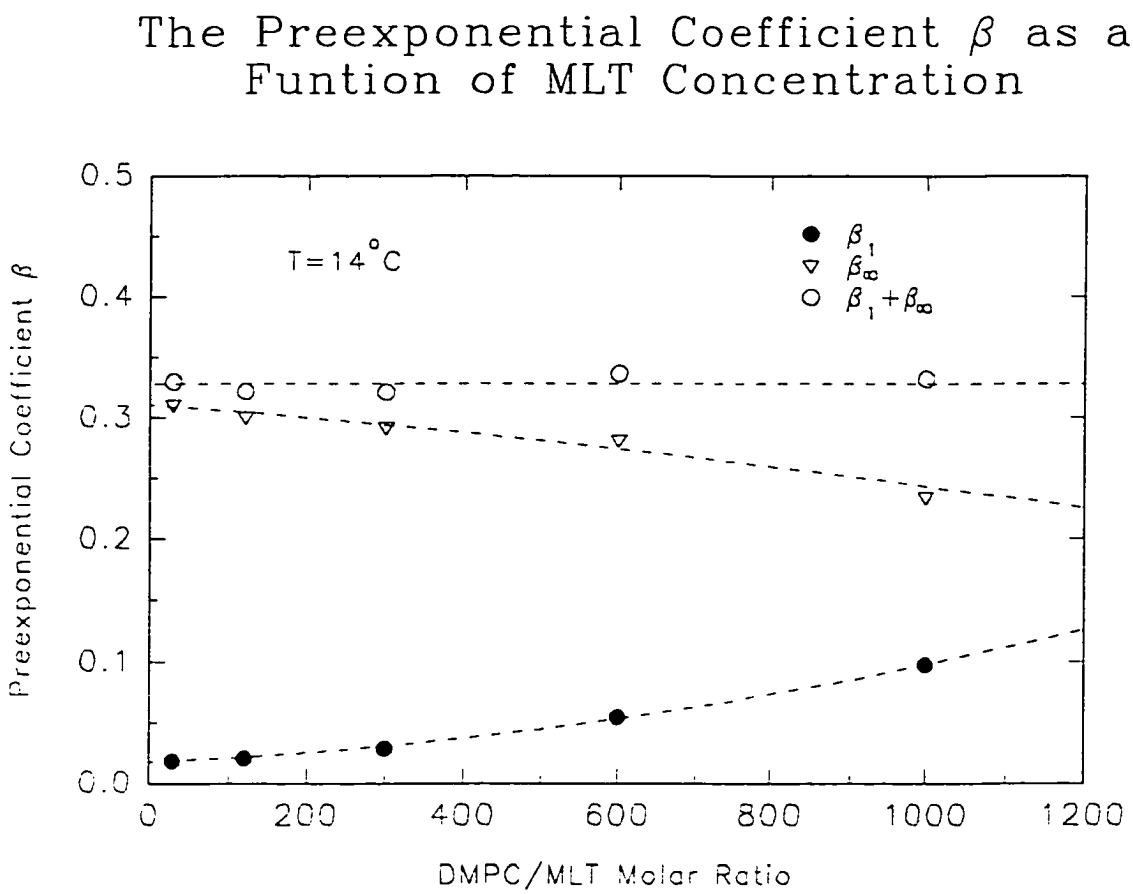

Figure 45. The pre-exponential coefficient (β) for DPH labeled DMPC SUVs as a function of melittin concentration. The excitation and emission wavelengths were 340 nm and 430 nm respectively. The DPH to DMPC labeling ratio was 1:500.

Table 13

The Calculated Semiangle θ_C (of a cone) for DPH Labeled DMPC SUVs at Different Melittin Concentrations

(DMPC:DPH = 500:1, T = 14°C)

Melittin Concentration	$\beta_{\perp}/(\beta_{\parallel} + \beta_{\perp})$	θ_C (radians)
No Melittin	0.7055	27.23
1:1000	0.7059	27.19
1:600	0.8365	19.62
1:300	0.9102	14.29
1:120	0.9350	12.10
1:30	0.9430	11.30

4. Summary

Fluorescent molecules have long been used to probe bilayer structure and dynamics. In this study, we have employed a new class of rotationally sensitive, long-lived fluorescence molecules (<τ>~200 ns) to probe the bilayer structure, particularly bilayer dynamics and changes arising from the interaction of a small peptide, on the *submicrosecond* time scale. The synthesis of a new phospholipid adduct, 4-coronenyl butyric-phosphatidylcholine (Cor-PC), proved successful and was obtained in high yield. Application of this novel fluorescence phospholipid probe to the study of localized peptide-lipid interactions was performed.

The new Cor-PC probe has the advantage over free coronene in that the position of the fluorophore within the lipid bilayer structure may be predicted and is fixed within the acyl chain region of bilayer. Indeed, fluorescence quenching experiments of lipid embedded Cor-PC and coronene using iodide anion suggest that coronene is buried deeper within the bilayer compared with Cor-PC, since the percentage of Cor-PC accessible to extrinsic quencher (I^-) within DMPC SUVs is greater than for embedded coronene. Thus, differences in rotational sensitivity of Cor-PC and coronene towards environmental changes arise in part from differing location of the probes in the lipid bilayer matrix. Cor-PC provides sensitivity to environmental changes occurring within the fatty-acyl chain region close to the phospholipid head group region. In contrast, free coronene which is expected to distribute randomly across the lipid bilayer width, appears somewhat less sensitive to alterations (such as addition of peptide) within the acyl chain region of the lipid bilayer.

Steady-state emission anisotropy values (<r>) were recorded as a function of increasing temperature for DMPC/melittin SUVs labeled with either coronene, Cor-PC or

DPH. Steady-state measurements reflect an *average* measure of both lipid membrane fluidity and ordering. However, the long fluorescence lifetimes of coronene and Cor-PC make their rotations sensitive to the chain ordering events which occur well after the decay of most other fluorescence probes, since the fluorescence lifetime exceeds the lifetime of the gel domains and equilibrium is established. This phenomenon is not observed for the rotational motions of embedded DPH labeled DMPC SUVs which reveals a sharp decrease in emission anisotropy at the phase transition temperature of 23°C. In contrast, coronene and Cor-PC labeled DMPC SUVs feature an overall broader lipid 'melting' curve shifted (10~15°C) towards lower temperatures (~20°C), and which reflect slower lipid fluctutations occurring within the submicrosecond 'time window", well below the lipid phase transition temperature (T_c).

Time-resolved emission anisotropy measurements of Cor-PC and coronene labeled DMPC vesicles thus provides further evidence of the relation between structure and dynamic change of lipids and time-resolved fluorescence parameters of these probes. While the average measured fluorescence lifetimes ($<\tau>$) for Cor-PC and coronene are not sensitive to the lipid phase transition, time-resolved emission anisotropy studies (TREA) reveal that the slower out-of-plane rotational correlation times (ϕ_2) for both these probes demonstrate sensitivity to the phospholipid phase transition (ϕ_2 is ~250 ns and ~30 ns for Cor-PC, and ϕ_2 is ~240 ns and ~10 ns for coronene embedded in DMPC SUVs (above and below T_c, respectively), and both Cor-PC and coronene are influenced by slow packing fluctuations in lipid bilayers. In contrast, for DPH where $<\tau>$ ~ 10ns, such persistent rotational motions of the probes are observed only as a residual anisotropy term (r_∞). Thus, these longer-lived probes can unravel

and offer more sensitivity to the presence of integral membrane components such as cholesterol or, as in this case, peptides, on the ordering of lipid bilayers.

The magnitude of ϕ_2 values for Cor-PC are somewhat comparable with coronene in the gel phase, although more hindered in the fluid phase. This is expected because the fluorophore in Cor-PC resides in a fixed position and is anchored to the lipid within the acyl chain region of the lipid bilayer reducing its rotational motions, whereas coronene is randomly distributed throughout the acyl chain region. Additionally, previous studies have shown that the fatty acyl chain of the phospholipid is less flexible from the glycerol backbone down through the C-9 methylene position [12] of the acyl chain. We thus expect that the coronenyl group of Cor-PC will reside in a somewhat more ordered environment above the lipid phase transition temperature compared with coronene.

For coronene, the short rotational correlation time (ϕ_1) represents the rotation of a subpopulation of molecules located in the fluid phase, and the relative proportion of this probe population (β_1) increases with temperature through T_c. The longer correlation time (ϕ_2) represents slower 'gated' packing fluctuations among the acyl chains of the lipid bilayer [5, 104] representative of a gel-fluid lipid exchange rate (k_{FG}). Similarly, decreasing values of ϕ_2 for Cor-PC suggest out-of-plane rotations dominated by the gel-fluid bilayer equilibrium within the bilayer.

Steady-state rotational studies of Cor-PC and coronene labeled lipid vesicles may be used to monitor important lipid-peptide interactions. While DPH showed little change in steady-state emission anisotropy values on introduction of melittin to the bilayer below T_c, sensitivity was observed for coronene, with a slight increase (~10%) in emission anisotropy

values (melittin, 1:50 peptide to phospholipid mole labeling ratio). Furthermore, Cor-PC labeled DMPC SUVs revealed a significant increase (~45%) in emission anisotropy values (<r>) below T_c with incorporation of melittin into the lipid bilayers (1:50 peptide to phospholipid molar labeling ratio). It appears that introduction of peptide to the lipid bilayer profoundly influences lipid dynamics occurring on the submicrosecond time scale where DPH exhibits little sensitivity. The submicrosecond time 'window' provided by Cor-PC and coronene probes thus offers a significant advantage for studies of lipid packing fluctuations and their modulation.

Time-resolved fluorescence experiments for coronene and Cor-PC labeled melittin containing vesicles provided quantitative dynamic information regarding the lipid ordering effects of melittin observed on the submicrosecond time scale. The fluorescence lifetime of Cor-PC does not change with the increasing amount of melittin in the lipid bilayers. The slower rotational correlation time (ϕ_2) of Cor-PC, which exhibits sensitivity to the slow lipid packing fluctuations through out-of-plane rotations exclusively, is increased on insertion of peptide to the DMPC SUV lipid bilayer reaching a value of 520 ns when the melittin to lipid molar ratio is 1:50. The increase of ϕ_2 with more melittin incorporated into the lipid bilayer suggests an ordering effect on lipid bilayers induced by peptide. The short rotational correlation time (ϕ_1) is not affected by the insertion of melittin into the lipid bilayer, which could mean the lipid ordering effect induced by melittin existing mostly in the gel-phase of the lipid. For coronene, the relative insensitivity of ϕ_2 to the presence of melittin may reflect unaltered k_{FG} rates (more likely), or alternatively potential exclusion of the probe from the peptide site of the bilayer.

Related fluorescence excimer experiments conducted in this study confirm that insertion of melittin in to the lipid bilayer decreases the microfluidity of the lipid bilayers. The diffusion controlled rate of excimer formation is reduced on titration of melittin into lipid vesicles, as evidenced by a decreased pyrene excimer-to-monomer intensity ratio. The fluorescence lifetime of pyrene is on the order of ~100 ns when embedded within lipid bilayers [9], which is on the same scale as the fluorescence lifetime of Cor-PC and coronene.

The effect of peptide on lipid packing is not detected on a nanosecond time scale as shown by time-resolved fluorescence emission anisotropy measurements using DPH labeled lipid/melittin vesicles. The average fluorescence lifetime of DPH is about 10 ns, which provides a limited time 'window' in which to detect peptide induced slow lipid fluctuation changes. The data in this research paper suggest that Cor-PC is a promising membrane probe for investigating of lipid-peptide interactions.

In summary, from the results of the above studies we can conclude that:

1. The synthesis of the Cor-PC probe adduct and its use for probing bilayer structure, lipid dynamics, and the effect of lipid-peptide interactions were successful.
2. Cor-PC and coronene exhibit a long mean fluorescence lifetime with rotational sensitivity to submicrosecond lipid dynamics, which are reflected in both steady-state and time-resolved fluorescence experiments.
3. Due to the known and fixed position of the fluorophore of Cor-PC within the bilayer, this probe can provide sensitivity to submicrosecond events occurring at a more localized position within the bilayer. From fluorescence quenching studies, the locations of Cor-PC and coronene within the lipid bilayer matrix are different.

4. Upon insertion of a peptide into DMPC SUV bilayers, the 'fluidity' of the lipid membrane appears to be decreased, as reflected in the rotational motions of both coronene and Cor-PC. Melittin appears to have a significant ordering effect on the lipid packing which can only be observed on a submicrosecond scale.

5. The magnitude of the fluorescence lifetime for the probes used is critical for the observation of 'slow' or submicrosecond lipid fluctuation events. Probes with lifetimes of several hundreds of nanoseconds are good candidates for such studies.

5. Bibliography

[1]. Habermann, E., Science, 1972, 177, 314-322.

[2]. Kreil, G. and Kreil-Kiss, G., Biochemical and Biophysical Research Communications, 1967, 27, 275-280.

[3]. Dempsey, C. E. Biochimica et Biophysica Acta, 1990, 1031, 143-161.

[4]. Canfield, R. E. J. Biol. Chem. 1963, 238, 2698-2707.

[5]. Davenport, L., Knutson, J. R. and Brand, L. SPIE Vol.909 Time-Resolved Laser Spectroscopy in Biochemistry ,1988, 263-270.

[6]. Cullis, P. R. And Hope, M. J. Biochemistry of lipid and membranes, (Vance, D. E. and J. E. Vance,J. eds.) The Benjamin/Cummings Publishing Company, Inc.1985, 1-250.

[7]. Rao, N. M., Biochem. & Biophys. Research Communication, 1992, 182 (2), 682-688.

[8]. Davenport, L., Knutson, J. R. and Brand, L. Faraday Discuss. Chem. Soc., 1986, 81, 81-94.

[9]. Davenport, L., Knutson, J. R. and Brand, L. Subcellular Biochemistry, Vol. 14 (Edited by Harris, J. R. and Edtemadi, A. H.) Plenum Publishing Corporation, 1989, 145-188

[10]. Nagle, J. F. and Scott, J. L. Jr. Biochim. Biophys. Acta, 1978, 513, 236-243.

[11]. Hudson, B. S. et. al, Application of Fluorescence in Biomedical Sciences, (D.L. Taylor, D. L. et. al. Eds.) Alan R. Liss., Inc. 1988, 159-202.

[12]. Seelig, A. and Seelig, J. Biochemistry, 1974, 13, 4839-4845.

[13]. Hinz, H. J. and Sturtevant, J. M., J. Biol. Chem. 1972, 247, 6071.

[14]. Suurkuusk, J., Lentz, B. R., Barenholz, Y., Biltonen, R. L. and Thompson, T. E., Biochemistry, 1976, 15, 1393-1401.

[15]. Hubbell, W. L. and McConnell, H. M., J. Am. Chem. Soc., 1971, 93, 383

[16]. Jost, P., Waggoner, A. S., and Griffith, O. H., Structure and Function of Biological Membranes (Rothfield, L. I. Ed.), Academic Press, New York, 1971, 83-143.

[17]. Seiter, C. H. A., and Chan, S. I., J. Am. Chem. Soc., 1973, 95, 7541-7553.

[18]. Davis, J. H., Biochim. Biophys. Acta, 1983, 737, 117-171.

[19]. Bansil, R., Day, J., Meadow, M., Rice, D. And Oldfield, E., Biochemistry, 1980, 19, 1938-1943.

[20] Litman, B. J., Lewis, E. N. and Levin, I. W., Biochemistry, 1991, 30, 313-319.

[21]. Castresana, J., Valpuesta, J. M., Arrondo, J. L. R. and Goni, F. M., Biochim. Biophys. Acta, 1991, 1065, 29-34.

[22]. Lentz, B. R., Barenholz, Y. and Thompson, T. E., Biochemistry, 1976, 15, 4521-4528.

[23]. Lentz, B. R., Barenholz, Y. and Thompson, T. E., Biochemistry, 1976, 15, 4529-4537

[24]. Jost, P. C. and Grifftih, O. H. Eds., Lipid-protein interactions, Vols. 1 and 2,Wiley New York, 1982, 1.

[25]. Stubbs, C. D. and Williams, B. W., Topics in Fluorescence Spectroscopy, Vol.3 (Lakowicz, J. R. Eds.), Plenum Press, New York, 1991, 232-271.

[26]. Holtzwarth, J. F., Eck, V and Genz,A. Spectroscopy and Dynamics of Molecular Biological Systems (Bayley, P. M. and R. E. Dale, R. E. Eds.) Academic Press, 1985, 351-401.

[27]. Wolber, P. K. and Hudson, B. S. Biochemistry, 1981, 20, 2800-2808.

[28]. Davenport, D. Method in Enzymology, 1997, 278, 487-512.

[29]. Wickner, W., Science, 1980, 210, 861-863.

[30]. Lingappa, V. R., Chaidez, J., Yost, C. S. and Hedgpeth, J., Proc. Natl. Acad. Sci. USA, 1984, 81, 456-460.

[31]. Friedlander, M. and Blobel, G., Nature, 1985, 318, 338-343.

[32]. Gierasch, L. M., Biochemistry, 1989, 28, 923-930.

[33]. Jones, J. D., McKnight, C. J. and Gierasch, L. M., J. of Bioenergetics and Biomembrane, 1990, 22, 213-232.

[34]. Ahn, T. and Kin, H., J. of Biological chemistry, 1996, 271 (21), 12372-12379.

[35]. Chen, H. and Kendall, D. A., J. of Biol. Chem., 1995, 270 (23), 14115-14122.

[36]. Wang, Q., Cui, D. and Lin, Q., Biochim. Biophys. Acta, 1997, 1324, 69-75.

[37]. Blobel, G. International Cell Biology, (Brinkly, B. R. and Porter, K. R. Eds) Rockefeller University Press, New York, 1977, 318.

[38]. Water, P., Gilmore, R. and Blobel, G. Cell, 1984, 38, 5-8.

[39]. Heigne, G. V. Eur. J. Biochem., 1981, 116, 419-422.

[40]. Engleman, D. M. and Steiz, T. A. Cell, 1981, 23, 411-422.

[41]. Sui, S. F., Wu, H., Guo, Y.and Chen, K. S., J. of Biochem., 1994, 116, 482-487.

[42]. DeGrado, W. F., Musso, G. F., Lieber, M., Kaiser, E. T., and Kezdy, F. J., Biophys. J., 1982, 37, 329-338.

[43]. Georghious, S., Thompson, M. and Mukhopadhyay, A. K., Biochim. Biophys. Acta, 1981, 642, 429-432.

[44]. Vogel, H., FEBS Lett., 1981, 134, 37-42.

[45]. Bechinger, B., J. of Membrane Biology, 1997, 156, 197-211.

[46]. Smith, R. et. al., J. of Molecular Biology, 1994, 241, 456-466.

[47]. Vogel, H. and Jähnig, F., Biophys. J., 1986, 50, 573-582.

[48]. Batenburg, A. M., Van Esch, J. H. and De Kruijff, B., Biochem., 1988, 27, 2324-2331.

[49]. Lasic, D, American Scientist, 1992, 80, 20-31.

[50]. Soutar, A. K., Pownall, H. J., Hu, S. A. and Smith, L. C., Biochemistry, 1974, 13, 2828-2836

[51]. Dangreau, H., Joniau, M., Cuyper, M. D., and Hanssens, I., Biochemistry, 1982, 21 3594-3598

[52]. Lakowicz, J. R. Principles of Fluorescence Spectroscopy, Plenum Press, New York

and London, 1983, 1-17.

[53]. Davenport, L., Knutson, J. R., and Brand, L., Biophys. J., 1987, 51, 537a.

[54]. Davenport, L., Knutson, J. R., and Brand, L., Biophys. J., 1988, 53, 508a.

[55]. Davenport, L., Markby, D. W., Knutson, J. R., and Brand, L., Photochem. Photobiol., 1983, 37, S20.

[56]. Chen, L. A., Dale, E. R., Roth, S., and Brand, L., J. Biol. Chem., 1977, 252, 2163-2169.

[57]. Hawton, M. H. and doane, J. W. Biophys. J., 1987, 52, 401-404.

[58]. Ruggiero, A. and Hudson, B. Biophys. J., 1989, 55, 1111-1124.

[59]. Michels, B., Fazel, N. and Cerf, R. Eur. Biophys. J., 1989, 17, 187-190.

[60]. Biltonen, R. J. Chem. Thermodynamics, 1990, 22, 1-19.

[61]. Lakowicz, J. R. Principles of Fluorescence Spectroscopy, Plenum Press, New York and London, 1983, 51-93.

[62]. Barkley, M. D., Kowalczyk, A. A. and Brand, L. J. Chem. Physics, 1981, 75, 3581-3593.

[63]. Goldenberg, M., Emert, J., and Morawetz, H., J. Am. Chem. Soc., 1978,100, 7171-7177.

[64]. O'Connor, D. V., and Phillips, D., Time-correlated Single Photon Counting, Academic Press, 1984, 1-209.

[65]. Eftink, M. R., Topics in Fluorescence Spectroscopy, Vol.2 (Lakowicz, J. R. Eds.) Plenum Press, New York, 1991, 53-120.

[66]. Steiner, R. F., Topics in Fluorescence Spectroscopy, Vol.2 (Lakowicz, J. R. Eds.) Plenum Press, New York, 1991, 1-52.

[67]. Brand, L., Knutson, J. R., Davenport, L., Beechem, J. M., Dale, R. E., Walbridge, D. G. and Kowalczyk, A. A. Spectroscopy and Dynamics of Molecular Biological Systems (Bayley, P. M. and R. E. Dale, R. E. Eds.), Academic Press, 1985, 259-305.

[68]. Birks, J. B., Photophysics of aromatic molecules, Wiley Press, New York, 1970, 1.

[69]. Lamotte, M., Merle, A. M., and Joussot-Dubien, J., Chem. Phys. Lett., 1975, 35, 410-416.

[70]. Katraro, R., Ron, A., and Speiser, S., Chem. Phys., 1979, 42, 121-132.

[71]. Morgan, C. G., Thomas, E. W., Moras, T. S. and Yiannis, P. Y. Biochimica Biophysica Acta 1982, 692, 196-201.

[72]. Shen, B., Joseph, T. W., Straher, M. P. and Davenport, L. J. Fluorescence, to be published

[73]. Clar, E. and Zander, M. J. Chem. Soc., 1958, 2, 1577-1579.

[74]. McClare, C. W. F. Anal. Biochem., 1971, 39, 527-532.

[75]. Dittmer, J. C. and Lester, R. L., J. Lipid Res. 1964, 5, 126-127.

[76]. Brocherhoff, H. Methods Enzymol., 1975, 35, 318.

[77]. Barenholz, Y., Gibbs, D., Litman, B. J., Goll, J., Thompson, T. E. and Garlson, F. D. Biochemistry, 1977, 16, 2806-2810.

[78]. Hope, M. J., Baly, M. B., Webb, G., and Cullis, P. R., Biochim. Biophys. Acta, 1985, 812, 55-65.

[79]. Dufourcq, J. and Faucon, J.-F., Biochimica et Biophysica Acta, 1977, 467, 1-11.

[80]. Mollay, C. And Kreil, G., Biochimica et Biophysica Acta, 1973, 316, 196-203.

[81]. Parker, C. A. and Rees, W. T. Analyst (London), 1960, 85, 587-600

[82]. Chen, R. F. and Bowman, R. L. Science, 1963, 147, 729-732.

[83]. Wahl, Ph. Biochim. Biophys. Acta, 1969, 175, 55-58.

[84]. Badea, M. G. and Brand, L. Methods Enzymol., 1979, 61H, 378-394.

[85a]. Grinvald, A., and Steinberg, I. Z., Anal. Biochem., 1974, 59, 583-598.

[85b]. Bevington, P. R., Data Reduction and Error Analysis for the Physical Sciences, McGraw-Hill Book Company, 1969, 134-163

[86]. Davenport, L., Dale, R.E., Bisby, R.E., and Cundall, R.B., Biochemistry, 1985, 24,

4097-4108.

[87]. Zimmerman, H. and Joop, N. Z. Elektrochem. 1961, 65, 138-142.

[88]. Vincent, M., deForesta, B, Gallay, J. and Alfsen, A. Biochemistry, 1982, 21, 708-716.

[89]. Shinitzky, M., Dianoux, A. C., Gilter, C., and Weber, G. Biochemistry, 1971, 10, 2106-2113.

[90]. Shinitzky, M. Physiology of Mrmbrane Fluidity, Vol. 1 (Shinitzky, M. Ed.), CRC Press, Boca, FL., 1984, 1-15

[91]. Dale, R. E., Chen, L. A. and Brand, L. J. Biol. Chem., 1977, 252, 7500-7510.

[92]. Beechem, J. M. and Brand, L. Photochem. Photobiol., 1984, 39, 41S.

[93]. D. M. Small, Handbook of Lipid Research, Vol.4, The Physical Chemistry of lipids (Edited by D. J. Hanahan), Plenum Press, 1986, 477-479.

[94]. Davenport, L., Wang, J. Z. and Knutson, J. R. Biological and Synthetic Membranes, Alan R. Liss, Inc., 1989, 97-106.

[95]. Andrch, M. P., and Vanderkooi, J. M., Biochemistry, 1976, 15, 1257-1261

[96]. Davenport, L., and Targowski, P., J. of Fluorescence, 1995, 5, 9-18.

[97]. Zandvoort, M. J., Gerritsen, H. C. and Levin, Y. K. J. of Phys. Chem., 1997, 101, 4142-4148

[98]. Jahnig, F., Vogel, H., and Best, L., Biochemistry, 1982, 21, 6790-6798.

[99]. Blatt, E., and Sawyer. W. H., Biochim. Biophys. Acta, 1985, 822, 43-62

[100]. Galla, H. J. and Sackmann, E. Biochim. Biophys. Acta, 1974, 339, 103-115.

[101]. Gratton, E. and Parasassi, T. J. Fluoresc., 1995, 5, 51.

[102]. Stubbs, C. D., Ho, C. and Slater, S. J. J. Fluoresc. 1995, 5, 19.

[103]. Tan, A. K. and Ramsay, R. Biochem., 1993, 32, 2137-2143

[104]. Beechem, J. M. and Brand, L. Photochem. Photobiol., 1986, 44, 323-329.

[105]. Dale, R.. E., Chen, L.A., and Brand L., J. Biol. Chem., 1977, 252, 7500-7510.

[106]. Kawato, S., Kinosita, K.,Jr., and Ikegami, A., Biochemistry, 1977, 16, 2319-2324.

[107]. Kinosita, K., Jr., Kataoka, R., Kimura, Y., Gotoh, O., and Ikegami, A., Biochemistry, 1981, 20, 4270-4277.

IMAGE EVALUATION
TEST TARGET (QA-3)

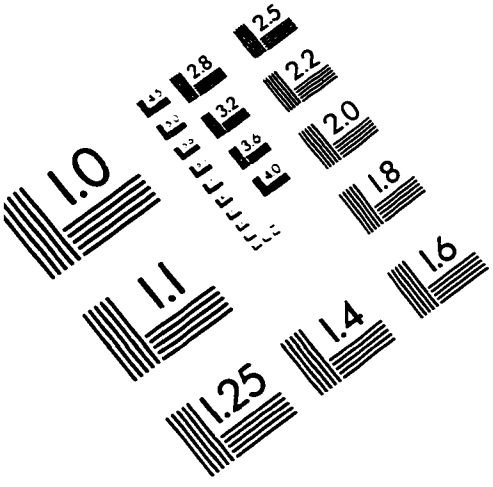

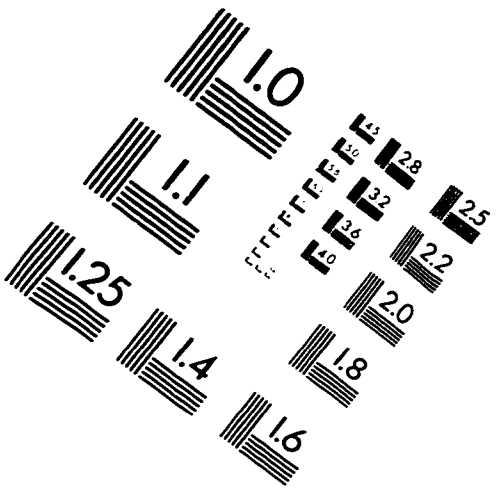

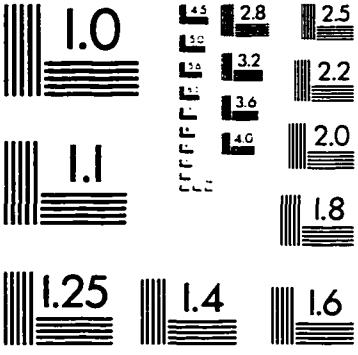

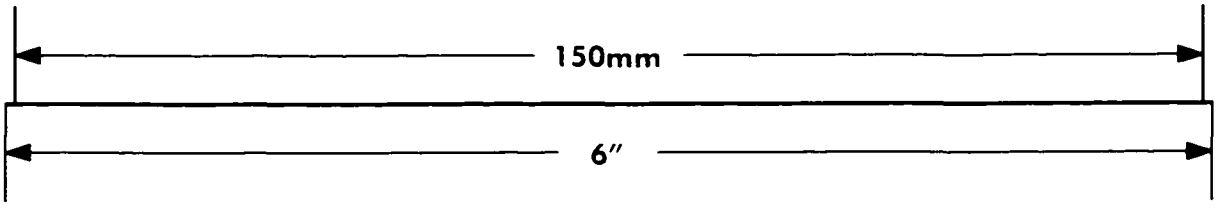

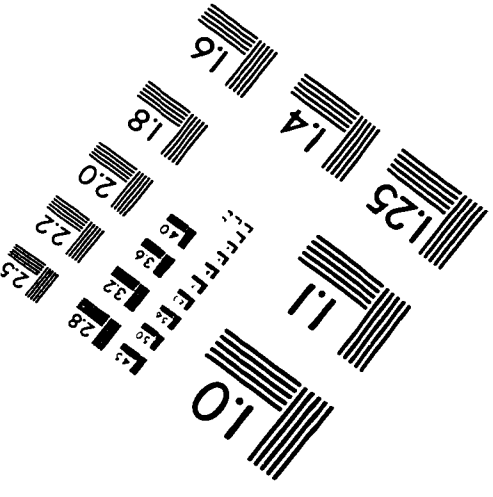

APPLIED IMAGE, Inc
1653 East Main Street
Rochester, NY 14609 USA
Phone: 716/482-0300
Fax: 716/288-5989